AD-A048 977 PRINCETON UNIV N J DEPT OF AEROSPACE AND MECHANICAL--ETC F/G 11/6
EROSIVE EFFECTS OF VARIOUS PURE AND COMBUSTION-GENERATED GASES --ETC(U)
OCT 77 A C ALKIDAS, S O MORRIS, C W CHRISTOE DAAG46-75-C-0088

UNCLASSIFIED AMS-1303 AMMRC-CTR-77-25 NL

1 OF 2
AD
A048977

AD

B.S. 12

AMMRC CTR 77-25

EROSIVE EFFECTS OF VARIOUS PURE AND COMBUSTION-GENERATED GASES ON METALS, PART II

OCTOBER 1977

A. C. ALKIDAS, S. O. MORRIS, C. W. CHRISTOE,
L. H. CAVENY AND M. SUMMERFIELD
DEPARTMENT OF AEROSPACE AND MECHANICAL SCIENCES
PRINCETON UNIVERSITY
PRINCETON, NEW JERSEY 08540

FINAL REPORT CONTRACT NUMBER DAAG46-75-C-0088

Prepared for

ARMY MATERIALS AND MECHANICS RESEARCH CENTER
Watertown, Massachusetts 02172

The findings in this report are not to be construed as an official Department of the Army position, unless so designated by other authorized documents.

Mention of any trade names or manufacturers in this report shall not be construed as advertising nor as an official indorsement or approval of such products or companies by the United States Government.

DISPOSITION INSTRUCTIONS

Destroy this report when it is no longer needed.
Do not return it to the originator.

SECURITY CLASSIFICATION OF THIS PAGE (When Data Entered)

REPORT DOCUMENTATION PAGE

READ INSTRUCTIONS BEFORE COMPLETING FORM

1. REPORT NUMBER: AMMRC CTR-77-25
2. GOVT ACCESSION NO.
3. RECIPIENT'S CATALOG NUMBER
4. TITLE (and Subtitle): EROSIVE EFFECTS OF VARIOUS PURE AND COMBUSTION-GENERATED GASES ON METALS. PART II.
5. TYPE OF REPORT & PERIOD COVERED: Final Report. 1 Jun [illegible] 75-31 Jan [illegible] 76
6. PERFORMING ORG. REPORT NUMBER: AMS-[illegible] 1303
7. AUTHOR(s): A. C./Alkidas, S. O./Morris, C. W./Christoe, L. H./Caveny M./Summerfield
8. CONTRACT OR GRANT NUMBER(s): DAAG46-75-C-[illegible]
9. PERFORMING ORGANIZATION NAME AND ADDRESS: Princeton University, Princeton, New Jersey
10. PROGRAM ELEMENT, PROJECT, TASK AREA & WORK UNIT NUMBERS: D/A Proj [illegible] 1T161102AH42, AMCMS Code: 611102.11.H42
11. CONTROLLING OFFICE NAME AND ADDRESS: U.S. Army Materials and Mechanics Research Center, Watertown, Massachusetts 02172
12. REPORT DATE: Oct [illegible] 77
13. NUMBER OF PAGES: 123 (122 p.)
14. MONITORING AGENCY NAME & ADDRESS (if different from Controlling Office)
15. SECURITY CLASS. (of this report): UNCLASSIFIED
15a. DECLASSIFICATION/DOWNGRADING SCHEDULE

16. DISTRIBUTION STATEMENT (of this Report)

Approved for public release; distribution unlimited.

17. DISTRIBUTION STATEMENT (of the abstract entered in Block 20, if different from Report)

18. SUPPLEMENTARY NOTES

19. KEY WORDS (Continue on reverse side if necessary and identify by block number)

Erosion of Metals.
Heating by Solid Propellant Gases.
High Pressure and High Temperature Heat Transfer.
Ballistic Compressor.
Steels.
Erosion Corrosion.
Surface Chemistry.
Propellant Gases.
Gun Tubes
Alloys

20. ABSTRACT (Continue on reverse side if necessary and identify by block number)

This study continues the experimental investigation of the thermal and chemical erosion characteristics of steel alloys which were begun under Contract DAAG46-72-C-0078. The high pressure (≥ 3 kbars) and high temperature (≥ 3000 K) environment to which the steel specimens are subjected is produced by a ballistic compressor and by a solid propellant combustor. Equilibrium thermochemical calculations of the possible reactions indicate that the most probable reaction products are oxides, nitrides, carbides, and

DD FORM 1 JAN 73 1473 EDITION OF 1 NOV 65 IS OBSOLETE

20. Abstract - Continued

carbonyls, in that order. The cause of surface cracks was found to be thermal and not relatable to the degree and severity of erosion. Erosion tests of the pure metals used as alloying elements revealed that molybdenum has the highest erosion resistance, followed by nickel. There is no evidence that alloying elements alter the chemical interaction between oxygen and iron. SEM studies revealed that when an accumulation of oxide scale occurs with successive firings, oxidation and thermal protection is provided. It is hypothesized that as long as steel remains below its solidus temperature, the primary erosion mechanism is the reaction of combustion gases with the steel surface to form scales and the subsequent carrying-away of the scales by the high speed flow.

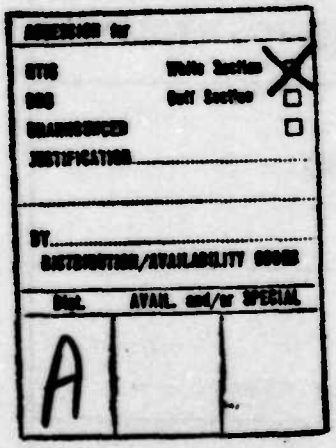

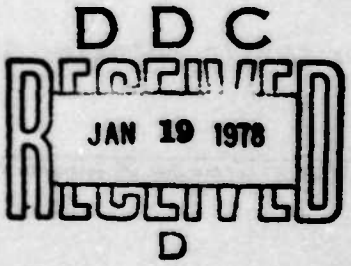

SUMMARY

The chemical erosion characteristics of steel alloys by high pressure and high temperature gases were investigated. Thermodynamic calculations of the reactions of the individual gaseous components of propellant gases with the alloying elements of steel showed that the most probable reaction products are the metal oxides followed by the nitrides, carbides and the carbonyls. Equilibrium calculations of the Fe-O_2, Fe-CO_2-CO and Fe-H_2O-H_2 system indicated that, for typical propellant compositions, wustite (FeO) is the most likely product of the chemical interaction between propellant gases and steel alloys.

Experimental investigations of the erosion of steel alloys were performed using as the hot, high pressure gas source for convective heating a vented-combustor and a ballistic compressor apparatus.

Scanning Electron Microscope (SEM) studies of the eroded surfaces of steel specimens subjected to the action of high pressure propellant gases revealed (a) the presence of a scale that becomes less abundant as the combustor peak pressure increased and (b) the presence of crack formations whose width increased with increasing combustor peak pressure. The crack dimensions were shown to depend on the isochoric flame temperature of the propellant (i.e., the higher the isochoric flame temperature of the propellant the wider the cracks on the underlying metal surface) and to be inversely dependent upon the thermal conductivity of the steel. Tests performed thus far (including high pressure and high temperature H_2 tests on steel) indicate that the mechanism of crack formation is thermal, i.e., cracks were formed to relieve the strain produced by the rapid heating and cooling processes. The role of cracks on the overall mass erosion experienced by the steel alloys is believed to be secondary.

The ballistic compressor was used to study the erosive action of individual gases at high pressure and high temperature on steel alloys. Comparison of rectangular and circular steel

orifices showed that both geometries experienced the same mass erosion per unit surface area. This result indicates that the depth of the thermal wave is much smaller than the radius of curvature of the circular orifices. In agreement with the results reported in Part I of this study,[1] hydrogen and molecular oxygen-containing gases (O_2/N_2 and $H_2/O_2/N_2$ mixtures) produced considerably more erosion of the AISI 4340 steel than N_2, A and CO and CO_2/A mixtures. At concentrations of 95% H_2 in N_2/H_2 mixtures and lower, the mass erosion experienced by the steel specimen is independent of the H_2 concentration. The erosion of AISI 4340 steel was shown to be linearly proportional to the mole fraction of O_2 in O_2/N_2 mixtures. Under some repetitive tests, erosion decreased with the number of firings; this demonstrates that the oxide scale produced by the iron/oxygen interaction may not be totally removed by the gas flow and, therefore, oxide accumulation, when it occurs, provides successively better thermal and oxidative protection. It is hypothesized that as long as steel remains below its solidus point, erosion results from the removal of the scale formed on the metal surface by the chemical interaction of iron with reactive gases.

Erosion tests performed on metals used as alloying elements showed that molybdenum has the highest resistance to erosion. The degree of erosion experienced by iron was similar to that of the three test steel alloys (i.e., AISI 4340, AISI 1020, and AISI 304). This indicates that the alloying elements of steel do not alter the chemical interaction between oxygen and iron.

Experimental investigation of known erosion-reducing additives (polyurethane foam, TiO_2/wax, talc/wax, paraffin wax and silicone lubricant) at high pressure, vented chamber conditions showed that the best additive is talc/wax, followed by paraffin wax. Polyurethane foam, an effective gun barrel erosion reducer, shows little promise under the vented chamber test conditions. The ineffectiveness of polyurethane foam is attributed to the lack of its coating action on eroded surfaces.

FOREWORD

The project summarized in this report was carried out under Contract DAAG46-75-C-0088 and administered by the Research Sciences Division, Basic Research Laboratories, of the U.S. Army Materials and Mechanics Research Center, Watertown, Mass. The Technical Monitor was Dr. J. Warren Johnson; his technical contributions materially aided this project.

Dr. C. W. Christoe of the U.S. Army's Explosives Laboratory at Picatinny Arsenal participated in this project as a Visiting Scientist at Princeton University.

Part I of this study summarized the results of the studies under Contract DAAG46-72-C-0078. This report is cataloged at Princeton University as AMS Report 1303.

TABLE OF CONTENTS

I. INTRODUCTION

The erosion of gun barrels is generally attributed to both thermal ablation (i.e., melting of the bore surface and subsequent removal of the melt by the aerodynamic forces of the flow) and chemical ablation (i.e., chemical interaction between the metal surface and the propellant gases and subsequent partial removal of the solid reaction products by the flow). The controversy among the various investigations of barrel erosion centers on which of the two above stated mechanisms is the primary cause of erosion. This difference in opinion centers on whether, during the firing cycle, the surface temperature, T_S, of the bore reaches its solidus temperature, T_M. Thus, we may define two regimes of erosion based on the value of the surface temperature of the bore:

1. When $T_S < T_M$ the primary mechanism of erosion is chemical ablation, and
2. when $T_S > T_M$ the primary mechanism of erosion is thermal ablation.

Whether the surface temperature of the material, T_S, reaches its solidus temperature will depend on a large number of parameters, such as the thermal and chemical characteristics of the propellant combustion gases and of the surface material; the experimental characteristics of the firing cycle, i.e., the effective test time and the pressure and temperature history of the propellant gases; and the physical characteristics of the flow. Even in the case where the surface temperature reaches the solidus temperature of the material of the bore, chemical ablation is very important, especially in the initial stages of erosion.

The overall objective of this study is to investigate in detail the chemical interaction of the individual gases that constitute the multi-component propellant gas mixture with steel alloys and to relate this information to the overall erosive action of propellant gases on steel alloys.

In the first part of this study,[1] results were presented

on the mass erosion experienced by three steel alloys (AISI 1020 carbon steel; AISI 4340 chrome-moly steel; and AISI 304 stainless steel) under the erosive action of propellant gases and individual gases constituting the multi-component propellant gases (CO_2, CO, O_2, N_2, H_2O).

In the present study, we undertook to:

a. determine, through thermodynamic calculations, the affinity of the reactive gases present in propellant gases (such as CO_2, CO, H_2O and O_2) have for the parent metal of steel alloys, Fe, and for the alloying metals of steel, Ni, Cr and Mn.

b. Characterize the eroded surfaces of steel alloys subjected to the erosive action of propellant gases and the individual gaseous components of propellant combustion products with respect to surface changes.

c. Identify the products of the gas/metal interactions both on eroded surface and in the effluent gas stream.

d. Study the erosion of pure metals that constitute the alloying elements of steel and compare the results to the erosion of steel alloys.

e. Obtain an experimental comparison of the erosion-reducing action of candidate wear-reducing additives.

It is obvious that under excessive or prolonged heating by combustion gases, melting will be the primary mode of mass removal. However, under most practical situations, this is a condition which is to be avoided by proper design. Thus, during this study, emphasis was on situations which produced high metal temperatures below the solidus temperature.

II. THERMODYNAMICS OF THE CHEMICAL REACTIONS BETWEEN METALS AND GASES

The complexity of the chemical interaction between a gas and an alloy occurs because the components of the alloy may have different affinities for the reactive gases (i.e., selective oxidation,[2,3] and the reactive species may not diffuse at the same rate through the scale formed on the surface or through the alloy phase. Also, a further complication may arise when a reactive gas dissolves in the alloys and reacts with one of the alloying components (usually the less noble component) within the alloy. In oxidation studies, this phenomenon is called internal oxidation.[2] Another complexity that may occur in gas alloy chemical interactions is when one of the alloying components forms a low melting point oxide. The presence of liquid oxide phase may lead to excessively fast reaction and disintegration of the alloy; this phenomenon is commonly termed, in oxidation studies,[2] catastrophic oxidation.

In erosion studies of steel alloys by high pressure and high temperature propellant gases, a further difficulty arises because the propellant gas is a multi-component mixture of gases and several of the species may enter into reactions with the parent metal or the alloying metals.

To study the contribution of the alloying elements of steel on the overall chemical reaction of steel with propellant gases, we examined:

a. the relative affinity of the reactive gases present in propellant gases such as CO_2 CO, H_2O and O_2 for the parent metal, Fe, and for the alloying elements of steel, Ni, Cr and Mn, and

b. the equilibrium conditions of iron-oxygen, iron-carbon monoxide-carbon dioxide and iron-hydrogen-water vapor system. Equilibrium calculations can be utilized to obtain information on the resulting products of reaction between reactive propellant gases and steel. Although the reactions occurring during the erosion process are not in equilibrium, it has been

shown (Ref. 4, p. 47) that at the boundaries between various oxide layers that form on the surface or between the parent metal and the neighborhood oxide layer, equilibrium may exist.

Reaction of Propellant Gases with Alloying Elements of Steel

For a reaction to proceed spontaneously at constant temperature and pressure, the process must be accompanied by a decrease in the Gibbs free energy of the system, i.e.,

$$(\Delta G)_{T,p} \leq 0 \qquad (1)$$

Equilibrium corresponds to the condition of minimum energy.

A quantitative measure of the stability of a product or of the relative affinity of a reactant gas for a particular compound is the standard Gibbs free energy ΔG°. In general, the larger the negative value of ΔG°, the greater the stability of the compound and the greater the likelihood of the reaction to produce this compound.

The relative affinity of the reactant gases present in propellant gases for the major alloying elements of steel are shown in Figs. 1-4. These figures are graphs of the standard Gibbs free energy of the oxides of the alloying elements of steel (Fe, Cr, Ni, and Mn) as a function of the reaction temperature. The reactant gases considered are CO_2, H_2O, CO, and O_2. The thermodynamic properties of the gas-metal reactions have been drawn from several references.[5,6,7,8,9] The form of the reactions represented in Fig. 1-4 are:

$$M + x/y\ CO_2 \rightarrow 1/y\ M_yO_x + x/y\ CO \qquad (2)$$

$$M + x/y\ H_2O \rightarrow 1/y\ M_yO_x + x/y\ H_2 \qquad (3)$$

$$M + x/y\ CO \rightarrow 1/y\ M_yO_x + x/y\ C \qquad (4)$$

$$M + x/2y\ O_2 \rightarrow 1/y\ M_yO_x \qquad (5)$$

where M represents the metal under consideration.

The points of discontinuities in the graphs marked by mp and d represent the melting point and decomposition of the oxide. Oxides with positive values of standard free energy of formation have been omitted.

The reaction of the metals with CO_2 (Fig. 1) show moderate negative values of $\Delta G°$. The most stable oxide is Cr_2O_3. The same characteristics are observed with the reactions with H_2O and CO (Figs. 2 and 3) although in the latter case at room temperature the oxides are more stable. As expected the oxides obtained from the reaction of the metals with oxygen are the most stable (see Fig. 4). However in most cases, the stability of the oxides decreased with increasing temperature. A further general observation is that Cr and Mn produce oxides that are more stable than the parent metal, Fe, whereas Ni produces less stable oxide. Stating this in other words, the reacting species of the propellant gases have greater affinity for Cr and Mn than Fe and Ni.

One must be cautioned that the standard Gibbs free energy for thermodynamic calculations does not provide information about the rate of the chemical reaction. The large negative value of $\Delta G°$ indicates only that a large driving force exists which should make the reaction more likely to occur. However, reaction kinetics information is required to investigate the rate of conversion of the particular reaction under investigation.

Figure 5 shows a plot of $\Delta G°$ as a function of temperature of the reactions between iron and the major gaseous components of propellant gas (CO_2, CO, H_2O and N_2). The plot indicates that none of the reacting gases have large affinity for iron, in comparison to the oxygen's affinity for iron (see Fig. 4).

When the oxide scale is thick the diffusion of reactants are slow and thermodynamic equilibrium[4,10] exists at the boundaries between the metal and the lower oxide or between two different oxides. Therefore knowledge of the equilibrium conditions of the oxidizer/metal system allows us to predict

the possible phase composition of the scale as a function of temperature and free stream oxidizer composition and the direction of the oxidation-reduction processes. In the next sections, we will consider the equilibrium of Fe/O_2, $Fe/CO_2/CO$ and $Fe/H_2O/H_2$. The gases under consideration represents the reactive gases present in propellant gases.

Chemical Equilibrium in Metal - Gas Systems

The general theory of chemical equilibrium presented in numerous textbooks,[11,12,13] has been summarized for the convenience of the reader in Appendix I. Considering the case of a simple reaction

$$Me + 1/2\ O_2 \rightleftharpoons MeO \tag{6}$$

the equilibrium constant (Eq. I-13) is given by the expression

$$K_a = \frac{a(MeO)}{a(Me)\,[a(O_2)]^{1/2}} = \exp -\left[\frac{\Delta G^\circ}{RT}\right] \tag{7}$$

At moderate pressures the activities of pure substances are equal to one, i.e.,

$$a(MeO) = a(Me) = 1$$

Assuming that the gas is ideal, i.e., $a(O_2) = p_{O_2}$ Eq. (6) becomes

$$K_p = p_{O_2}^{-1/2} = \exp -\left[\frac{\Delta G^\circ}{RT}\right] \tag{8}$$

When the partial pressure of oxygen in the gaseous phase, $(p_{O_2})'$, is less than the equilibrium pressure p_{O_2}, MeO will tend to reduce to Me. Conversely when p'_{O_2} is greater than p_{O_2} then Me will tend to oxidize to MeO.

The Iron - Oxygen System

The reaction of iron with oxygen may result in the formation of three oxides: Fe_xO (wustite), Fe_3O_4 (magnetite) and Fe_2O_3 (hematite). The wustite of stoichiometric composition FeO is unstable. However, for the sake of simplicity we will adopt the stoichiometric form of wustite for subsequent equilibrium calculations.

Figure 6a shows a plot of the dissociation pressures of the iron oxides as a function of the reaction temperature. The reactions representing the solid lines in Fig. 6a are:

$$2\ FeO \rightleftharpoons 2Fe + O_2 \tag{9}$$

$$1/2\ Fe_3O_4 \rightleftharpoons 3/2\ Fe + O_2 \tag{10}$$

$$2\ Fe_3O_4 \rightleftharpoons 6\ FeO + O_2 \tag{11}$$

$$6\ Fe_2O_3 \rightleftharpoons 4\ Fe_3O_4 + O_2 \tag{12}$$

The equilibrium constant associated with each of the above reactions is related to the equilibrium pressure of oxygen by the relation

$$K_p = p_{O_2} = \exp(-\Delta G^\circ/RT) \tag{13}$$

Two or more compounds exist together in equilibrium at temperatures and pressures that are defined by the lines in Fig. 6a. To elucidate this point, let us consider the upper line of Fig. 6a separating the iron oxides Fe_2O_3 and Fe_3O_4. Hematite (Fe_2O_3) and Magnetite (Fe_3O_4) co-exist in equilibrium at temperatures and partial pressures of oxygen that lie on the boundary line separating the two regions. If for example, for a given temperature the partial pressure of oxygen p_{O_2} is less than the equilibrium partial pressure $(p_{O_2})_e$ corresponding to that temperature, then Fe_2O_3 will decompose to O_2 and Fe_3O_4. Conversely if p_{O_2} is greater than $(p_{O_2})_e$, then Fe_3O_4 will be further oxidized to Fe_2O_3.

A schematic representation of the above argument for the general reaction

$$Me + 1/2\ O_2 \rightleftharpoons MeO$$

is shown in Fig. 6b.

The equilibriums

$$2/3\ Fe_2O_3 \rightleftharpoons 4/3\ Fe + O_2 \qquad (14)$$

and

$$2\ Fe_2O_3 \rightleftharpoons 4\ FeO + O_2 \qquad (15)$$

do not exist and, therefore, are not in Fig. 6a.

The basic assumption for the development of Fig. 6a and similar figures is that when gas and a metal compound react together, their ultimate products will be the ones that require the lowest equilibrium partial pressure of the gas. To understand fully Fig. 6a, all the reactions of the iron-oxygen system (Eqs. 9-12, 14 and 15) have been included in Fig. 6c. For example, the equilibrium state of Eq. (14) does not exist because at temperatures of 500 K and above, the equilibrium partial pressure of oxygen, $(p_{O_2})_e$ for reaction (14' is higher than the equilibrium partial pressure of oxygen for the reaction (9); thus wustite, Fe_xO, will be produced instead of hematite, Fe_2O_3. On the other hand, at temperatures below 500 K the equilibrium partial pressure of oxygen of the reaction (14) is higher than the corresponding value of the reaction (10); thus when iron and oxygen reacts, at this temperature range, Fe_3O_4 will be produced.

Figure 6a shows that Fe_2O_3 cannot be in equilibrium with either Fe_xO or Fe. Furthermore, at high reaction temperatures (above 500 K) and high oxygen partial pressures, all three oxides of iron are formed. The outer layer is Fe_2O_3, the middle layer is Fe_3O_4 and the layer in contact with iron is Fe_xO. However, based on these idealized calculations, wustite is not formed when the temperature is below 500 K.

The Iron-Carbon Dioxide-Carbon Monoxide System

Figure 7 shows the equilibrium partial pressure ratio of CO to CO_2 as a function of temperature. The reactions considered are:

$$Fe + CO_2 \rightleftharpoons FeO + CO \quad (16)$$

$$3/4Fe + CO_2 \rightleftharpoons 1/4Fe_3O_4 + CO \quad (17)$$

$$3FeO + CO_2 \rightleftharpoons Fe_3O_4 + CO \quad (18)$$

$$2Fe_3O_4 + CO_2 \rightleftharpoons 3Fe_2O_3 + CO \quad (19)$$

The equilibrium constant associated with each of the above reactions is related to p_{CO}/p_{CO_2} by

$$K_p = \frac{p_{CO}}{p_{CO_2}} = \exp\left[-\Delta G^\circ/RT\right] \quad (20)$$

The equilibriums

$$2/3\ Fe + CO_2 \rightleftharpoons 1/3\ Fe_2O_3 + CO \quad (21)$$

$$2FeO + CO_2 \rightleftharpoons Fe_2O_3 + CO \quad (22)$$

do not exist. The region of Fe_2O_3, defined by Eq. (17) is not shown because it lies below $p_{CO}/p_{CO_2} = 0.01$. Fe_2O_3 will be formed only when the gaseous phase is very rich in CO_2, i.e., $p_{CO}/p_{CO_2} > 10^{-5}$. A typical value of p_{CO}/p_{CO_2} in propellant gases is 0.4. Thus from Fig. 7 it can be deduced that neglecting the effects of other reactive gases, the oxide scale produced will be largely Fe_xO. The usefulness of the information obtained from Fig. 7 is demonstrated in Table 1[14] which presents an experimental identification of the relative amounts of FeO and Fe_3O_4 present in eroded steel surface under the erosive action of CO/CO_2 mixtures. As predicted from Fig. 7, in the case of $p_{CO}/p_{CO_2} = 0.84$ the oxide scale produced will be mainly FeO.

The Iron-Hydrogen-Water Vapor System

The equilibrium diagram of this system is shown in Fig. 8. This is a plot of the equilibrium pressure ratio p_{H_2}/p_{H_2O} versus the reaction temperature. The reactions considered are

$$Fe + H_2O \rightleftharpoons FeO + H_2 \quad (23)$$

$$3FeO + H_2O \rightleftharpoons Fe_3O_4 + H_2 \quad (24)$$

$$2Fe_3O_4 + H_2O \rightleftharpoons 3Fe_2O_3 + H_2 \quad (25)$$

The equilibriums

$$2/3\ Fe + H_2O \rightleftharpoons 1/3\ Fe_2O_3 + H_2 \quad (26)$$

$$3/4\ Fe + H_2O \rightleftharpoons 1/4\ Fe_3O_4 + H_2 \quad (27)$$

$$2FeO + H_2O \rightleftharpoons Fe_2O_3 + H_2 \quad (28)$$

do not exist. As in the case of the $Fe\text{-}CO_2\text{-}CO$ system, the region of Fe_2O_3 is not shown because it exists when the gaseous phase is very rich in H_2O, i.e., p_{H_2}/p_{H_2O} is greater than 10^{-5}. The hydrogen to water vapor partial pressure ratio in typical propellants is about 0.5. Thus, generally the scale will be predominantly wustite.

Products of the Chemical Interaction of Propellant Gases and Steel in Barrel Erosion

The large array of the chemical products produced during the erosion of gun barrels that have been identified and the respective position where they have been found is shown in Table 2.[15] Of these products the most important are the iron oxides, nitrides, and carbides. Thermodynamic calculations of the standard Gibbs free energy showed that the order of likelihood of these products forming is: oxides first, nitrides second, carbides third and carbonyls last. The Gibbs free energy of the carbonyl and carbide reactions were positive with the exception of the carbides formed by the reaction with

solid carbon.

The interest in the carbonyl formation and in particular to the iron pentacarbonyl [$Fe(CO)_5$] resulted from the hypothesis set forth by Evans and co-workers [16,17] that the erosion of steel by CO/CO_2 mixtures is due to the reaction:

$$Fe + 5CO \rightarrow Fe(CO)_5 \ .$$

This reaction is catalyzed by SO_2, H_2S, NH_3 and H_2. Trace concentration of the above compounds have been found to increase considerably the erosion of steel orifices.

However, tests to isolate and identify experimentally iron carbonyl[14] as the erosion products of the CO/CO_2 gas mixture interaction with steel did not reveal the existence of iron carbonyl. This may have been due to the possible rapid decomposition of the iron carbonyl after its formation that makes it difficult to detect. At 500 K iron carbonyl is a stable product with a free energy of formation of -88 kcal/mole. Its free energy of formation, however, decreases with increasing temperature.

III. EROSIVE EFFECTS OF HIGH PRESSURE COMBUSTION GASES ON STEEL ALLOYS

The first report of this study[1] presented results of the correlation of the mass removal of steel alloys resulting from the erosive action of high pressure and high temperature propellant gases with such parameters as:

a. type of steel alloy,
b. type of propellant,
c. geometry of the orifice, and
d. number of successive exposures.

These correlations provided substantial data base on the erosion of steel alloys. However, very little was learned about the chemical aspects of erosion. In the present study, we undertook to obtain further insights into the erosion process by examining the effect of erosion on the steel surfaces. Accordingly, we sought to:

a. Characterize the eroded surfaces with respect to surface changes, and
b. Identify the products of the gas/metal interaction both on the eroded surface and in the effluent gas stream.

Apparatus and Materials

Experiments of the erosion of steel alloys by combustion generated gases were carried out in the vented-combustor apparatus shown schematically in Fig. 9 and described in detail elsewhere.[1,18,19] In order that the interior surfaces of the test orifice be accessible to optical microscopy and SEM examination, matched split disks containing a milled rectangular slot in one semicircle (see Fig. 10) were assembled and clamped to the test part of the combustor. The combustor was then charged with propellant (0.6 to 1.2 gm) which was then ignited by means of a primer. In the present experiments, unlike the earlier investigations,[1,18,19] no vent orifice was used so that to increase the effective test time. Fig. 11 shows a comparison

of the pressure history of the combustor using a 0.15 cm vent orifice (Fig. 11a) and using no vent orifice (Fig. 11b). The effective test time increases by a factor of 2.5 when the combustor does not have a vent orifice.

Most of the erosion tests were performed on AISI 4340 chromium-molybdenum steel. However, for comparative purposes a number of tests were performed on AISI 304 stainless steel and AISI 1020 carbon steel. Typical nominal compositions and room temperature properties of the above steels are shown in Tables 3 and 4.

The propellants used in this study were IMR-4198 and M1 single-base propellants. The M1 (T_v = 2528 K) propellant is a cooler propellant than the IMR-4198 (T_v = 3000 K) propellant. The chemical composition and propellant gas properties of the two propellants are shown in Table 5.

After each experiment, the test disk halves were cleansed of combustion products with acetone and trichloroethylene, weighed and the eroded surface examined. No qualitative differences were observed when comparing the milled surface with the opposed unmilled region of the matching half-disk. For simplicity, therefore, all results, except mass loss, given in subsequent sections refer to the unmilled side of the orifice. The mass losses quoted are the sum of that measured on both matched halves.

Results and Discussion

1. Mass Removal

The simplest quantitative measure of the erosion of a test specimen subjected to the action of high pressure and high temperature propellant gases is the mass difference before and after exposure to hostile gases.* Figure 12 shows a plot of the mass erosion experienced by the rectangular orifices as a function of the peak pressure of the combustor. These tests were performed without a vent orifice in the combustor (i.e., the width of the pressure trace at $p_{MAX}/2$ is of the order of 3.6 msec). The plot is linear after a pressure threshold

*It should be noted that the thicknesses removed from the surfac during our laboratory experiments are on the same order as those experienced during gun firings.

corresponding to about 90 MN/m^2. The relation between mass erosion and peak pressure obtained without a vent orifice differs greatly from the corresponding relation using a vent orifice (i.e., width of the pressure trace at $p_{MAX}/2$ is of the order of 1.3 msec). In the shorter effective test time experiments, the mass erosion rate accelerated rapidly as peak pressure increases, whereas in the longer test time experiments the mass erosion is linearly dependent to the combustor peak pressures. The difference in the characteristic shape of the mass erosion curves may indicate a shift in the mechanism of erosion, as the heating time of the specimen is increased, i.e., chemical ablation at short test times to thermal ablation at the longer test times. At the present time, we are not prepared to resolve this point. Plans, however, have been formulated to elucidate this change in the character of the erosion curve, by performing heat transfer calculations to estimate the surface temperature of the test specimen as a function of the experimental parameters.

2. Geometric Effects

A detailed examination of the geometric changes of the test specimen resulted from the erosive action of propellant gases as a function of the space coordinates was performed using profilometry.* A typical topograph of one symmetric half of eroded planar surface of AISI 4340 steel is shown in Fig. 13. In the middle of the orifice, the depth of regression is seen

---

* The profilometric studies as well as the Scanning Electron Microscope studies have been performed at the RCA David Sarnoff Research Center, Princeton, New Jersey.

to decrease monatomically from the upstream section (where the surface heat transfer is the greatest) to near the downstream end (where the surface heat transfer is the lowest). The edges of the downstream section channel are higher than the original untested planar surface which indicates that metal removed by the erosion process in the upstream section accumulated on the lip of the downstream section. A comparison of the erosion experienced by the steel specimen at three positions along the length of the specimen is shown in Fig. 14. This figure shows clearly that the greatest mass removal occurs at the upstream section.

3. Characterization of the Eroded Surface by Means of SEM

Figure 15 is a photograph of a Scanning Electron Microscope (SEM) image and shows a typical test surface prior to exposure to high pressure and high temperature propellant gases. The horizontal bands shown in Fig. 15 are machine marks and serve as convenient reference lines. Figure 16 shows a series of three eroded surfaces that have been exposed to IMR-4198 propellant gases. These SEM photomicrographs are situated from high to low to correspond to increasing combustor peak pressure. Examination of Fig. 16 reveals two important observations:

a. the presence of a scale on the eroded surface which is less abundant as the peak pressure increases, and
b. the presence of cracks on the underlying metal surface itself which appears to increase in width, and probably depth, as the peak pressure increases.

The relative decrease of area occupied by the scale at higher pressures suggests that this scale lacks sufficient cohesive strength to resist the higher shearing forces corresponding to the increased combustor pressure. Where the scale does form it has a brittle, flaky appearance.

Electron Microprobe Analysis (EMP) of these eroded surfaces indicated the presence of markedly more carbon in comparison with an unexposed specimen. The oxygen levels were shown to be comparable. It should be kept in mind that EMP quantitative

capabilities are limited with respect to light elements. The EMP also detected trace amounts of sulphur which were not present in the unexposed specimen. However, the Electron Microprobe Analysis is incapable of distinguishing whether these erosion products are bound into chemical compounds of iron or whether they have been merely deposited onto the surface with sufficient cohesive strength to resist the cleansing operations that were performed prior to examination. Moreover the EMP's insensitivity to oxygen does not rule out the presence of one or more of the iron-oxide scales.

The increase of the width of surface cracks with pressure observed in Fig. 16 is also shown in Fig. 17 which is a plot of width of the surface cracks measured from the SEM photomicrographs versus combustor peak pressure. Since the width of cracks varies over the surface a representative range of widths observed for each combustor peak pressure was plotted. Figure 17 shows a test performed using, instead of IMR-4198 propellant, a lower isochoric flame temperature propellant, an M1 propellant. As shown in Fig. 17 and also in Fig. 18, which is a photomicrograph of the eroded surface, the width of the surface cracks resulting from the erosive action of M1 propellant gases was markedly reduced. This reduction may be attributed largely to the cooler isochoric flame temperature (2500 vs 3000 K) of the M1 propellant which results in a correspondingly lower metal surface temperature.

A comparison of the crack formation on the eroded surface of the three test alloys, namely AISI 1020 carbon steel, AISI 4340 chromium-molybdenum steel and AISI 304 stainless steel is shown in Fig. 19. The cracks are shown to be wider in the case of the stainless steel than of the AISI 4340. The smallest width was in the case of the carbon steel AISI 1020. Examination of the room temperatures thermal properties of these alloys shows that AISI 1020 has the highest thermal conductivity, whereas AISI 304 has the lowest thermal conductivity. Thus crack dimensions are seen to be inversely dependent upon the thermal conductivity of the steel. This again points to the

effect of surface temperature on crack formation because the lower the thermal conductivity of a material the higher its surface temperature assuming the same environmental conditions.

All indications thus far are that the mechanism of crack formation is thermal in nature and that cracks are probably formed due to strains produced by volume changes resulting from the rapid heating and cooling processes that are relieved by surface cracking. However there is a possible alternative mechanism of crack formation which is known to be pressure-dependent namely hydrogen embrittlement.[20,21] Hydrogen embrittlement is a general term used to describe a variety of phenomena in which the shear or tensile strength of hard metals has been reduced due to the presence of hydrogen in its environment or composition. Hydrogen embrittlement can cause microscopic surface and internal cracking following the absorption of a very small average concentration of hydrogen. This is because the hydrogen tends to concentrate at grain boundaries and to interfere with intergranular attractive forces. Accordingly, hydrogen embrittlement is most apparent in materials under stress. The usual tests for embrittlement involve measuring the failure limit of a stressed specimen as a function of parameters such as external hydrogen pressure or temperature of the strain rate. Experiments indicate that up to pressures of about 70 MN/m^2 (Ref. 20, p. 139, 171) the yield strength decreases roughly as the square root of hydrogen pressure and that the temperature dependence of hydrogen embrittlement peaks at about room temperature (Ref. 20, p. 146, 172; Ref. 21, p. 256).

Notch tests carried out on nickel at room temperature and a hydrogen pressure of 70 MN/m^2 show a reduction of notch strength from a nominal value of 900 MN/m^2 to about 200 MN/m^2, or a reduction of about 80%. The way in which such mechanical properties as loss of ductility relate to metal erosion in general, and to crack formation in particular, is not obvious.

To attempt to identify the mechanism of crack formations,

whether thermal or chemical, a series of tests were performed using the Princeton University ballistic compressor.[1] A detailed description of this apparatus is given in a subsequent section of this report.

4. Studies of the Mechanism of Crack Formation Utilizing the Ballistic Compressor

The objective of the tests performed utilizing the ballistic compressor was to compare the surface characteristics of eroded specimens resulting from the action of hydrogen versus that of an inert gas such as argon.

Table 6 shows a summary of the test conditions and test specimen mass losses achieved in these tests.

Figures 20 and 21 show a comparison of SEM photomicrographs of eroded surfaces produced by the action of H_2/CO_2 and A. Neither the tests performed with H_2 nor with A produced surface cracks. However in the argon tests and in high pressure H_2 tests (620 MN/m^2) there is evidence that melting of the surface during the test occurred.

The Role of Cracks on the Erosion Mechanisms of Steel Alloys

A general observation of the SEM photomicrographs of eroded surfaces is that the cracks follow grain boundaries. The removal of such loosened grains by the subsequent firings might be an important process on the overall erosion of steel alloys subjected to repeated exposures of hot, high pressure propellant gases. Indeed the surface regression of the metal surface per firing ($\sim$ 20μm) allows the possibility that whole grains (which appear to be of the order of 5μm in diameter) might be removed in their entirety during a single firing.

Figure 22 shows the surface of a sample exposed five times to IMR-4198 propellant gas at a chamber pressure of 290 MN/m^2. The nature, abundance, and dimensions of the cracks fit the trends established above for single firings so well that it can be concluded that with regard to crack formation, each firing acts independently. This is in agreement with results presented in Ref. 1 that show that mass erosion rate

of steel specimens is independent of the number of firings.

The results presented on the examination of an eroded surface suggest that while crack formation growth can be correlated with the mass loss of the specimen, the relationship is more coincidental than causal and that crack formation is not a major factor in the erosion of steel alloys exposed to the environmental conditions achieved in the present study.

SEM Investigation of Collected Residues of Erosion

SEM examination of the solid erosion products removed from the test surface by the flowing hot gases were made by allowing the test gas exiting from the test orifice to impinge on a cool (room temperature) surface located 6 - 10 cm downstream from the test orifice. A small quantity of the erosion products along with some propellant products accumulate on the cool surface which is then subjected to microscopic examination. The collector surface was either made of copper or steel and was in the form of a disk with its surface perpendicular to the direction of the flow. In addition to this type of stationary collector, a rotating collector was employed that provides for a movement of the substrate (surface of the collector) at right angles to the flow. The flow was collimated by a masking slit as shown in Fig. 23. This collector provides time-resolved samples of the deposited erosion products. Fig. 24 shows depositions on stationary copper substrates resulting from the exposure to IMR-4198 propellant gases of AISI 1020, 304 and 4340 steels respectively. These deposits were a flat black color when observed optically and electron microprobe analysis indicated the presence of relatively large amounts of lead and potassium although minor quantities of iron were detected.

Accordingly, one is lead to the conclusion that the bulk of the materials deposited were propellant products, as might be expected. A fine crystalline after-growth, discernable at higher magnification, of the deposits associated with the latter two steels (Fig. 25) has not yet been identified. The flowery

crystallites of Fig. 25b, however, have the same general appearance as larger crystals which were observed a few days later on the same sample. These larger crystal colonies appeared light blue and translucent under an optical microscope and are assumed to be due to hydration of copper salts formed at the time of the exposure.

Figure 25c shows a somewhat different crystal growth pattern when IMR-4198 propellant gases following erosion of AISI 4340 steel were allowed to pass over a stationary steel substrate.

The results of deposition into the moving bands of iron and copper are ambiguous in that although the amount of deposited material (as well as the abundance of impact craters) was resolved as a function of time, no qualitative differences could be observed throughout the deposition period. Moreover, no distinction between deposits on the copper band versus the steel band could be made, and no occurrence of the fine crystalline structures discussed above were noted anywhere.

Spectral Investigation of Exhaust Plume

A search for spectral evidence of gaseous iron compounds was carried out using a Spex "Mini-mate" spectrometer, modified[22] to accept a Polaroid camera. Polaroid Type 57 film was used which has an ASA speed of 3000. Taking into account the film speed, geometric limitations and average mass-loss per firing, the apparatus should have been sensitive to spectral emission from trace amounts (e.g., one molecule in 10^8) of Fe atoms or Fe compound molecules. No emission spectra were obtained when the plume was observed at 90° to its axis. A panoramic still photograph of the experiment revealed very weak and diffuse illumination in the plume which could have arisen from scattering of the propellant flame light originating inside the combustor.

Since the propellant flame inside the combustor gives rise to intense broad-band spectra in the 600μm region the possibility existed that radiation might be selectively

absorbed by unexcited molecules of reaction products to produce absorption spectra in a "down-the-tube" axial configuration. A series of experiments using stainless steel discs (for maximum erosion) and a variety of pressures failed to produce any identifiable lines.

It is believed either insufficient chemical energy is released in the formation of iron compounds to excite optical transitions or that the iron compounds produced, such as Fe_2O_3, form crystals on the surface which then break up as solid particles and that molecular, uncondensed Fe_2O_3, or other iron complexes, never exist to be spectrally active.

IV. EROSIVE EFFECTS OF STEEL ALLOYS BY PURE GASES

Exposure of steel[1] and aluminum[18,19] alloys to a stream of high pressure and high temperature combustion gases in many cases produce regression rates of the metal surface that are much higher than the rates calculated from the theory of inert ablation (melt-and-wipe-off). The augmentation of the regression rate of these alloys is attributed to the chemical interaction between the metal and the combustion gases. In the case of aluminum alloys, for example, the very high mass loss rates experienced by the test specimen were attributed to the combustion of aluminum vapor in the boundary layer of the flow that results in an increase in the surface heat feedback which in turn increases the rate of mass removal.

The interpretation, however, of the gas-metal interactions in the propellant-gas experiments is always obscured to a large degree by the simultaneous presence of a great number of gaseous species formed by the combustion of the propellant. The problems associated with large numbers of gaseous species (i.e., using combustion gases) were overcome be developing and using a ballistic compressor.[1] The ballistic compressor is a device that generates hot, high pressure pure gas or prescribed gas mixture which can be brought into contact with a metal specimen for the study of the reaction processes.

Part I of this study[1] presented results of the mass loss experienced by three steel alloys (AISI 4340 chromium-molybdenum steel, AISI 1020 carbon steel, and AISI 304 stainless steel) exposed to high pressure and high temperature pure gases.

The purpose of the present investigation was to provide further information on the erosion of steel alloys by pure gases. We have sought to:

a. study the effects of orifice configuration on the erosion of steel alloys by pure gases,
b. characterize the eroded surface resulting from the interaction of each test gas with the steel specimen,

c. identify the products of the test gas/steel interaction on the surface, and

d. study in greater detail the mechanism of erosion of steel alloys by a hydrogen and O_2/N_2 mixture which produces unusually high mass removal rates.

Apparatus and Materials

A detailed description of the ballistic compressor apparatus is given in Ref. 1. In brief, the ballistic compressor apparatus, shown schematically in Fig. 26, utilizes a reservoir of driver gas (e.g., 2.5 MN/m^2, 300 K) to drive a piston to compress adiabatically the desired test gas. In this way the apparatus produces a quantity of hot, high pressure gas (e.g., 400 MN/m^2, 3000 K) that flows through the test orifice. The pressure history of the test gas was monitored by a high frequency Kistler 607 piezoelectric pressure transducer. A typical pressure trace is shown in Fig. 27. In comparison with the test time produced by the vented combustor apparatus (1.5 to 4 msec) the ballistic compressor has an effective test time which is less than 1 msec.

As in the case of the vented combustor tests most of the ballistic compressor tests were performed on AISI 4340 chromium-molybdenum steel. Both circular and rectangular orifice geometries were tested. The dimensions of the orifices are shown in Fig. 10. The flat test surfaces, provided by the rectangular configuration orifices were utilized for SEM and microprobe studies. The method of preparation of the test specimen is described on page 13 of this report.

Test gases used in this study to obtain a qualitative and quantitative measure of their erosive effect on steel alloys were: N_2, H_2, CO, CO_2, A and O_2/N_2, $H_2/O_2/N_2$, CO_2/A and H_2/O_2 mixtures.

Metal test specimen mass loss and regression depths (measured by a profilometer) are the primary quantitative data used to indicate the severity of the gas-metal interaction

during test exposure.

Performance of the Ballistic Compressor

The versatility and wide range of the ballistic compressor as a generator of high pressure and high temperature gases is depicted in Fig. 28. This shows a comparison of the ranges of temperature and density that can be produced by three techniques, namely, shock tube, static compression, and ballistic compressor.

A comparison between the actual pressure attained by the ballistic compressor and theoretical performance predicted by (a) assuming isentropic compression and (b) taking into account valve losses and blow-by is shown in Fig. 29. The isentropic compression assumption overestimates the generated pressure by as much as 30%.

At test gas pressure levels up to 140 MN/m^2 the predictions made by the nonideal theory agree with the experimental results obtained using pistons without o-rings (negligible friction). Above this pressure level ($\sim$ 140 MN/m^2) leakage begins to reduce the performance of the ballistic compressor.

Results and Discussion

1. Mass Removal

Table 7 shows the erosion results of both circular and rectangular steel AISI 4340 orifices. For comparative purposes, both the total mass erosion and the mass erosion per unit surface area of the test orifice are presented. The results show that the total mass removed from the rectangular orifice is greater than for the circular orifice. However, the erosion per unit surface area is approximately the same as that of the circular orifices. This was not the case for the vented chamber results (propellant gases) reported in Ref. 1. There, the rectangular orifices experienced greater mass removal per unit surface area. The explanation of the vented-combustor results was based on the effect of curvature of the orifice on the heat transfer. The higher the ratio of the thermal-

wave thickness to the radius of curvature the greater the heat dissipated to the interior of the disk and, thus, the lower the surface temperature. However, in the ballistic compressor tests, the test time is very short (compared to the vented chamber) and, thus, the depth of heat penetration is small compared to the radius curvature. Thus, one-dimensional slab heat transfer adequately represents both the circular and rectangular configurations.

Comparing the erosive action of the gases tested, it is evident that the gas mixtures containing molecular O_2 and molecular H_2 produce high mass removal rates. CO_2, CO, and N_2 produce relatively small effects. Based on SEM studies discussed later in this report, the molecular oxygen-containing gases produce erosion of steel by formation of low shear strength oxide scale that is swept away by the flowing gases. On the other hand the augmented erosive action of H_2 in comparison to N_2 is not clear. A possible explanation is that due to the higher thermal diffusivity of hydrogen, the surface heat transfer is increased which results in greater erosion. At room temperature, for example, the thermal conductivity of H_2 is 4.02×10^{-4} cal/cm-sec-K, whereas the thermal conductivity of N_2 is 5.77×10^{-5} cal/cm-sec-K. The possibility that the mechanism of erosion of steel alloys by hydrogen may be other than thermal cannot be ignored and therefore a series of tests have been performed to investigate this. These tests will be discussed later in this section.

2. Geometric Effects

Topographs of one symmetric half of an eroded planar surface of AISI 4340 steel subjected to the erosive action of high pressure and high temperature air and hydrogen are shown in Figs. 30 and 31.

As shown in Fig. 30 the surface of the specimen, tested in air is irregular (wavy in the direction perpendicular to the flow). Highest mass removal occurred at the upstream edge as expected. The surface regression at this section

is of the order of 60μ. On the other hand, in some areas of the downstream section, the surface is above the original level indicating possible mass deposition or more likely (see SEM results) oxide formation that was not removed by the flow.

The topograph of the steel surface tested in H_2 is highly irregular (see Fig. 31). The highest surface regression is at the upstream edge. Proceeding downstream, the regression decreases up to 400μm from the upstream edge where it begins to increase until 750μm from the upstream edge where it begins to decrease to a minimum at the downstream edge. The observed hill on the surface at 400μm from the upstream edge resulted from metal removed at the upstream edge, transported and deposited downstream. The process of deposition is also evident at the side edges of the eroded surface.

3. Characterization of the Eroded Surfaces by Means of SEM

To facilitate the study of the erosive action of the above gases on steel surface, SEM and microprobe examinations of the eroded surface have been performed. The surface modifications of the test specimens for each gas tested were as follows:

Nitrogen Gas

Nitrogen produces little effect on the surface of the test specimen. Fig. 32 is an SEM photomicrograph of the surface of AISI 4340 subjected to the erosive action of high pressure and high temperature (359 MN/m^2) N_2 gas. A comparison of Fig. 32 with that of an untested specimen (Fig. 15) shows that minor modifications of the surface occurred. The grinding tool marks observed in Fig. 15 are shown in Fig. 32 to be distinct and largely unaffected. The amount of metal removed in the N_2 test was below our threshold of detectability (< 0.1 mg).

Carbon Monoxide

Examination of the test surface under the erosive action of CO shows the formation of a thin scale that seems to originate at the original machining marks of the surface.

A closer look at the scale (Fig. 33) shows the formation of cracks which may cause the flaking-away of the scale leaving the substrate metal unchanged. In this particular test, no mass loss could be detected.

Carbon Dioxide

As shown in Fig. 34 with the exception of the presence of granular residue on the test surface, the surface is largely unaffected by CO_2. The origin of these residues is not clear.

Hydrogen

The surface modifications occurring due to the hydrogen/steel interaction is shown in Fig. 35. The SEM photomicrograph was taken on the edge of the rectangular test channel. The right side of the photograph represents the untested surface, the left side is the eroded surface. The scale formed in the channel is shown to be very porous. Optically, however, the test surface appears smooth and polished.

The mass removal of the test specimen in the above H_2 test was 0.64 mg. At higher mass removal (3.14 mg in five consecutive tests) the surface appeared to be markedly smoother.

Air

Fig. 36 shows the surface appearance of a test specimen subjected to a pulse of high pressure and high temperature air. Microprobe analysis of the porous scale reveals large concentrations of oxygen that indicate that it is presumably an iron-oxide scale. The mass removal can be attributed to the partial removal of the low shear strength oxide scale by the aerodynamic forces of the flow.

Mechanism of Erosion of CO_2, CO, H_2 and O_2 on Steel Alloys

Carbon Dioxide

The most comprehensive study of the chemical erosion of steel was made during WW II by Evans and co-workers[16,17] who studied the erosive effects of high pressure and high

temperature gases produced by the combustion of O_2 with excess amounts of CO. They found that, in general, erosion increases as the CO_2 concentration in the combustion increases. This result does not agree with our finding that CO_2 produces erosion of the same magnitude as that of an inert gas (N_2). It should be kept in mind, however, that the results reported in Ref. 19 were obtained using the combustion products produced by burning O_2/CO mixtures. Accordingly an appreciable amount of free O_2 is present in the test gas mixture which may have produced the erosion attributed to CO_2. This hypothesis is in agreement with their result that erosion increases with CO_2 concentration because it implies a corresponding increase in O_2 concentration in the reactive mixture.

Carbon Monoxide

The inability of CO to produce erosion of the steel alloys above the inert background erosion (N_2), coupled with the scale formation observed in our experiments are in strong contradiction to the carbonyl mechanism of steel erosion.

The carbonyl mechanism proposed by Evans and co-workers[16,17] states that erosion of steel in the chemical region is due to the formation of volatile iron carbonyl by the reaction of CO with Fe

$$Fe + 5CO \rightarrow Fe(CO)_5$$

Their efforts[14] however to isolate and identify iron carbonyl as the erosion product of the action of CO/CO_2 mixtures on steel vents were not conclusive.

Oxygen

The augmentation of mass removal of steel alloys due to surface chemical attack by oxygen is demonstrated in Fig. 37. This is a plot of mass removal versus mole fraction of O_2 in O_2/N_2 mixture. This relation is linear indicating that the overall chemical reaction between O_2 and iron is a first order reaction. This linear relation, however, is correct when the mole fraction of O_2 is greater than 0.15. When the mole fraction is less than 0.15, mass removal is negligible.

Based on the SEM studies presented earlier and the above results, we postulate the following mechanism of erosion of steel alloys by oxygen: oxygen produces mass removal by formation of low shearing-strength oxide scale(s) that is partly or wholly swept away by the flowing gases.

To test this hypothesis a series of 5 consecutive erosion tests were performed on the three test alloys. In each test the mass loss experienced by the specimen was recorded. Figs. 38 and 39 show the results. Fig. 38 is a plot of mass erosion versus number of firings whereas Fig. 39 is a plot of mass eroded per firing versus number of firings. These results show that:

a. mass erosion decreases with increase in the number of firings, and
b. the erosion experienced by the stainless steel, AISI 304, is greater than the erosion of the other steels. The chromium-molybdenum steel, AISI 4340, exhibits the best erosion characteristics of the three test steels.

The decrease of erosion experienced by the steel alloys with repetitive testing indicates that the oxide scale formed by the reaction of Fe with O_2 is not completely removed by the flowing gases, and that as the number of firings increase an accumulation of oxide scale occurs which provides successively better thermal and oxidative protection.*

The order of erodibility of the steel alloys obtained using the ballistic compressor is not the same as obtained using the vented-combustor apparatus. In the latter apparatus, the carbon steel, AISI 1020 show the best erosion resistance, with AISI 4340 and AISI 304 following. The stainless steel, AISI 304 showed considerably greater mass losses than the other two. In the combustor, AISI 1020 and AISI 4340 experience similar mass losses, although AISI 304 experiences the greatest mass loss.

The removal of oxide scale by the flowing gases has been verified by collecting erosion residue inside a quartz tube which was then inserted in an electron paramagnetic resonance

*It should be noted that whether the oxide scale accumulates is very dependent on the exposure conditions.

(EPR) chamber. The signal from the chamber was positively identified as Fe^{3+} ion in axial symmetry.* Fe_2O_3 which has a hexagonal structure, satisfies this requirement and is a highly probable product in the erosion of steel by high pressure and high temperature oxygen. The presence of Fe^{2+} cannot be identified by EPR at temperatures much higher than 4 K and since liquid helium apparatus was not available, the possibility of FeO in the efflux gases cannot be excluded at this time.

Hydrogen

To identify the mechanism of erosion of steel alloys by high temperature and high pressure hydrogen, a series of tests were made on AISI 1020 carbon steel where the mass loss of the specimen was measured as a function of H_2 concentration in H_2/N_2 mixtures. The results are presented in Fig. 40. They show that erosion is considerable only when the mixture is 100% H_2; at lower values of hydrogen concentration the erosion is similar to the erosion obtained using N_2 and, moreover, is independent of the hydrogen concentration.

The above result contradicts the hypothesis that the large mass removals experienced by the steel alloys due to the erosive action of H_2 in comparison to that of N_2 was due to the high thermal diffusivity of H_2 that increases the surface heat transfer of the specimen, which in turn increases the erosion rate. If the hypothesis was true then the erosion should have been proportional to the hydrogen concentration.

---

*A resonance was obtained in which the g-value attained a value of about 6 (free electrons have a g-value of 2) in the formula

$$\text{Energy} = g\beta H$$

where β = electron charge, H = magnetic field.

V. EROSION OF PURE METALS BY HIGH PRESSURE AND HIGH TEMPERATURE GASES

As stated in Section II, the mechanism of erosion of steel alloys by reactive gases may be strongly influenced by the alloying metals present in steel. Typical alterations in the chemical interaction between an alloy and a reactive gas in comparison to the pure metal-gas interaction are:

a. the occurrence of selective chemical attack oxidation that results when the gas has greater chemical affinity for one or more components of the alloy than the remainder of the components. This selective chemical attack by the reactive gas may result in erosion by weakening the structural strength of the alloy surface.

b. The formation of low melting oxide by one of the components of the alloy that may lead to excessively fast oxidation of the alloy. The detailed mechanism of the catastrophic effect of the presence of liquid oxides on the reaction (oxidation) of alloys with gases has not been fully understood.[2] It has been hypothesized that liquid phases penetrate the scale along grain boundaries to the alloy surface thus providing a path for the rapid diffusion of reactive gas molecules or ions to the metal surface.

Our objective was to initiate a study on the erosion of pure metals that constitute the alloying elements of steel by propellant gases and pure gases and to compare the erosion characteristics of these metals to the erosion characteristics of steel.

Presently we have examined the mass removal experienced by Fe, Ni and Mo under the erosive action of high pressure and high temperature propellant gas and air. These erosion results have been compared to the corresponding results of the three test alloys considered in this investigation (i.e., AISI 1020 carbon steel, AISI 4340 chrome-moly steel and AISI 304 stainless steel).

Apparatus

The erosion of the pure metals by propellant gases was studied in the vented-combustor apparatus described in Section III of this report. The propellant used was IMR-4198 single-base propellant.

The erosive action of high pressure and high temperature air on Fe, Ni and Mo was investigated utilizing the ballistic compressor apparatus described elsewhere in the report (Section IV).

The geometry of the test orifices was cylindrical. No tests were performed on rectangular orifices, although future plans exist to utilize the erosion of rectangular orifices in conjunction with SEM studies of the surface modifications of eroded pure metal specimens.

The room temperature thermal properties of iron, nickel, molybdenum and the three steel alloys tested are shown in Table 4.

Results

A comparison of the erosive action of propellant gases on iron, nickel, molybdenum and the three steel alloys considered in this investigation is shown in Table 8. Tests were performed at two pressure levels 230 and 360 MN/m^2. This Table includes also the average enlargement of the diameter of the test orifice computed from the mass loss experienced by the test specimen. At the high pressure level, molybdenum shows the least amount of erosion, with iron next, then the two steel alloys AISI 4340 and 1020, then nickel and last the stainless steel AISI 304. At the low pressure level, the order of the nickel is the same as that of iron (second) whereas the chrome-moly steel AISI 4340 eroded more than twice as much as the carbon steel AISI 1020.

In general, the order of erodibility of the above materials can be predicted by examining their thermal properties. For example, molybdenum has the highest melting or solidus temperature and also the highest thermal conductivity. On the other hand, AISI 304 stainless steel has the lowest solidus

temperature and the lowest thermal conductivity. Comparison of the thermal properties of iron and nickel shows that although nickel has a lower melting temperature than iron, it has a larger thermal conductivity than iron.

The erosion results of the three pure metals are also in agreement with the chemical affinity of the reactive components of the propellant gas for these metals. Molybdenum has the least chemical affinity for the reactive gases followed by nickel and then iron.

The erosion of the above test specimens by high pressure and high temperature air is shown in Table 9. These ballistic compressor tests provide better information on the chemical interaction between metals and gases, because due to the much shorter effective test time (0.2 msec in comparison to 2 msec for the vented-combustor) the chemical effects are better isolated from the thermal effects.

Comparison of the erosion results of Table 9 shows that molybdenum erodes the least followed by nickel and then iron in agreement with the chemical affinity calculations of these elements with oxygen. The most important result, however, is that iron and the three test steels experience the mass removal rates which are higher than either Ni or Mo which indicates, admittedly not conclusively, that the alloying elements of steel are not preferentially attacked.

VI. A STUDY OF THE EROSION REDUCING ACTION OF ADDITIVES

In recent years efforts to reduce the erosion of gun barrels have been centered on the use of wear reducing additives because this technique is simple and relatively inexpensive and has shown very promising results. The most effective additives are: polyurethane foam, TiO_2/wax (Swedish additive) and Talc/wax. Attempts, however, by various investigators to examine the relative effectiveness of the above three additives as erosion reducing agents were not conclusive.[23] Tests[24] on a 105 mm tank cannon showed that the Swedish additive is superior to polyurethane foam. However, recent laboratory tests[25] with a 37 mm gun indicated that the superiority of the Swedish additive vs. the polyurethane foam may be attributed to improper experimental comparison. When the Swedish additive (TiO_2/wax) was tested, flaps that cover the base of the projectile were incorporated whereas in the case of polyurethane foam no flaps were used. Laboratory tests performed by Picard and co-workers[26,27] showed that erosion reduction obtained by the talc/wax additive is significantly greater than that of the Swedish additive. This result was also verified in tests performed on a 105 mm tank cannon. On the other hand, recently Schroeder et al,[28] using a 37 mm caliber gun, found that polyurethane foam was superior to both TiO_2/wax and talc/wax additives as long as the additives were tested in the same configuration. Their study, however, was performed at lower combustor pressures in comparison to the pressures commonly encountered in interior ballistics.

The apparent discrepancies in the results of the various investigations on the relative effectiveness of the wear-reducing additives stems mainly from the non-uniform experimental conditions used to compare the additives. The effectiveness of the additives as erosion reducers strongly depends on their positioning in the propelling charge. Furthermore the relative effectiveness varies with the mass fraction of the additive present in the propelling charge and

on particle size, although experimental confirmation of the latter has yet to be achieved. A deeper root of the inconsistency of the results is that the development of these additives has been mainly empirical; little effort has been applied to study the mechanisms of the erosion-reducing action of these additives.

The present investigation is an experimental study of the reducing action of several known additives on the erosion of AISI 4340 chrome-moly steel and AISI 304 stainless steel by propellant gases. Recognizing that in gun systems the critical parameter is the available volume, comparison of the additives has been performed by keeping the positioning and the volume of these additives with respect to the test specimen the same in all tests.

Several test specimen surfaces have been subjected to SEM examination to obtain the effect of the additives on the surface modifications of the test specimen.

Apparatus

The tests were performed in the vented-combustor apparatus described in Section III of this report. The test specimen configuration and the positioning of the additive relative to the test specimen is shown schematically in Fig. 41. The additive was placed immediately upstream of the test specimen; the orifice of the additive is smaller than the test orifice in order that the protruding mass of the additive be easily transported by the flow of the combustion gases to the metal surface.

The additives under investigation were:

a. polyurethane foam,
b. TiO_2/wax (46/54% by mass),
c. talc/wax (40/60% by mass),
d. paraffin wax, and
e. silicone lubricant (vacuum grease).

The combustion gases were generated by burning IMR-4198 single base propellant. The combustor pressure in all tests was kept approximately constant at 290-324 MN/m^2.

Results and Discussion

A summary of the results for both types of steel tested are given in Table 10. The most effective erosion reducer is shown to be talc/wax additive; second is the paraffin wax. The surprising result is that the polyurethane foam, which has been shown to be in many investigations very effective as an erosion reducer, produced minor changes in the mass removals experienced by the test specimen under the erosive action of high pressure and high temperature propellant gases. It must be emphasized, however, that this comparison is based on constant volume of the additive. A comparison by mass of additive present may produce different results. As shown in Table 9 the mass of the talc/wax additive is 3 times greater than the mass of the polyurethane foam. However, as stated earlier, the comparison of the performance of the additives should be made based on the volume of the additives because the volume is a critical parameter in the design of guns.

Another noteworthy point of these results is that the percentage reduction of erosion obtained by using a particular additive is similar in both types of steel tested.

An indication of the mechanisms of the erosion reducing action of the additives is provided by SEM photomicrographs of the eroded surface. Fig. 42 shows an eroded surface without the use of additives. The cracks present on the eroded surface have been shown to result from thermal stresses; the contribution of the crack formation to the overall mass removal process is believed to be minor. Surface modifications resulting from the use of additives are shown in Figs. 43 and 44. In Fig. 43, polyurethane foam was used as the additive; Fig. 44 shows the effect of the Swedish additive. It is apparent from a comparison of Figs. 42, 43 and 44 that in the case of polyurethane foam, the eroded surface remains unchanged whereas in the case of the Swedish additive a thick deposit of the additive exists on the metal surface which may probably provide a protection for further erosion.

The coating action of the additives to provide thermal and chemical insulation of the test surface from the erosive

attack of propellant gases has been suggested in earlier studies. Analysis[23] of the bore coating material of the Swedish additive shows that about 77% by mass is TiO_2.

VII. CONCLUSIONS

Reactions of Propellant Gases with Steel Alloys

Thermodynamic calculations of the reactions of the individual gaseous components of propellant gases with the alloying elements of steel show that:

1. The order of likelihood for the products to be formed is: 1) oxides 2) nitrides 3) carbides and 4) carbonyls.
2. Oxygen has the greatest affinity to combine with a metal to produce an oxide, followed by CO_2 and H_2O.
3. Chromium and manganese produce more stable oxides than iron, whereas the oxides of nickel are less stable than the iron-oxides.
4. The Gibbs free energy of most of the reactions considered increases with temperature, indicating that these reactions are less favorable at higher temperatures.
5. Equilibrium calculations of the iron-oxygen, iron-CO_2-CO and iron-H_2O-H systems indicate that, for typical propellant gas compositions, the scale formed by the chemical interaction of propellant gases with steel will consist largely of wustite (FeO). This finding is in agreement with experimental identification of the products of erosion of gun barrel steel.

Erosion of Steel Alloys by Propellant Gases

Scanning Electron Microscope studies of steel surfaces subjected to the erosive action of propellant gases, using the vented-combustor apparatus, provided the following conclusions:

1. The eroded surfaces of steel alloys were covered largely by a scale which is presumably formed by the chemical interaction between propellant gases and steel alloy. Electron Microprobe Analysis indicated the presence of appreciably more carbon in comparison with an unexposed specimen.
2. The relative decrease of area occupied by the scale at higher pressures suggested that the cohesive forces between

the scale and the underlying test metal were not sufficiently strong to resist the high shearing forces of the flow.

3. Crack formations were shown to be present on the underlying metal surface of an eroded test specimen.
4. The width and, probably, the depth of these cracks were found to increase with increasing combustor peak pressure.
5. The width of the cracks were shown to increase using a higher isochoric flame temperature propellant.
6. A comparison of the crack formations of the eroded surface of the three test alloys, namely, AISI 1020 carbon steel, AISI 4340 chromium-molybdenum steel, and AISI 304 stainless steel showed that the cracks were wider in the case of AISI 304 steel than of the AISI 4340 steel. The smallest width of cracks was in the case of carbon steel AISI 1020. These results indicate that crack dimensions were inversely independent upon the thermal conductivity of the steel.
7. Repetitive tests showed that crack formation did not increase appreciably with the number of firings.
8. Tests performed using the ballistic compressor to investigate hydrogen embrittlement as the mechanism of crack formations were not conclusive.
9. The tests performed thus far indicate that the mechanism of crack formation is thermal; cracks were probably formed to relieve strains produced by volume changes resulting from the rapid heating and cooling processes.
10. No evidence was found to relate crack formations to the erosion of steel alloys exposed to the environmental conditions used in the present study.

Erosion of Steel Alloys by Pure Gases

The erosion of steel alloys under the action of high temperature and high pressure pure gases or gas mixtures was studied utilizing the ballistic compressor. The test gases used were N_2, A, CO, H_2 and CO_2/A, N_2/O_2, $N_2/H_2/O_2$ mixtures.

Comparison of the mass erosion experienced by circular

orifices versus rectangular orifices shows that the total mass removed from the rectangular orifices was greater than for the circular orifices. However, the erosion per unit surface area was approximately the same for both of the flow configurations tested. This was attributed to the fact that the depth of heat penetration in the ballistic compressor tests was small compared to the radius of curvature of the circular orifices. Thus these orifices behave as if they were one-dimensional slabs.

In accordance with the results reported in Part I of this study,[1] hydrogen and molecular oxygen-containing gases (Air, O_2/N_2 and $H_2/O_2/N_2$ mixtures) provided considerably more erosion of the AISI 4340 steel than the inert gases, N_2, A, and CO and CO_2/A gas mixtures.

Based on SEM studies, the following characterization of the eroded surfaces resulting from the high pressure and high temperature action of various gases were observed:

1. Nitrogen produced little effect on the surface of a steel specimen.
2. Carbon monoxide produced a scale that partly covers the substrate metal. Examination of the scale showed the formation of cracks that may have caused the flaking-away of the scale.
3. Hydrogen produced considerable modifications of the eroded surface. The scale formed on the metal surface was shown to be very porous. Evidence of melting was observed also.
4. Air and O_2/N_2 mixtures produced a relatively thick scale on the eroded surface. Microprobe analysis of this scale revealed large concentrations of oxygen which indicates that it is an iron-oxide scale.

The mechanism of the erosive action of H_2 on steel alloys was investigated by varying the molar concentration of H_2 in N_2/H_2 mixtures. These results show that appreciable erosion was obtained only with 100% H_2. At concentrations of 95% H_2 and lower, the mass erosion experienced by the steel specimen was independent of the mole fraction of H_2 in N_2/H_2 mixtures.

A profilometric study of a surface eroded by high pressure and high temperature H_2 indicated that mass removal upstream may be transported and deposited elsewhere downstream.

The role of H_2 on the erosion of steels was not elucidated; further investigation is required.

The erosion of AISI 4340 steel was shown to be linearly proportional to the mole fraction of O_2 in O_2/N_2 mixtures. Under some conditions, repetitive tests indicated that mass erosion decreases with increasing number of firings. This suggested that the oxide scale formed by the reaction of Fe and O_2 was not completely removed by the flowing gases and as the number of firings increased, an accumulation of oxide occurred which provided successively better thermal and oxidative protection.

Comparison of the mass erosion experienced by the three steel alloys under the action of high pressure and high temperature air showed that AISI 304 experienced the greatest mass loss; AISI 1020 and 4340 experienced similar mass losses.

Erosion of Pure Metals by High Pressure and High Temperature Gases

To study the influence of the alloying metals of steel on the overall erosion of steel alloys, the mass removal experienced by Fe, Ni and Mo under the erosive action of high pressure and high temperature propellant gases and air was examined and compared to the corresponding results of the three test alloys.

In both the vented-combustor and ballistic compressor tests, molybdenum exhibited the best erosion characteristics. However, it was observed that molybdenum is structurally weak; under the extreme conditions of pressures produced in our apparatus, molybdenum disks showed large cracks.

In the vented-combustor apparatus at a high pressure level, iron was shown to have the next best erosion characteristics followed by the two steel alloys AISI 4340 and AISI 1020, then nickel and, last, the stainless steel AISI 304. The

mass erosion experienced by these test specimens can be grossly correlated with their thermal conductivities. The higher the thermal conductivity of a material the smaller the mass removal, assuming the solidus or melting temperature is sufficiently high.

The chemical interactions of the above test specimens with oxygen were observed utilizing the ballistic compressor.

Molybdenum, in these tests, eroded the least, followed by nickel and then iron, in agreement with the calculated affinity of these elements for oxygen.

Iron was shown to experience the same mass removal as the three test steel alloys. This indicates that the alloying elements of steel do not alter the chemical interaction between oxygen and iron.

The Erosion Reducing Action of Additives

An experimental study of the erosion-reducing action of known additives (polyurethane foam, TiO_2/wax, talc/wax, paraffin wax and silicone lubricant) on the erosion of AISI 4340 chrome-moly steel and AISI 304 stainless steel by propellant gases was performed. The positioning and the volume of these additives with respect to the test specimen was kept the same throughout the experimental comparison.

At the high pressures utilized in these tests (p_{MAX} = 290 MN/m^2) the most effective erosion reducer was shown to be the talc/wax additive; second, was the paraffin wax. Polyurethane foam, known to be very effective in the reduction of gun barrel erosion, showed little promise. SEM investigation of the eroded surfaces indicated that, unlike the TiO_2/wax additive, the polyurethane foam did not leave a deposit on the eroded surface. The coating action of the additives is hypothesized to contribute greatly to their role as erosion reducers.

The reduction percentage of erosion achieved by using a particular additive was similar in both steels, AISI 4340 and AISI 304.

VIII. OVERALL CONCLUSIONS AND RECOMMENDATIONS OF THIS STUDY

Based on both the vented-combustor tests and the ballistic compressor tests of this study, we have come to the preliminary conclusion that the erosion of steel alloys (under normal gun firing conditions*) by high pressure and high temperature gases is due to the chemical interaction between the reactive gases and the steel surface that results in the formation of a scale; the adhesive forces between the product scale and the metal surface are not sufficiently high to overcome the frictional forces induced by the flow. Thus, the scale partly or wholly is removed by the flow.

To investigate further the mechanism of erosion of steel alloys by propellant gases and to isolate the reactive gases present in propellant gases that are responsible for the chemical attack on the steel surface, future research should be directed toward:

a) The precise identification of the molecular species present as reaction products on the eroded surfaces.
b) The prediction of the surface temperature attained by the steel specimens both in the vented-combustor apparatus and the ballistic compressor apparatus.
c) Further investigations of the mechanisms of the erosive action of H_2 and H_2O on steel alloys.
d) The use of the ballistic compressor to study the erosion of steel by gas mixtures such as CO/CO_2 and H_2/H_2O. These gases are the major components of propellant gases.

*Thus, we considered the situations which avoid the extremes that produce high rates of melting.

REFERENCES

1. Alkidas, A. C., Morris, S. O., and Summerfield, M., "Erosive Effects of Various Pure and Combustion-Generated Gases on Metals, Part I," AMMRC CTR 75-23, Army Materials and Mechanics Research Center, Watertown, Mass., Oct. 1975.

2. Kofstad, P., High-Temperature Oxidation of Metals, Chapter VIII, John Wiley & Sons, Inc., N.Y., 1966, pp. 269-299.

3. Fast, J. D., Interaction of Metals and Gases, Vol. 1, Thermodynamics and Phase Relations, Chapter 5, Academic Press, New York and London, 1965, pp. 74-93.

4. Argent, B. B. and Birks, N., "Rate-Limiting Reactions in High Temperature Oxidation Processes," in High Temperature Materials: The Controlling Physical Processes, Ed. Kennedy, A. J., Oliver & Boyd, Edinburgh and London, 1968, pp. 36-64.

5. Perry, R. H., (Ed.), Chemical Engineer's Handbook, 5th Ed., McGraw Hill, New York, 1973.

6. Glassner, A., "The Thermochemical Properties of the Oxides, Fluorides and Chlorides to 2500 K," ANL 5750,

7. Smithells, C. J., Metals Reference Book, Butterworth & Co., London, 1962.

8. Kubaschewski, O., Thermochemical Data of Alloys, Pergamon Press Ltd., London, 1956.

9. JANNAF Thermochemical Tables, Thermal Research Laboratory, The Dow Chemical Co., Midland, Mich.

10. Chufarov, G. I., et al, "Thermodynamics of the Oxidation of Metals," in Surface Interactions Between Metals and Gases, Arkharov, V. I., and Gorbunova, K. M., (Eds.), Transl. by Consultants Bureau, N.Y., 1966, pp. 5-20.

11. Moore, W. J., Physical Chemistry, 4th Edition, Chapter 8, Prentice Hall, Inc., Englewood Cliffs, N.J., 1972, pp. 279-320.

12. Lay, J. E., Thermodynamics, Chapter 18, C. E. Merrill Books, Inc., Columbus, Ohio, 1963, pp. 500-532.

13. Williams, F. A., Combustion Theory, Appendix A, Addison-Wesley Publishing Co., Inc., Reading, Mass., 1965, pp. 327-356.

14. Frazer, J. C. W., et al, "Vent-Plug Erosion by the Carbon Monoxide-Carbon Dioxide Gas System," NDRC Report No. A310, National Defense Research Committee, Office of Scientific Research & Development, Washington, D.C., Oct. 1944.

15. Taylor, D. J. and Morris, J., "Gun Erosion and Methods of Control," Proceedings of the Interservice Technical Meeting on Gun Tube Erosion and Control, Ahmad, I. and Picard, J. P., eds., Watervliet Arsenal, Watervliet, N.Y., February 1970, p. 1.3.

16. Evans, R.C., et al, "The Chemical Erosion of Steel by Hot Gases under Pressure," J.Phys.Col.Chemistry, Vol. 51, 1947, pp. 1404-1429.

17. Frazer, J. C. W. and Horn, F. H., "Interaction of Carbon Monoxide and Iron," NDRC Report No. A-92, National Defense Research Committee, Office of Scientific Research & Development, Washington, D.C., September, 1942.

18. Summerfield, M., et al, "Erosion of Aluminum by High Pressure Propellant Gases," Tenth JANNAF Combustion Meeting Proceedings, Vol. I, Aug. 1973, pp. 227-276.

19. Plett, E. G., Alkidas, A. C., Shrader, R. E., and Summerfield, M., "Erosion of Metals by High Pressure Combustion Gases: Inert and Reactive Erosion," J.Heat Transfer, Vol. 97, February 1975, pp. 110-115.

20. Hydrogen Embrittlement Testing, ASTM Special Tech. Publ. No. 543, American Society for Testing and Materials, Philadelphia, 1974.

21. Smialowski, M., Hydrogen in Steel, Addison-Wesley Publishing Co., Inc., Reading, Mass., 1962.

22. Plett, E.G., Shrader, R. E. and Summerfield, M., "Erosive Effects of Combustion Gases on Metallic Combustion Chambers," Final Report on Contract DAA-25-71-C0109, Part II, Princeton University, October 1972, p. 21.

23. Alkidas, A. C., Summerfield, M., and Ward, J. R., "A Survey of Wear-Reducing Additives and of the Mechanisms Proposed to Explain their Wear-Reducing Action," BRL Memorandum Report No. 2603, Ballistic Research Laboratories, Aberdeen Proving Ground, Md, March 1976.

24. Hassman, H., "Review and Trend of Wear Reducing Additives in Large Caliber Tank and Artillery Cannon," Proceedings of the Interservice Technical Meeting on Gun Tube Erosion and Control, Ahmad, I., and Picard, J. P., eds., Watervliet Arsenal, Watervliet, N.Y., February 1970, p. 2-1.

25. Brosseau, T. L., and Ward, J. R., "Reduction of Heat Transfer to Gun Barrels by Wear Reducing Additives," BRL Memorandum Report No. 2464, Ballistic Research Laboratories, Aberdeen Proving Ground, Maryland, March 1975.

26. Picard, J. P., and Trask, R. L., "A New Gun Barrel Erosion Reducer," J. Spacecraft and Rockets, Vol. 5, 1968, p. 1487.

27. Picard, J. P. and Trask, R. L., "Talc, A New Additive for Reducing Gun Barrel Erosion," Proceedings of the Interservice Technical Meeting on Gun Tube Erosion and Control, Ahmad, I., and Picard, J. P., eds., Watervliet Arsenal, Watervliet, N.Y., February 1970, p. 2.3.

28. Shroeder, M. A., Inatome, M., and May, I. W., "Use of Polyvinyltetrazoles as Wear-Reducing Additives for Reducing Gun Barrel Erosion," BRL Memorandum Report, Ballistic Research Laboratories, Aberdeen Proving Ground, MD., in press.

Table 1

Identification* of the Relative Concentrations of FeO and Fe_3O_4 on Eroded Surface of Steel Subjected to the Action of CO/CO_2 Gas Mixture. (CO/CO_2 = 0.84)

Adiabatic Flame Temperature K	Mass Percentage of Oxide Present in the Sample	
	FeO	Fe_3O_4
3320	47	--
3170	65	--
2990	53	--
2765	56	--
2495	36	3

*X-ray diffraction analysis

Table 2

Products of Erosion Identified and the Position in Which They Were Found

Alteration Product	Superficial Surface Layer	Surface layers near C. of R.	Entrapped in coppering	In Cracks	Beneath Cartridge Case
Cementite Fe_3C		X	X		
Fe_2C			X		
Austenite		X	X	X	
Magnetite	X		X	X	X
Wastite FeO		X	X		
Iron nitride ε		X	X		
Iron nitride γ		X	X		
Chalcocite Cu_2S			X	X	
Wurtzite ZnS		X	X	X	X
Sphalerite ZnS				X	
Digenite Cu_9S_5				X	
Pyrrhotite FeS_x				X	
Barium carbonate				X	
Barium sulphate				X	
Barium nitrate					X
Chromium carbide		X			
Nickel carbide		X			

Table 3

Nominal Composition of the Steel Alloys
Used in the Erosion Tests

	STEEL ALLOYS, AISI #		
NOMINAL COMPOSITION	304	1020	4340
C	0.08(MAX)	0.18-0.23	0.38-0.43
Mn	2.00(MAX)	0.30-0.60	0.60-0.80
Si	1.00(MAX)	0.10	0.20-0.35
Ni	8-12		1.65-2.00
Cr	18-20		0.70-0.90
Mo			0.20-0.30

Table 4

Thermal Properties of Test Specimens
Used In This Study

METAL OR ALLOY	DENSITY ρ g/cm^3	THERMAL* CONDUCTIVITY k cal/cm-s-K	HEAT* CAPACITY c cal/g-K	SOLIDUS TEMPERATURE T_M K
IRON	7.87	0.192	0.108	1810
NICKEL	8.90	0.215	0.106	1726
MOLYBDENUM	10.22	0.335	0.060	2893
AISI 1020	7.86	0.124	0.107	1789
AISI 304	8.02	0.041	0.12	1700
AISI 4340	7.86	0.090	0.107	1778

*At room temperature.

Table 5

Propellant Compositions and Combustion Gas Properties

PROPELLANT	COMPOSITION	PRODUCT COMPOSITION MOLE FRACTION	PROPERTIES
IMR 4198	90.5 NITROCELLULOSE (13.15% N) 6.0 DINITROTOLUENE 0.7 DIPHENYLAMINE 0.3 GRAPHITE 0.5 POTASSIUM SULPHATE 2.0 MOISTURE	CO = 0.439 CO_2 = 0.104 H_2 = 0.126 H_2O = 0.215 N_2 = 0.111 [a]F.R = 0.005 [b]X_{ox} = 0.319	T_v = 3000.K M = 24.25 F = 344.041 FT-LBF/LBM a = 1122.9 M/S γ = 1.226
M-1	82.75 NITROCELLULOSE (13.15% N) 10.0 DINTROTOLUENE 5.0 DIBUTYLPHALATE 1.0 DIPHENYLAMINE 1.25 MOISTURE	CO = 0.501 CO_2 = 0.056 H_2 = 0.201 H_2O = 0.140 N_2 = 0.099 F.R = 0.003 X_{ox} = 0.319	T_v = 2528.K M = 22.26 F = 315.829 FT-LBF/LBM a = 1087.4 M/S γ = 1.252

[a]F.R = FREE RADICALS

[b]$X_{ox} = \sum(H_2O + CO_2)$ MOLE FRACTION

Table 6

Special Tests Performed to Study the Mechanism of Crack Formation of Steel Alloys Under the Action of High Pressure Propellant Gases.

TEST NO.	TEST GAS (MOLE FRACTION)	PEAK PRESSURE MN/m^2	MASS ERODED mg
10-6	H_2	324.0	0.52
27-6	H_2/CO_2 (20/80)	482.6	0.0
27-1	H_2/CO_2 (20/80)	620.5	0.0
27-3	Ar	78.6	0.0

Table 7 Steel alloy AISI 4340 erosion results obtained using ballistic compressor.

TEST GAS (MOLE FRACTIONS)	PEAK PRESSURE MN/m^2	MASS ERODED* mg		AVERAGE DEPTH ERODED PER TEST* μm	
		CIRCULAR ORIFICE	RECTANGULAR ORIFICE	CIRCULAR ORIFICE	RECTANGULAR ORIFICE
N_2	348 - 401	0.072	0.17	1.7	1.7
CO	300 - 372	0.052	0.13	1.3	1.3
Ar/CO_2 (60/40)	314 - 345	0.072	0.13	1.7	1.3
H_2	276 - 365	0.436	1.39	10.5	13.9
Air	372 - 407	0.518	1.49	12.5	14.9
$N_2/H_2/O_2$ (80/13.3/6.7)	224-275	0.218	0.30	5.3	3.0

*Average erosion in 5 consecutive tests.

Table 8

The Erosive Action of Propellant Gases on Iron, Nickel, Molybdenum and the Three Test Steel Alloys*

TEST MATERIAL	P_{MAX} = 230 MN/m^2		P_{MAX} = 360 MN/m^2	
	MASS ERODED mg	AVERAGE DEPTH ERODED µm	MASS ERODED mg	AVERAGE DEPTH ERODED µm
IRON	0.47	11.3	2.99	72.1
NICKEL	0.49	10.4	4.72	100.7
MOLYBDENUM	0.03	0.5	0.14	2.6
AISI 1020	0.83	20.0	3.56	36.0
AISI 304	3.45	81.6	8.67	205.2
AISI 4340	1.83	44.2	3.28	79.2

*Circular orifices tested with IMR 4198; average of two tests.

Table 9

The Erosive Action of High Pressure and High Temperature Air on Iron, Nickel, Molybdenum and on the Three Test Steel Alloys

TEST MATERIAL	PEAK PRESSURE MN/m^2	MASS ERODED* mg
MOLYBDENUM	370	0.11
NICKEL	376	0.38
IRON	383	1.33
AISI 1020	334	1.23
AISI 4340	341	0.85
AISI 304	334	1.96

*Average of two or more exposures of circular orifices.

Table 10

Erosion Reducing Action of Various Additives on AISI 4340 and 304 Steel Alloys (Vented-Combustor Tests).

		AISI 4340		AISI 304	
ADDITIVE	MASS OF ADDITIVE mg	MASS ERODED[a] mg	% REDUCTION OF EROSION	MASS ERODED[a] mg	% REDUCTION OF EROSION
NONE		6.42	--	16.69	--
POLYURETHANE FOAM	3.32 mg	6.18	3.7	17.13	2.6
TiO_2/WAX (46/54)	9.76	2.98	53.6	8.52	49.0
TALC/WAX (40/60)	10.6	1.44	77.6	4.86	70.9
PARAFFIN WAX	9.85	2.44	62.0	6.64	60.2
SILICONE LUBRICANT (VACUUM GREASE)	16.7	4.73	26.3	11.67	29.1

[a]Mass eroded in 3 consecutive tests

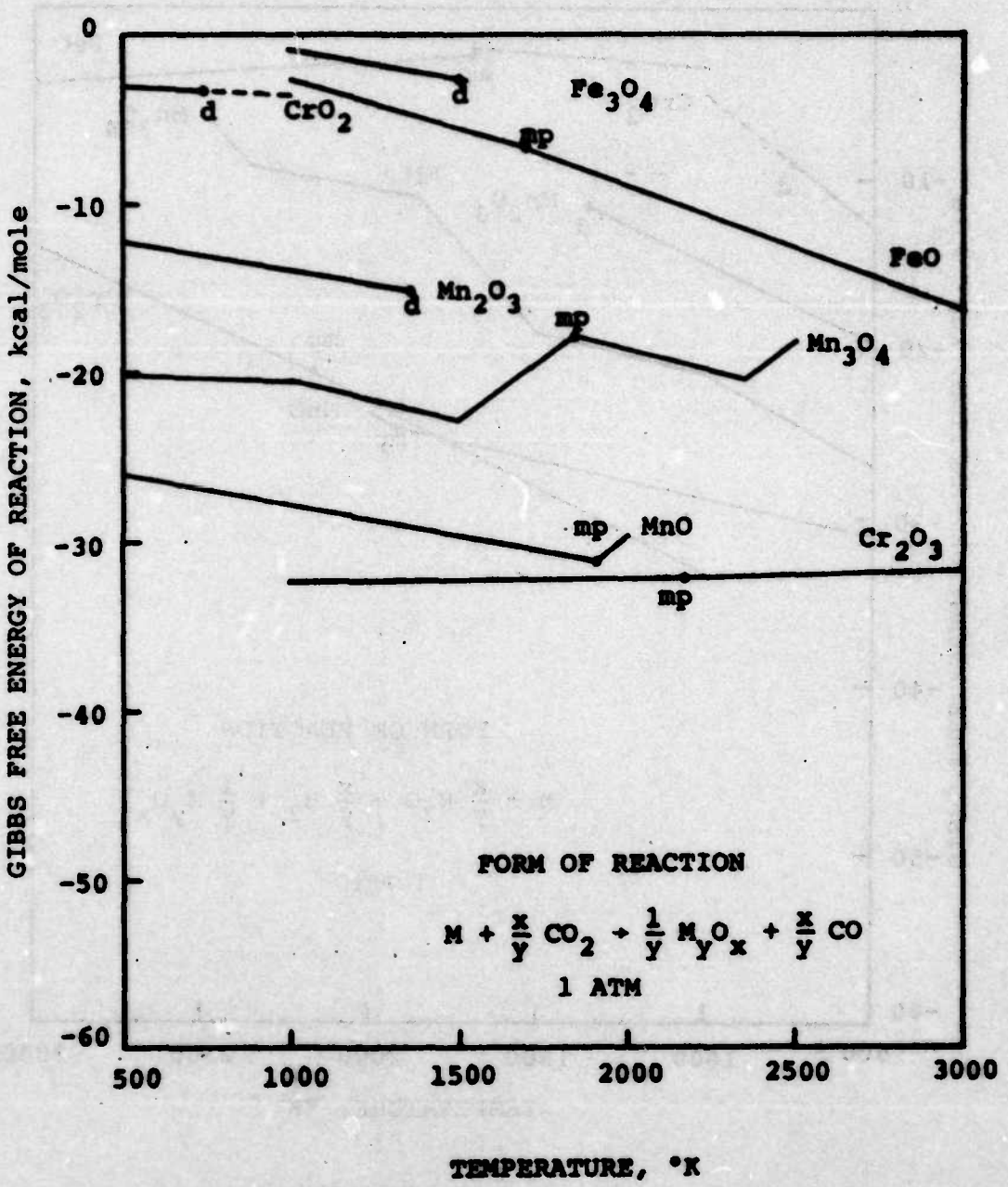

Fig. 1 Free energy of reaction of CO_2 gas, at 1 atmosphere pressure, with major metallic constituents of steel to form metallic oxides.

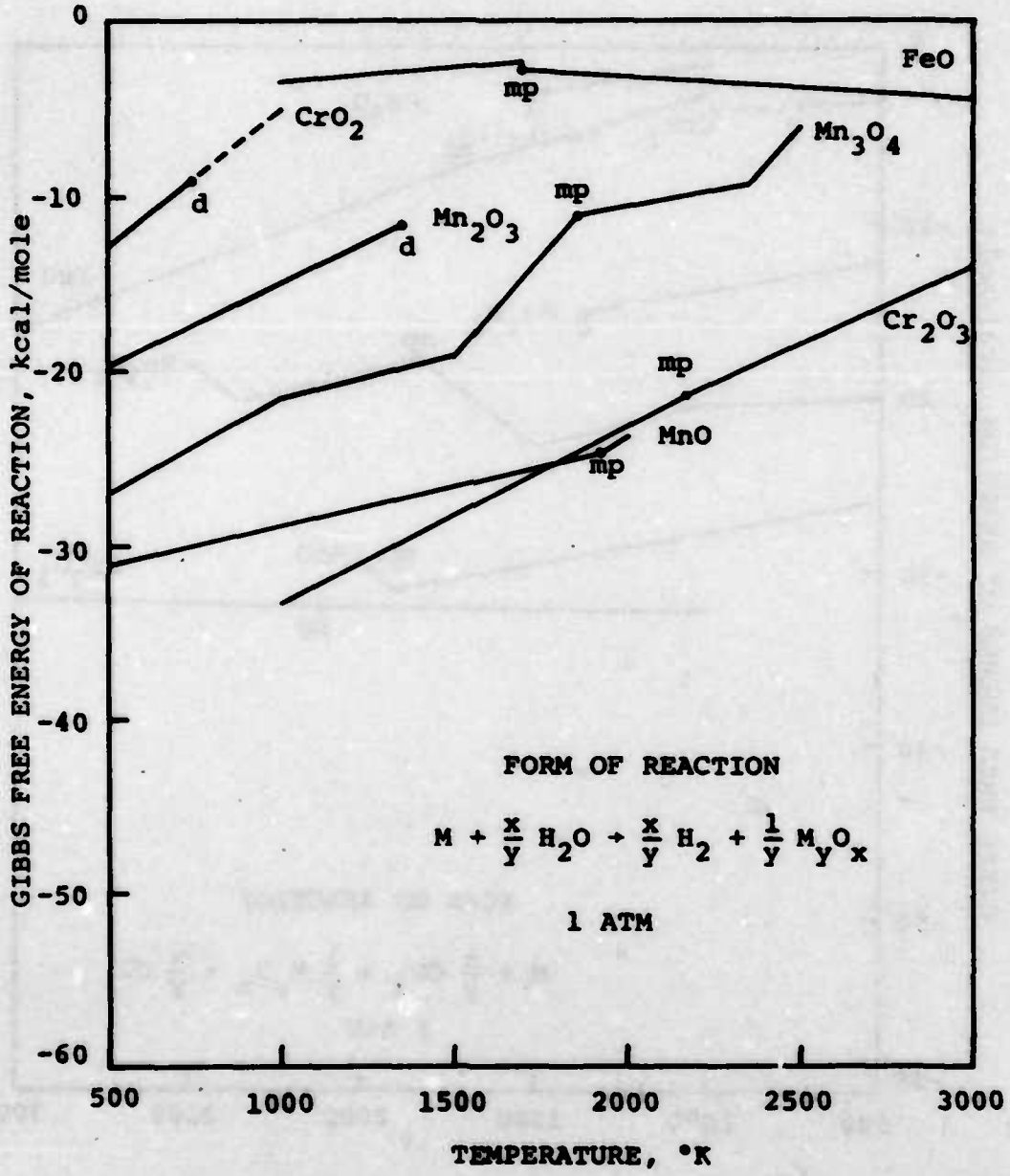

Fig. 2 Free energy of reaction of H_2O gas, at 1 atmosphere pressure, with major metallic constituents of steel to form metallic oxides.

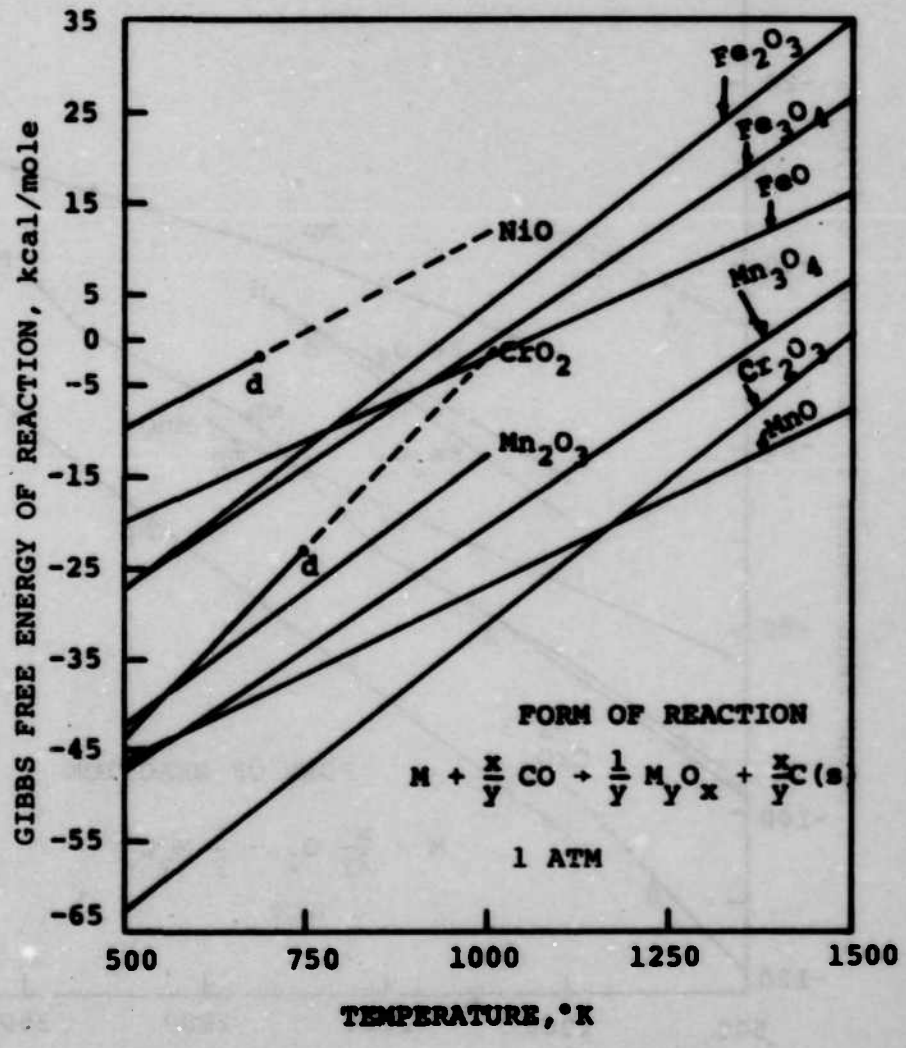

Fig. 3 Free energy of reaction of CO gas, at 1 atmosphere pressure, with major metallic constituents of steel to form metallic oxides.

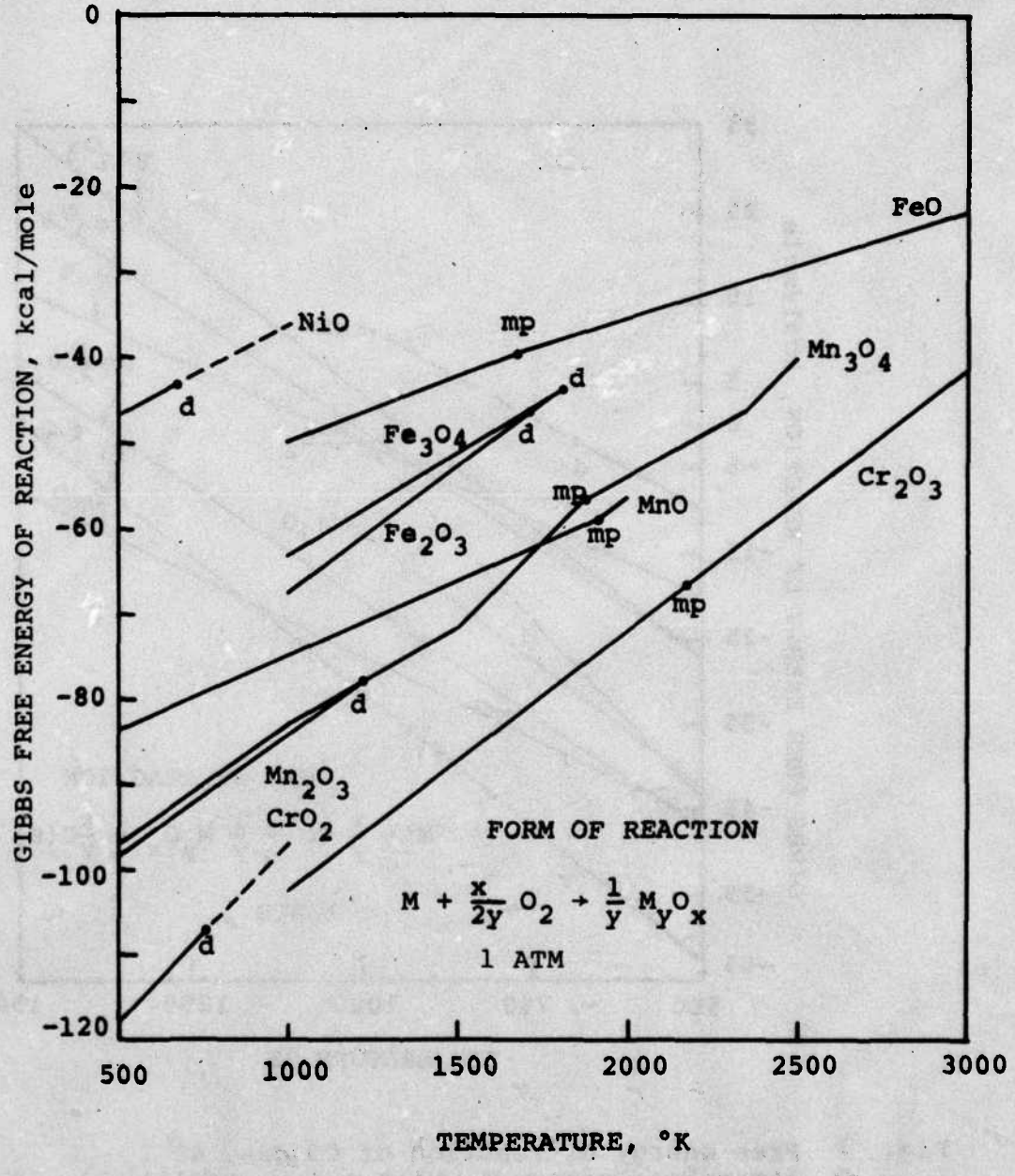

Fig. 4 Free energy of reaction of O_2 gas, at 1 atmosphere pressure, with major metallic constituents of steel to form metallic oxides.

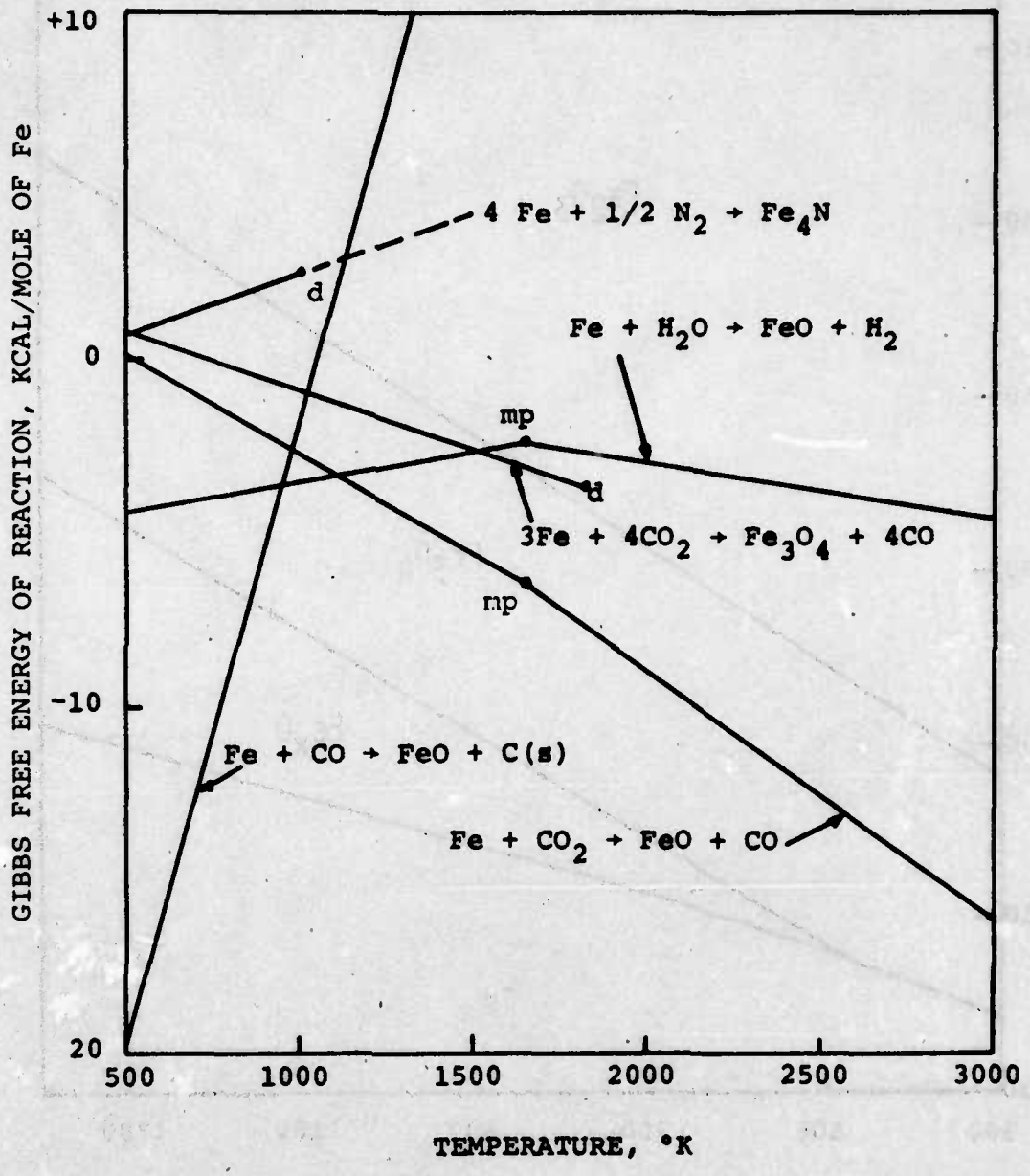

Fig. 5 Order of thermodynamic likelihood for reactions between iron and the major gaseous components of propellant gas.

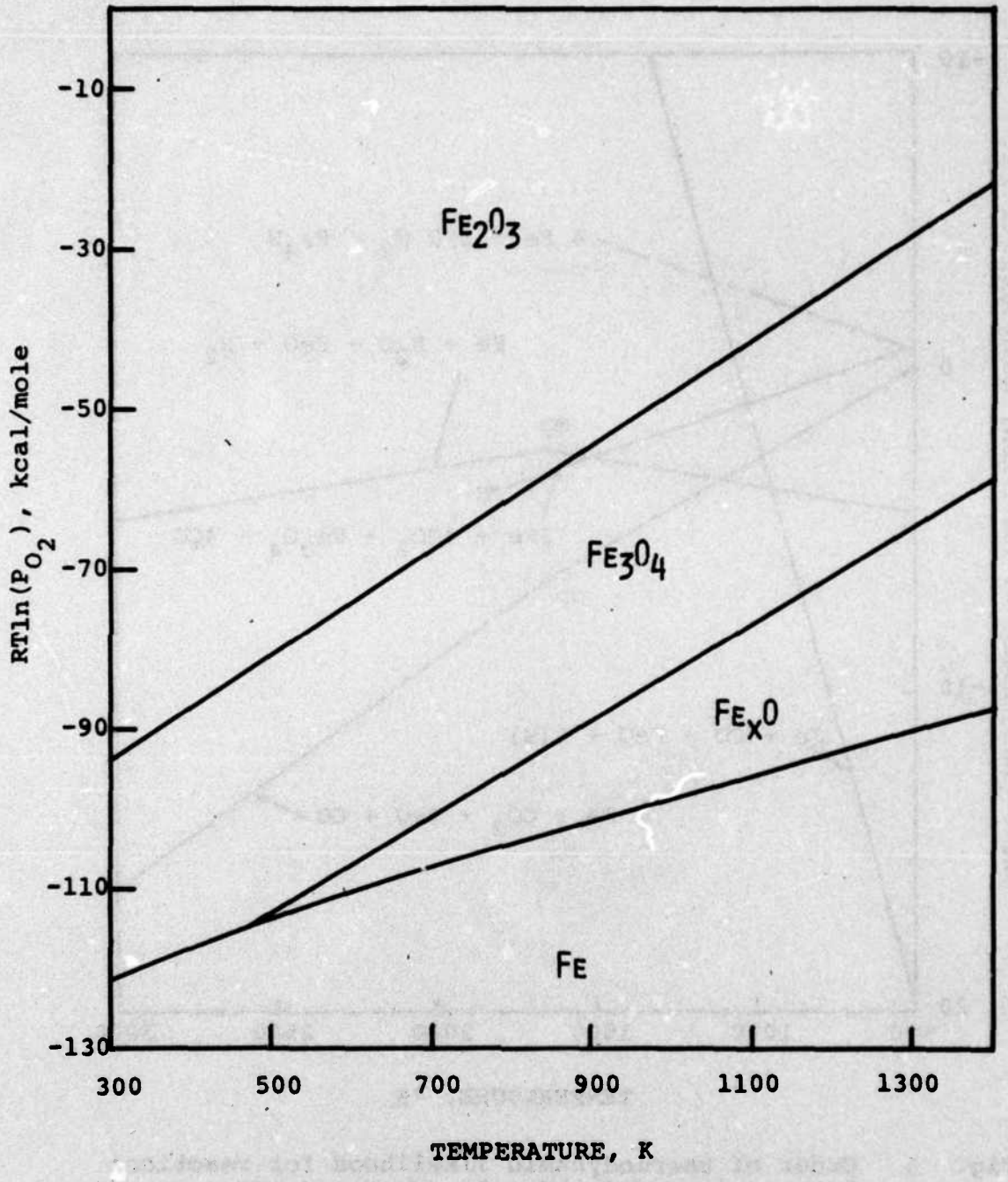

Fig. 6a Equilibria of the iron-O_2 systems.

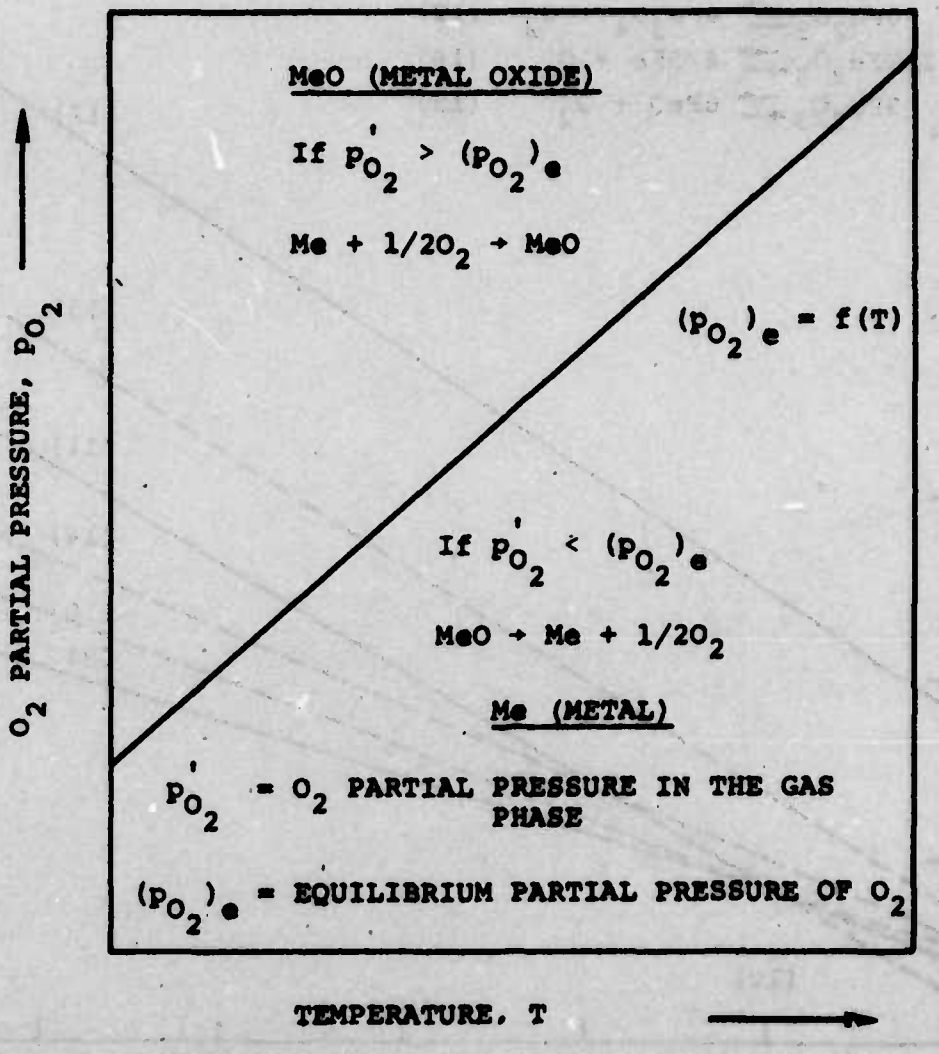

Fig. 6b Schematic diagram of the equilibrium states (p_{O_2} versus T) of the reaction:
$Me + \frac{1}{2}O_2 \rightleftharpoons MeO$.

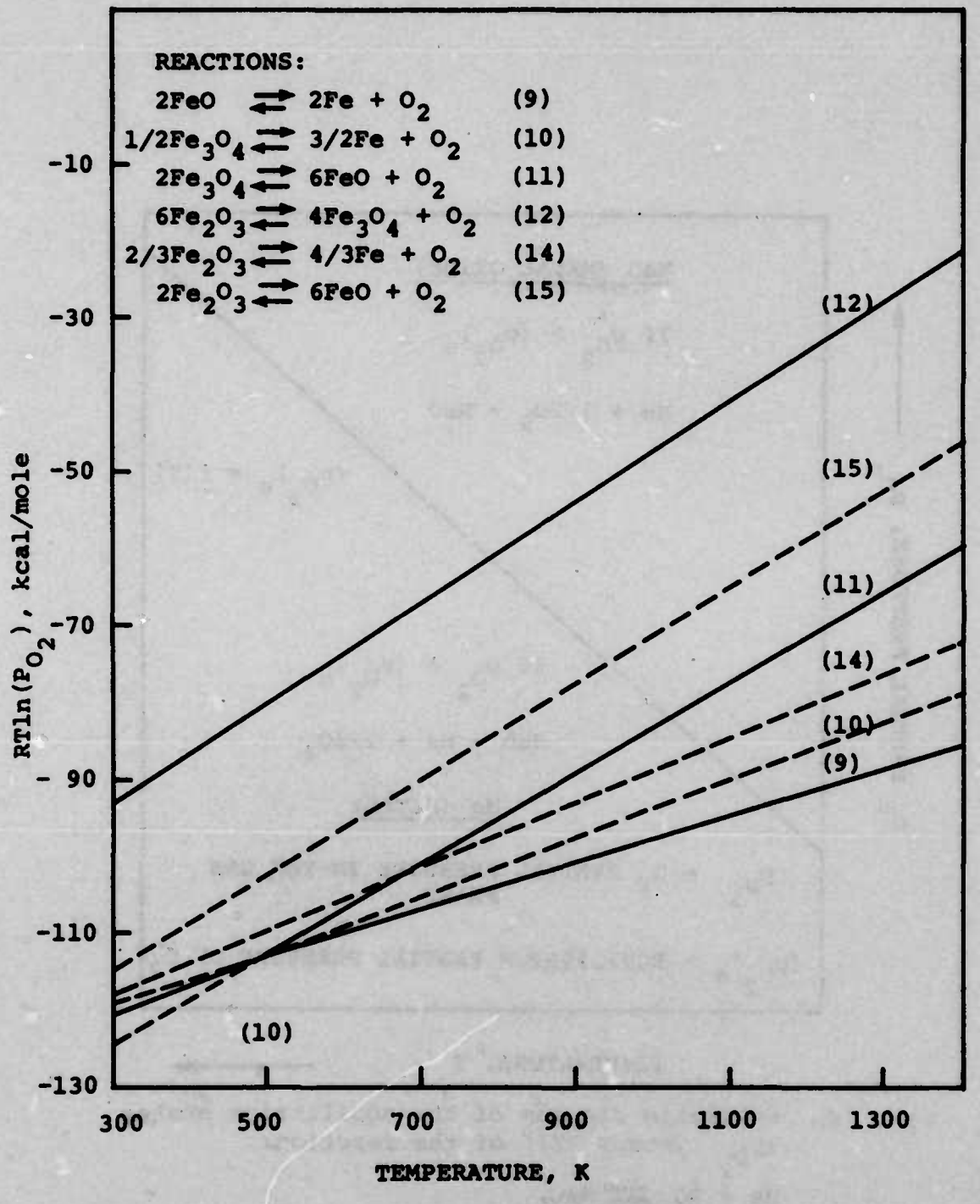

Fig. 6c Equilibrium curves of all the iron-oxygen reactions. Dotted lines indicate equilibria of reactions that do not occur.

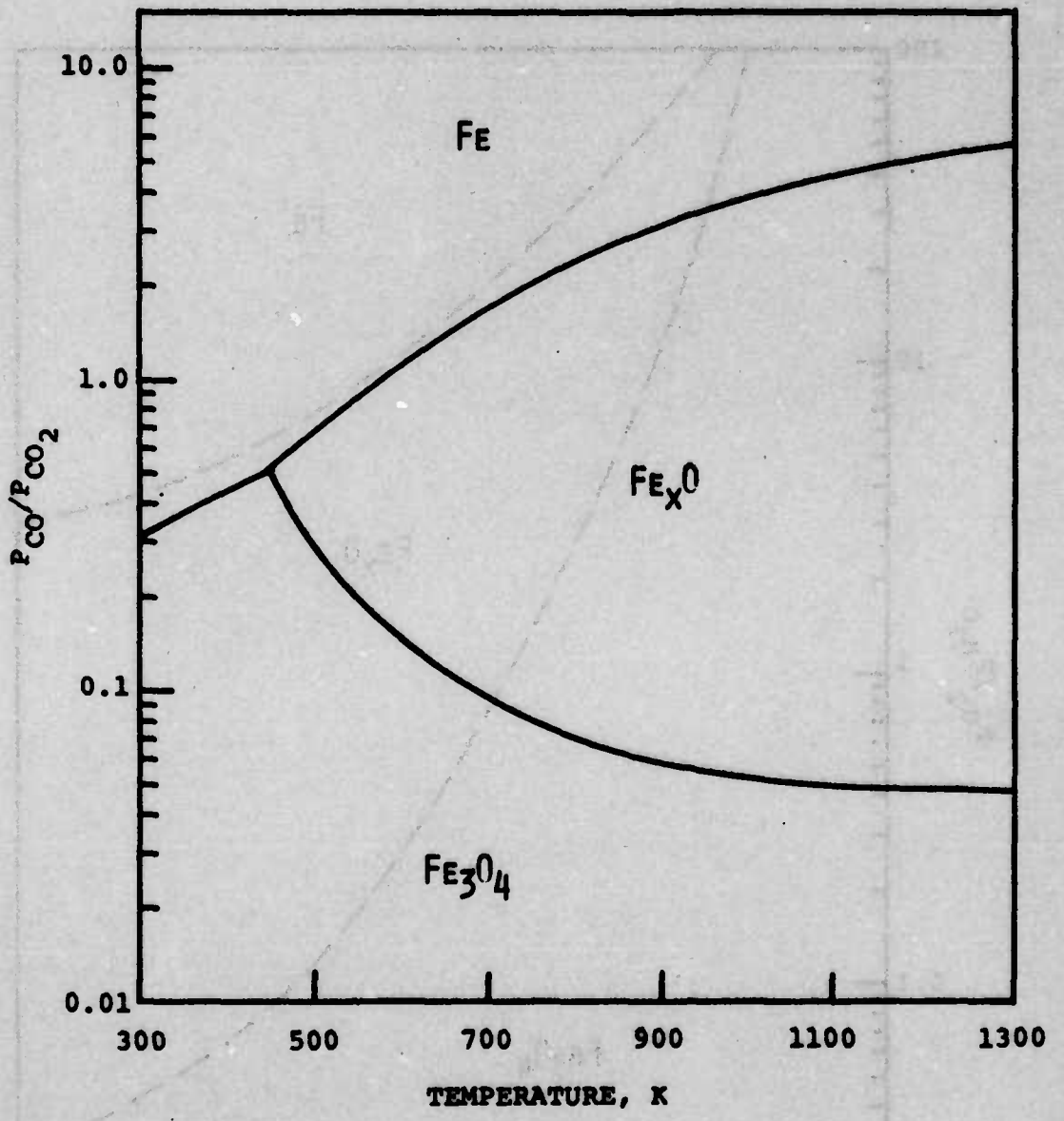

Fig. 7 Equilibria of the iron-CO_2-CO system.

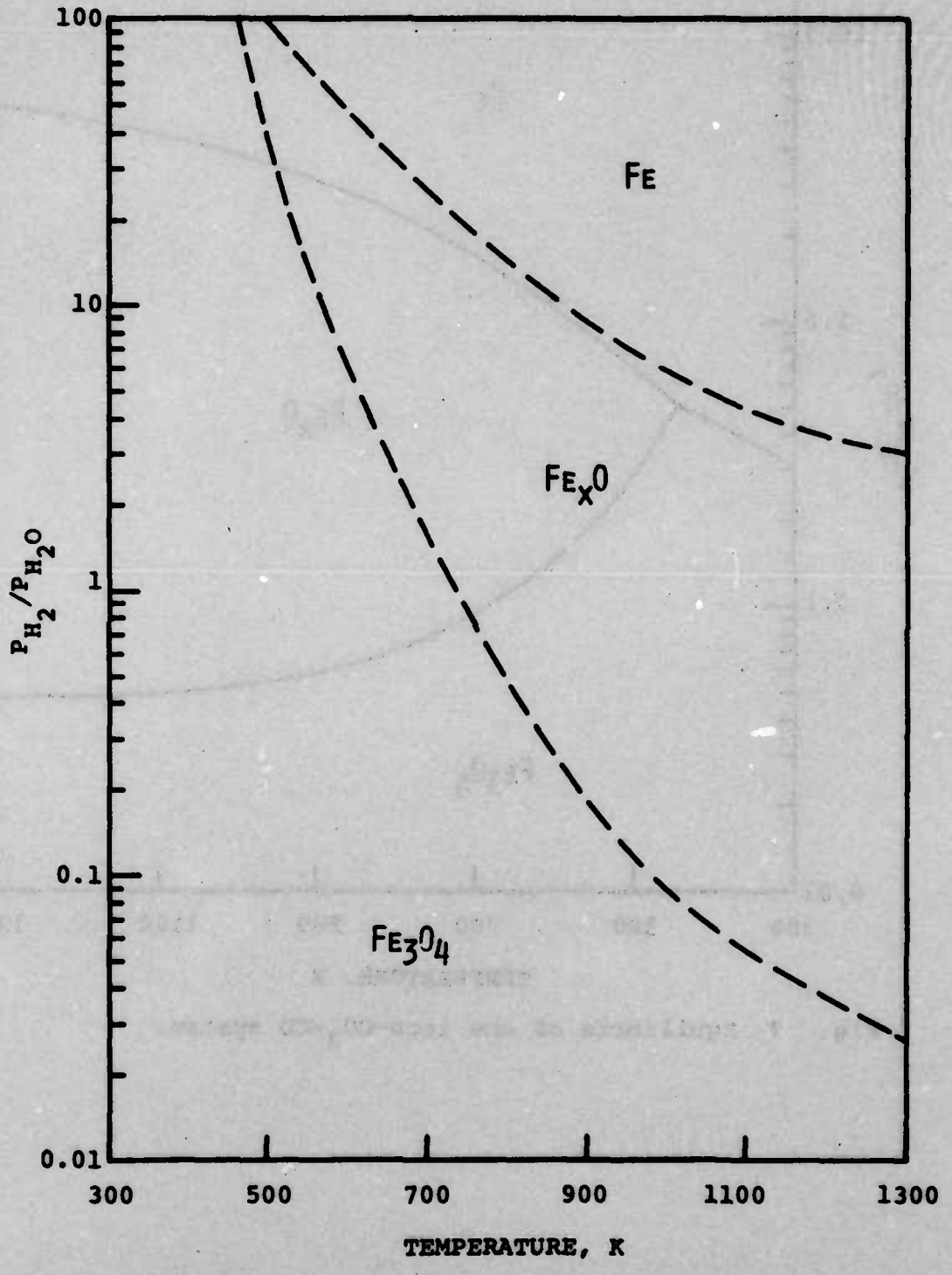

Fig. 8 Equilibria of the iron-H_2O-H_2 system.

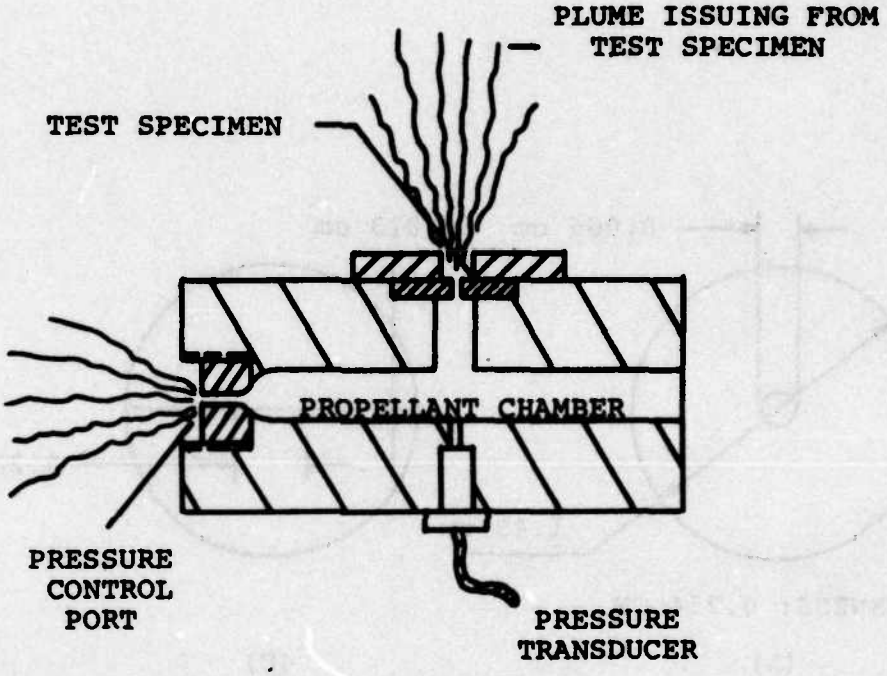

Fig. 9 Schematic diagram of the vented-combustor apparatus.

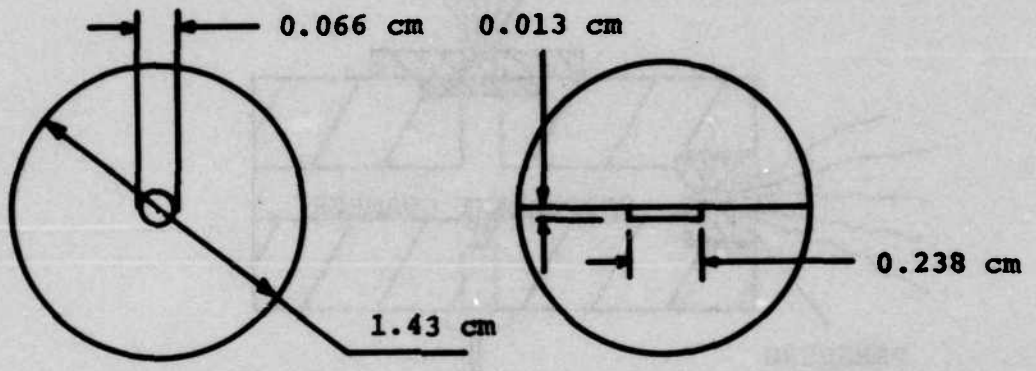

Fig. 10 Dimensions of test specimens; (A) cylindrical orifice, and (B) rectangular orifice.

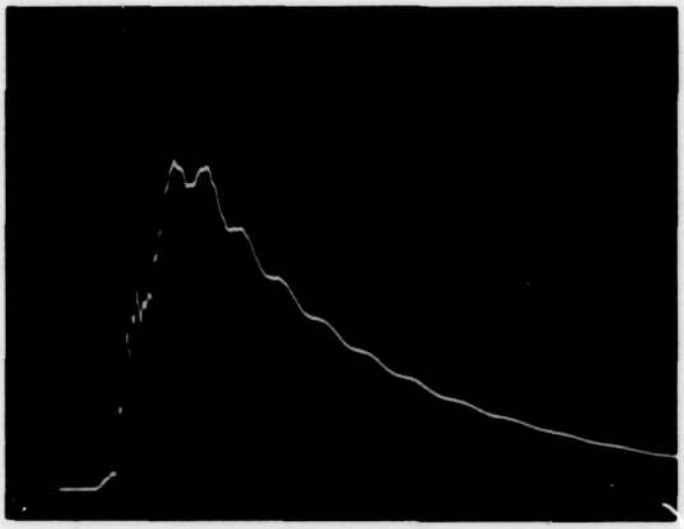

(a) COMBUSTOR WITH 0.15 CM DIA VENT ORIFICE

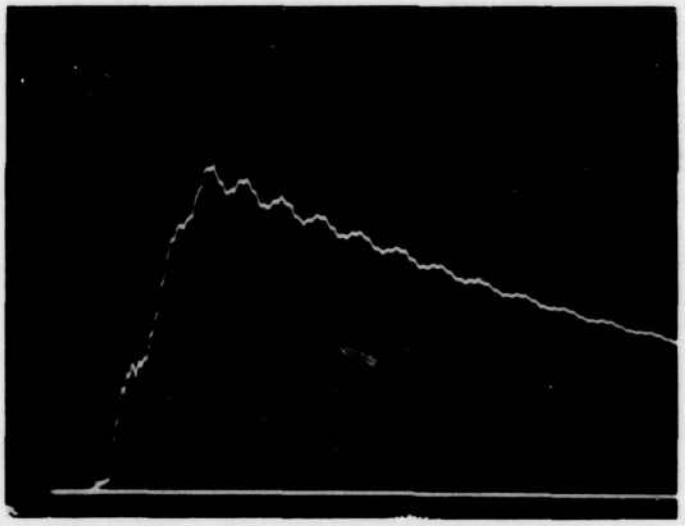

(b) COMBUSTOR WITH NO VENT ORIFICE

VERTICLE SCALE: 68.9 MN/m^2/DIVISION
HORIZONTAL SCALE: 0.5 MSEC/DIVISION

Fig. 11 Comparison of the pressure history of the vented combustor using (a) 0.15 cm dia. vent orifice, and (b) no vent orifice. The effective test time is increased by a factor of 2.5 when no vent is used.

Note: 1 MN/m^2 = 145.04 lbf/in^2

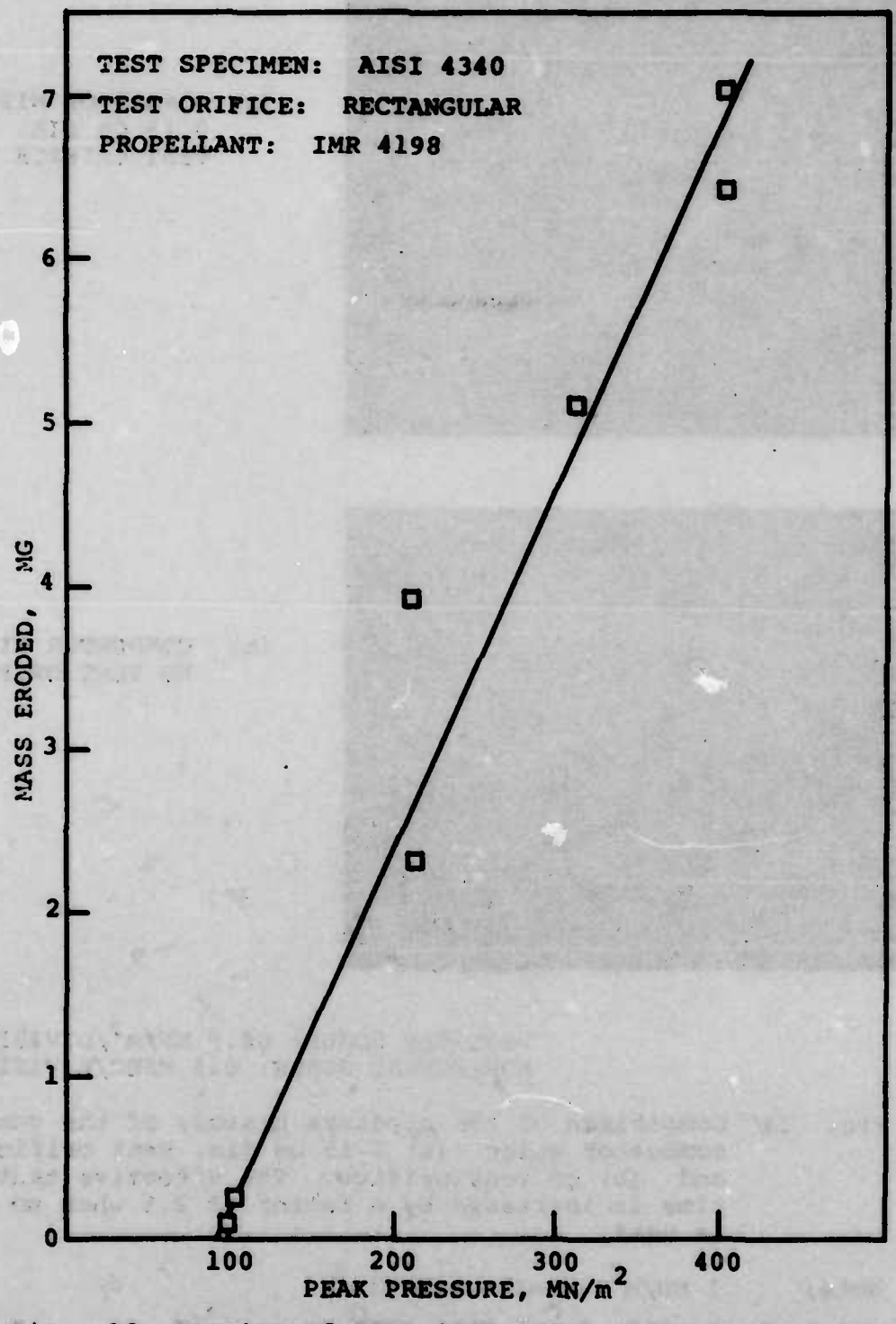

Fig. 12 Erosion of AISI 4340 steel alloy rectangular orifices as a function of combustor peak pressure.

Note: 1 MN/m^2 = 145.04 lbf/in^2

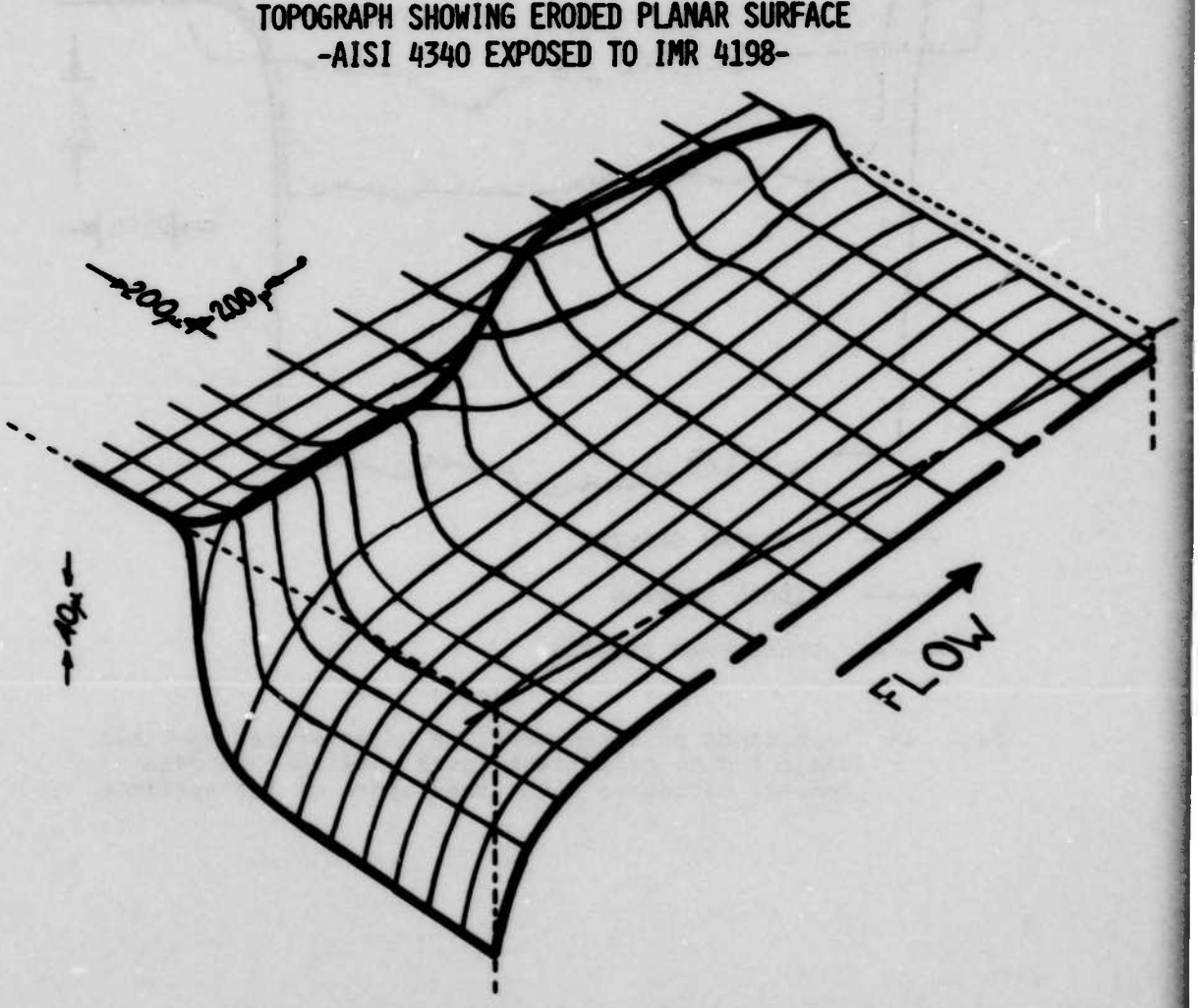

Fig. 13 Topograph of one symmetric half of eroded planar surface of AISI 4340 steel showing details of mass removal due to the erosive action of propellant gases. (Roughness of the order of 10 μm or less is not shown.)

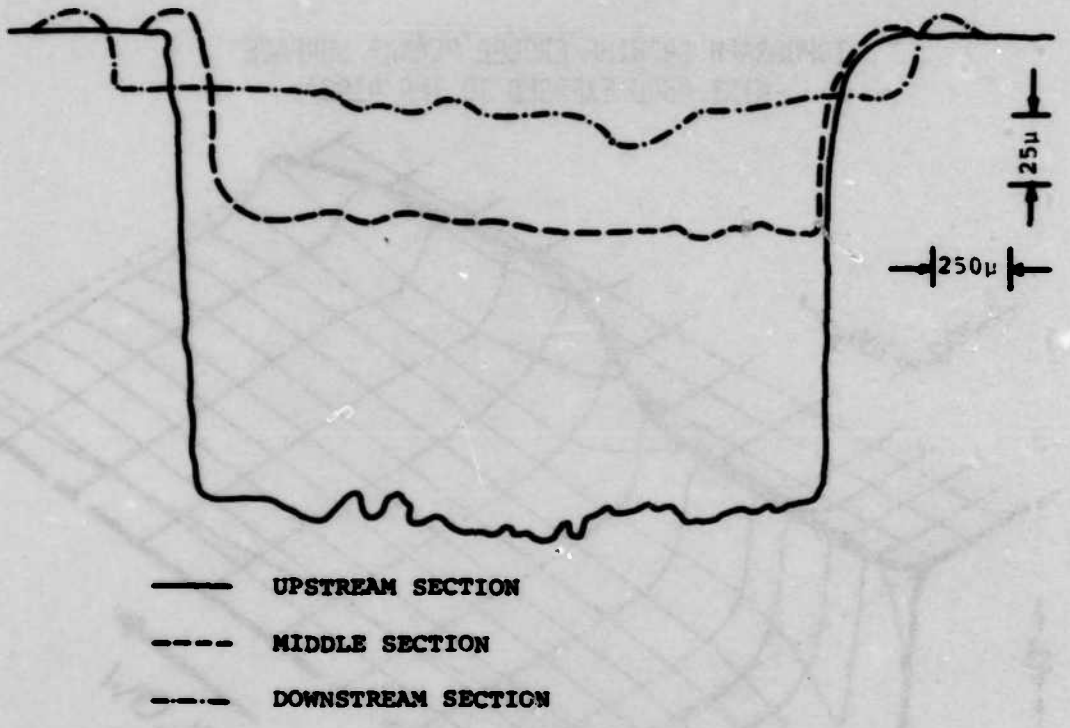

Fig. 14 Topographs of three sections of an eroded specimen subjected to propellant gases showing that mass removal decreases along the length of the specimen.

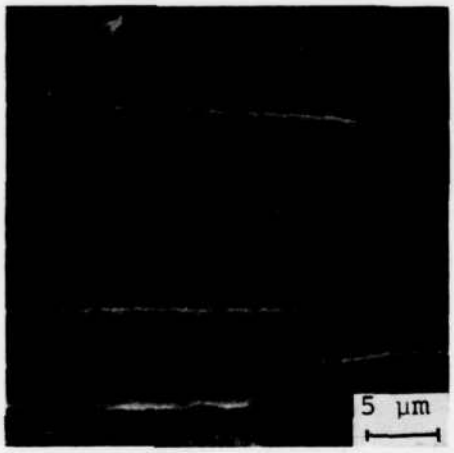

Fig. 15 SEM photograph of the surface of an untested specimen. The horizontal bands are machine tools marks.

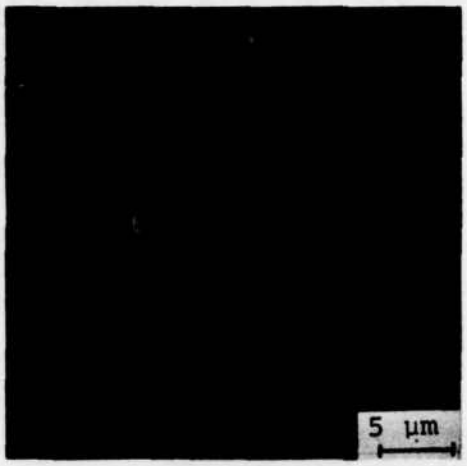

p_{max} = 103.4 MN/m^2

Δm = 0.26 mg

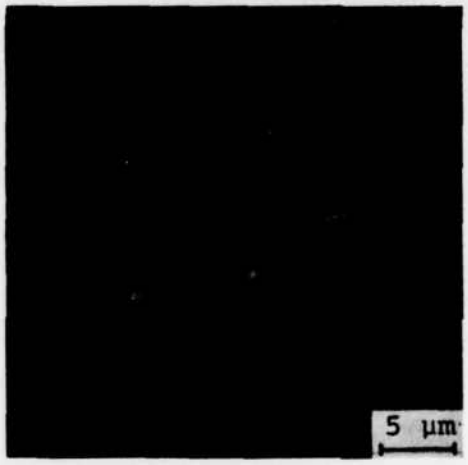

p_{max} = 213.7 MN/m^2

Δm = 2.32 mg

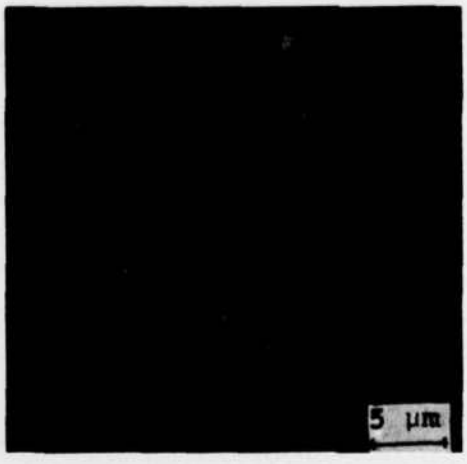

p_{max} = 403.4 MN/m^2

Δm = 7.02 mg

Fig. 16 SEM photographs of the surface of AISI 4340 steel specimens showing that the width of cracks produced by the action of IMR 4198 propellant gases increases with increasing pressure.

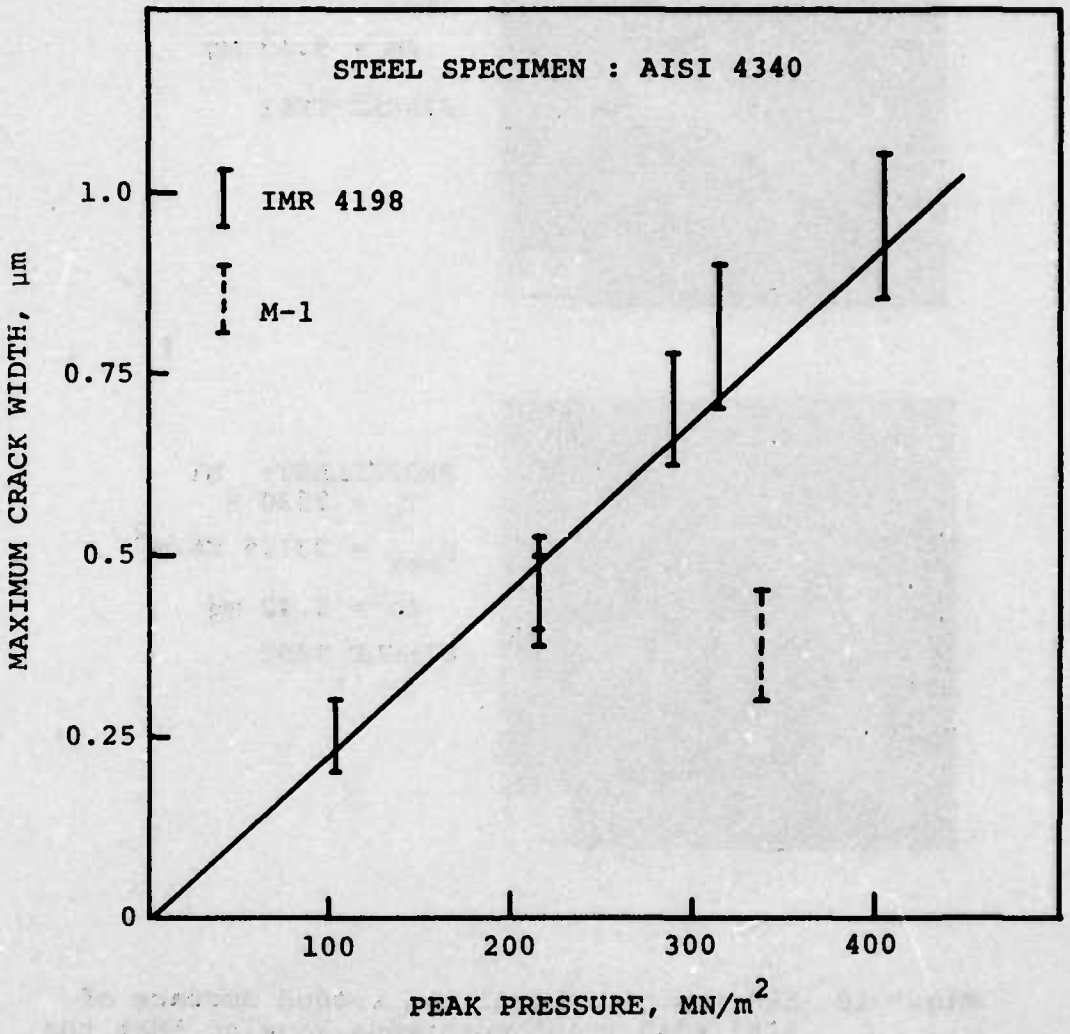

Fig. 17 Maximum crack width vs combustor peak pressure. The width of cracks increases with increasing peak pressure.

PROPELLANT: IMR 4198
T_v = 3000 K
p_{max} = 313.7 MN/m^2
Δm = 5.13 mg
SINGLE TEST

PROPELLANT: M1
T_v = 2530 K
p_{max} = 337.9 MN/m^2
Δm = 5.42 mg
SINGLE TEST

Fig. 18 SEM photographs of the eroded surface of AISI 4340 steel specimens showing that the width of cracks increases with increasing flame temperature.

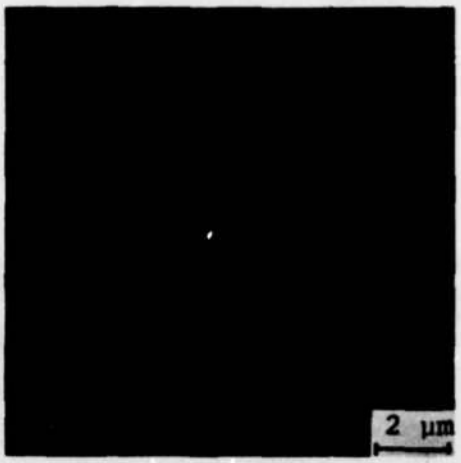

AISI 4340
p_{max} = 313.7 MN/m^2
Δm = 5.13 mg
K = 37.66 WATTS/mK

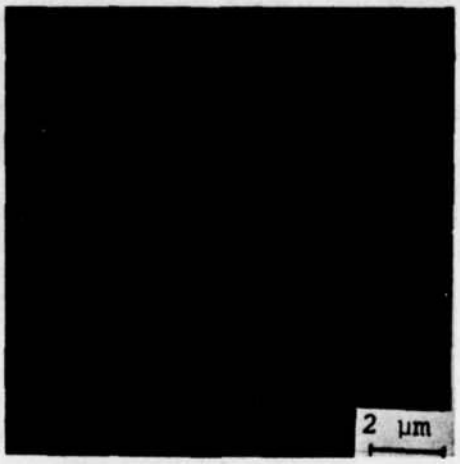

AISI 1020
p_{max} = 320.6 MN/m^2
Δm = 4.81 mg
K = 51.88 WATT/mK

AISI 304
p_{max} = 310.3 MN/m^2
Δm = 12.91 mg
K = 17.15 WATT/mK

Fig. 19 SEM photographs of steel specimens under the erosive action of propellant gases showing that the crack width increases with decreasing conductivity of the steel.

TEST GAS: H_2/CO_2 (20/80%)

p_{max} = 620 MN/m^2

Fig. 20 SEM photograph of an eroded surface showing that high pressure H_2 does not produce cracks on the metal surface (AISI 4340 steel).

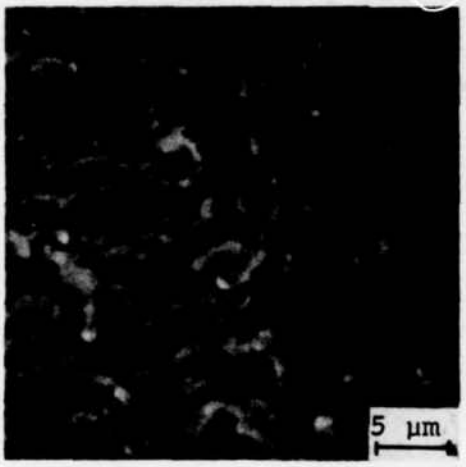

p_{max} = 78.6 MN/m^2

Δm = 0.0 mg

Fig. 21 SEM photograph showing the inert erosive action of Argon on AISI 4340 steel surface. Surface modifications are believed to result from surface melting.

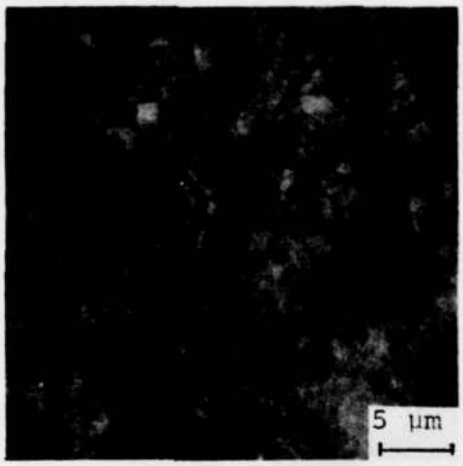

PROPELLANT: IMR 4198

T_v = 3000 K

p_{MAX} = 290 MN/m^2

ΔM = 10.12 mg

5 Consecutive Tests

Fig. 22 SEM photograph of the eroded surface of AISI 4340 steel specimen showing that consecutive tests do not augment crack formation.

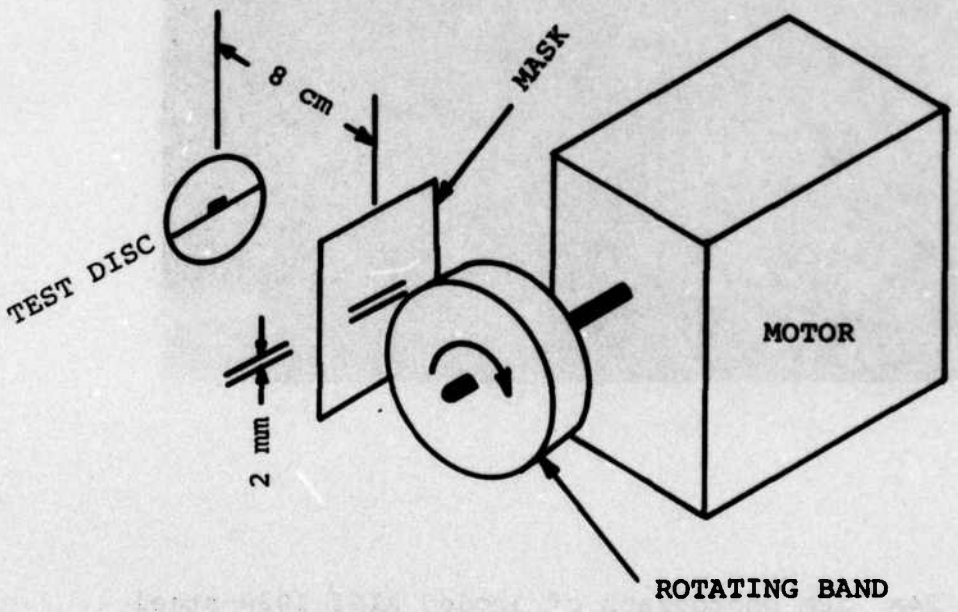

Fig. 23 Schematic diagram of the rotary collector utilized to obtain time-resolved samples of erosion products.

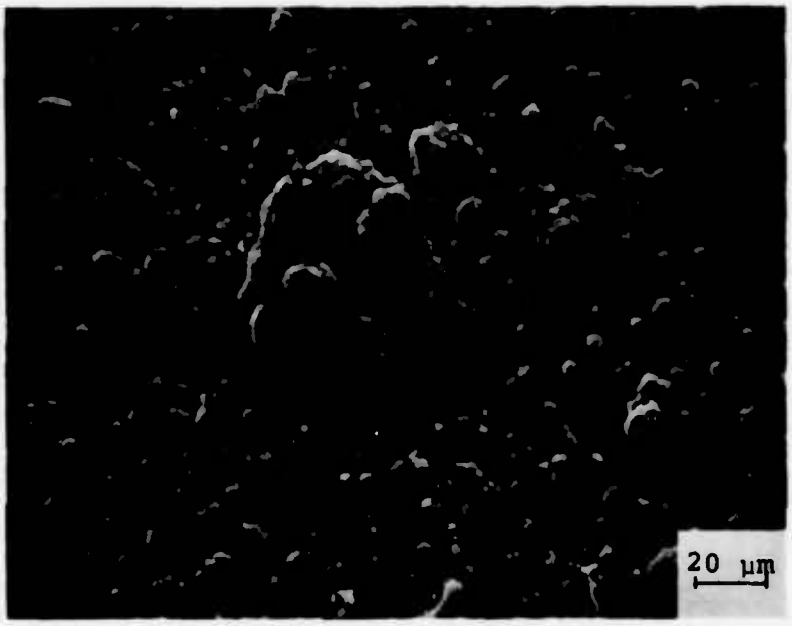

Fig. 24a SEM photograph of eroded AISI 1020 steel collected on a copper substrate.

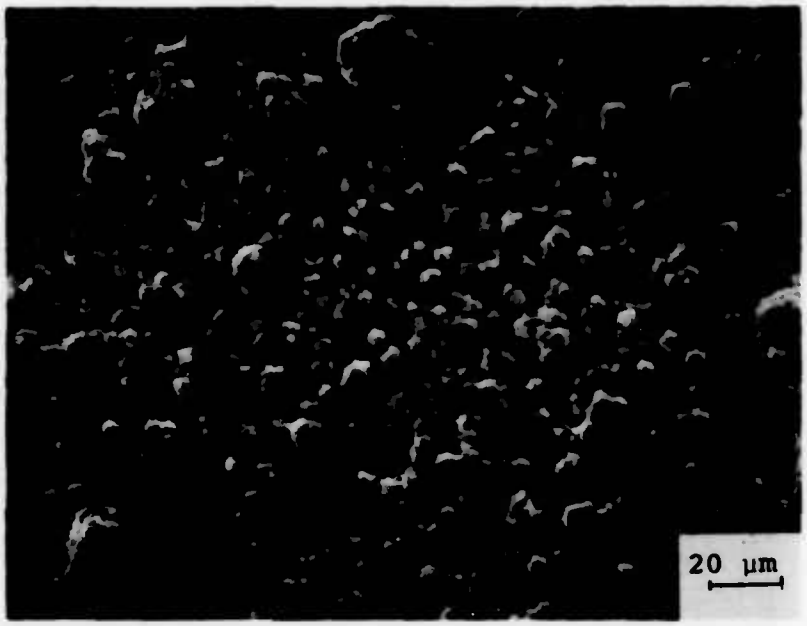

Fig. 24b SEM photograph of eroded AISI 304 steel collected on a copper substrate.

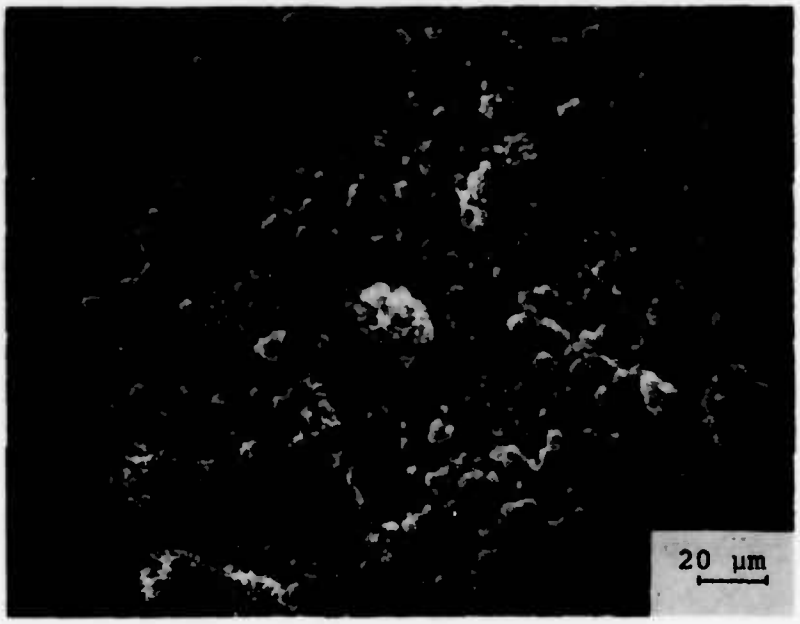

Fig. 24c SEM photograph of eroded AISI 4340 steel collected on a copper substrate.

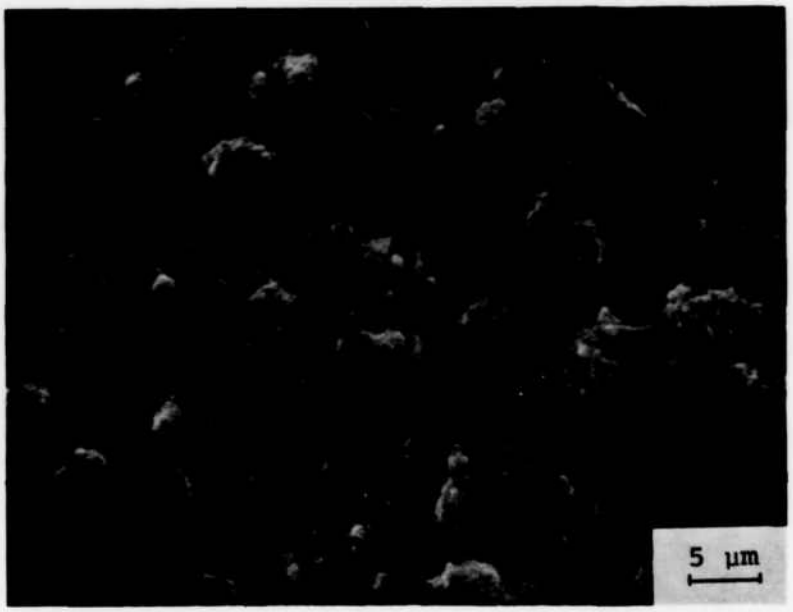

Fig. 25a Same as Fig. 24b but at a higher magnification.

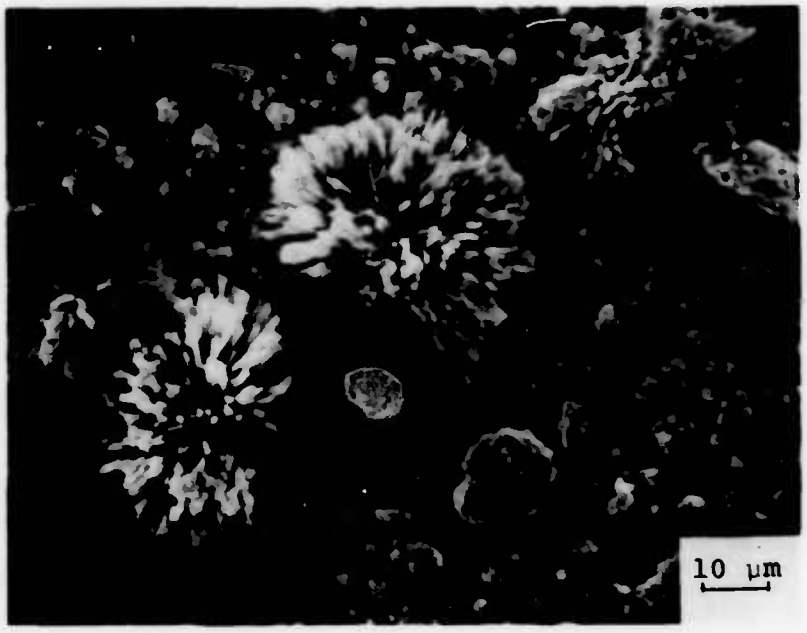

Fig. 25b Same as Fig. 24c but at higher magnification.

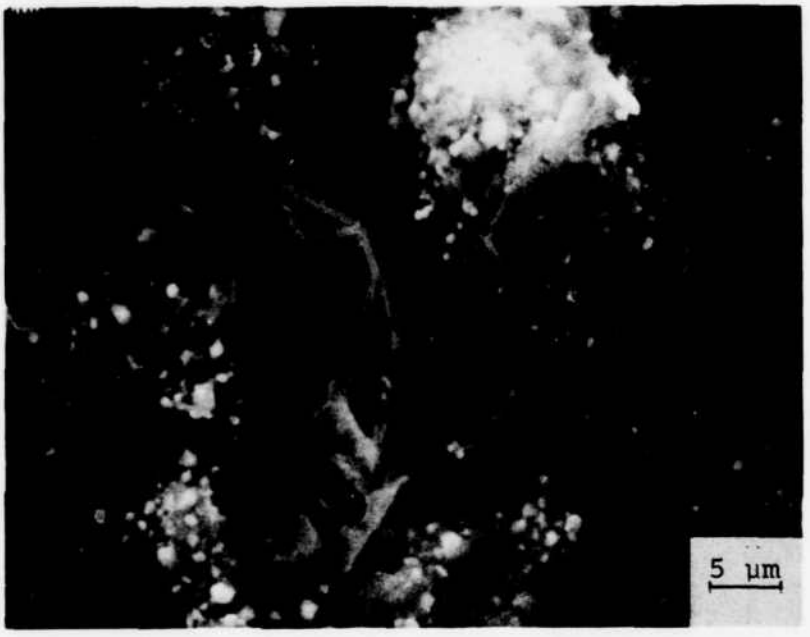

Fig. 25c SEM photograph of eroded AISI 4340 steel collected on a steel substrate.

AD-A048 977 PRINCETON UNIV N J DEPT OF AEROSPACE AND MECHANICAL--ETC F/G 11/6
EROSIVE EFFECTS OF VARIOUS PURE AND COMBUSTION-GENERATED GASES --ETC(U)
OCT 77 A C ALKIDAS, S O MORRIS, C W CHRISTOE DAAG46-75-C-0088

UNCLASSIFIED AMS-1303 AMMRC-CTR-77-25 NL

2 OF 2
AD
A048977

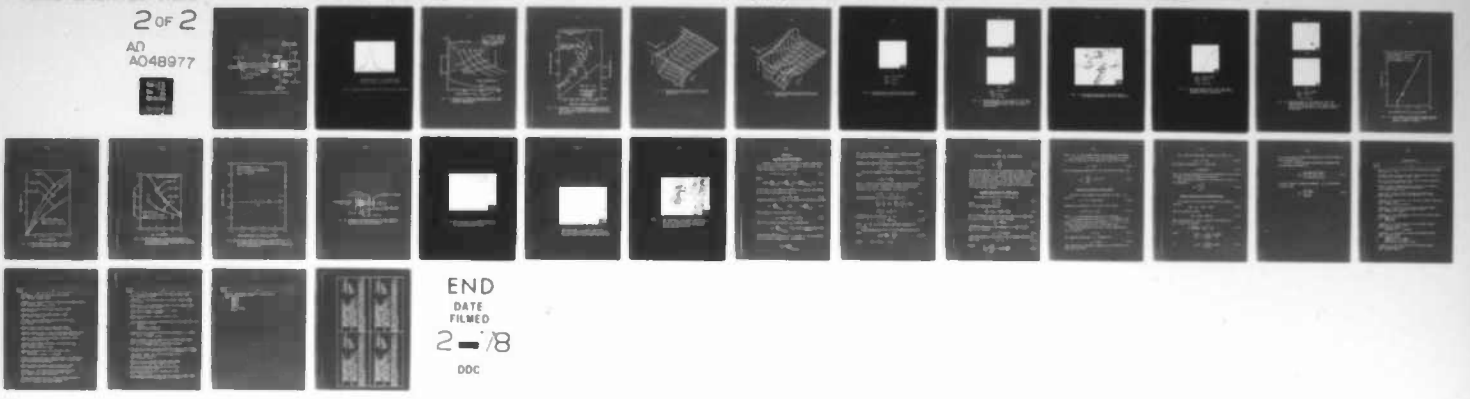

END
DATE
FILMED
2-78
DDC

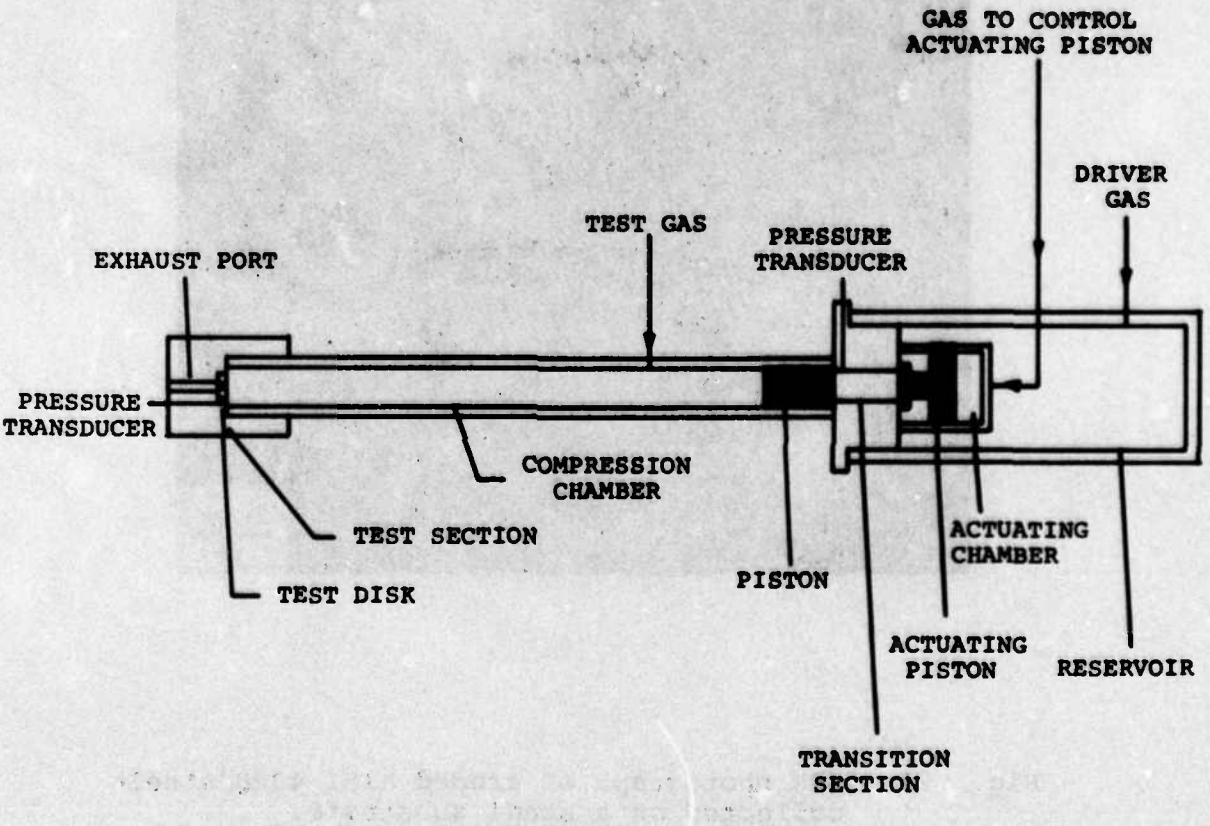

Fig. 26 Schematic diagram of the ballistic compressor.

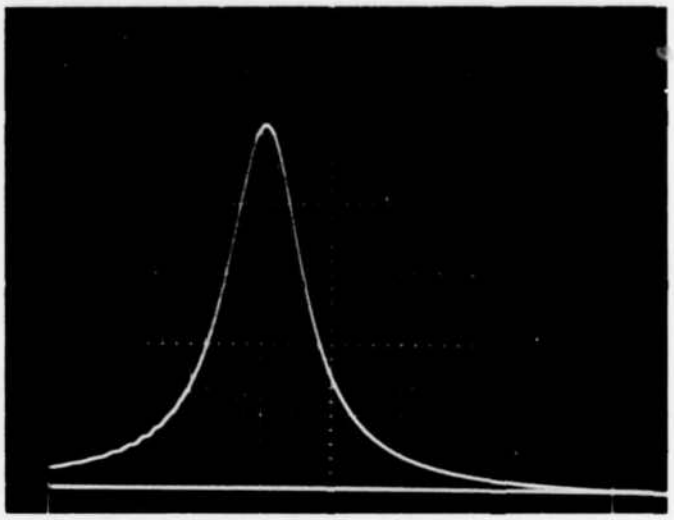

HORIZONTAL SCALE = 0.2 msec/DIVISION
VERTICAL SCALE = 68.9 MN/m^2/DIVISION

Fig. 27 Typical pressure-time trace of ballistic compressor.

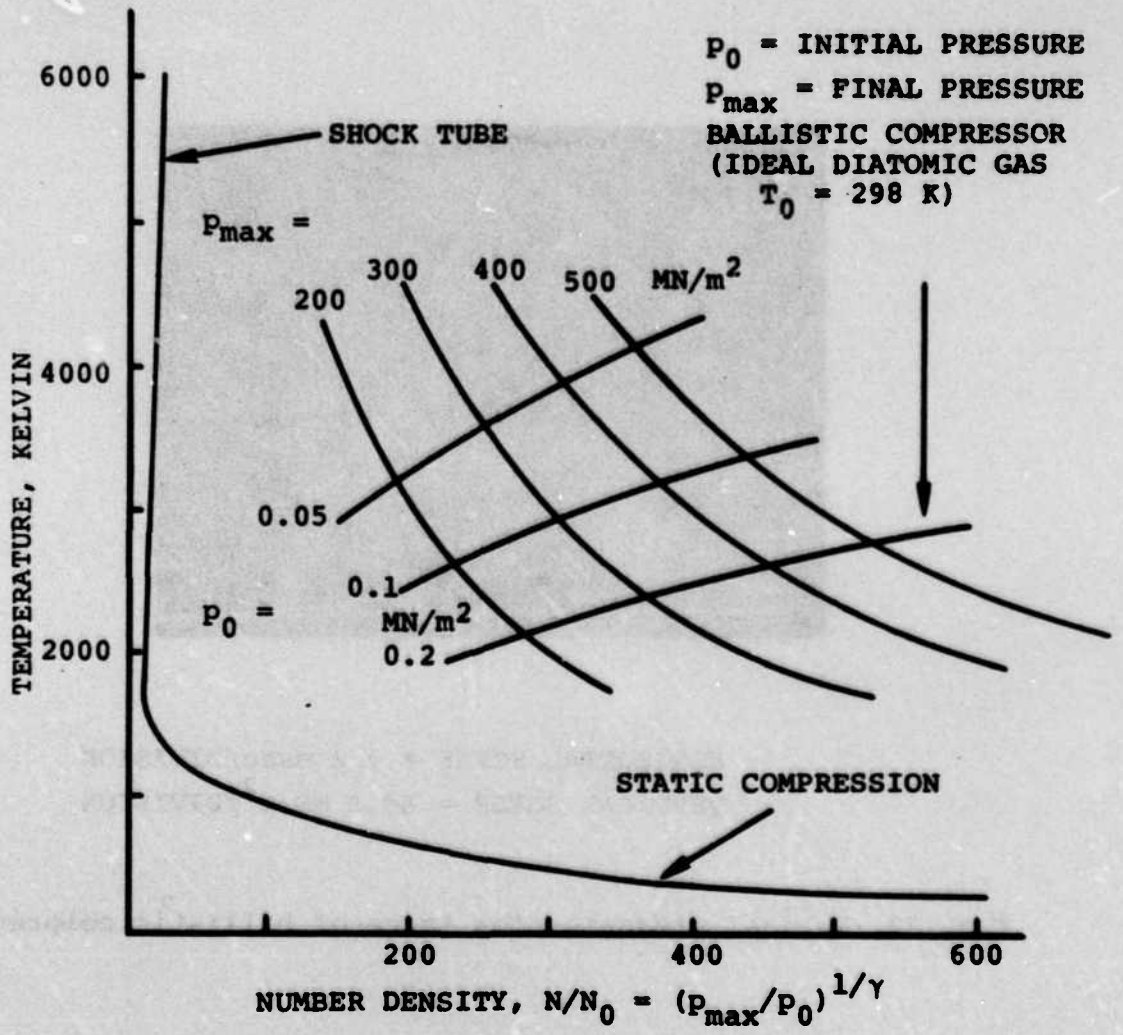

Fig. 28 Comparison of modes of production of hot, high pressure gases showing the versatility of the ballistic compressor.

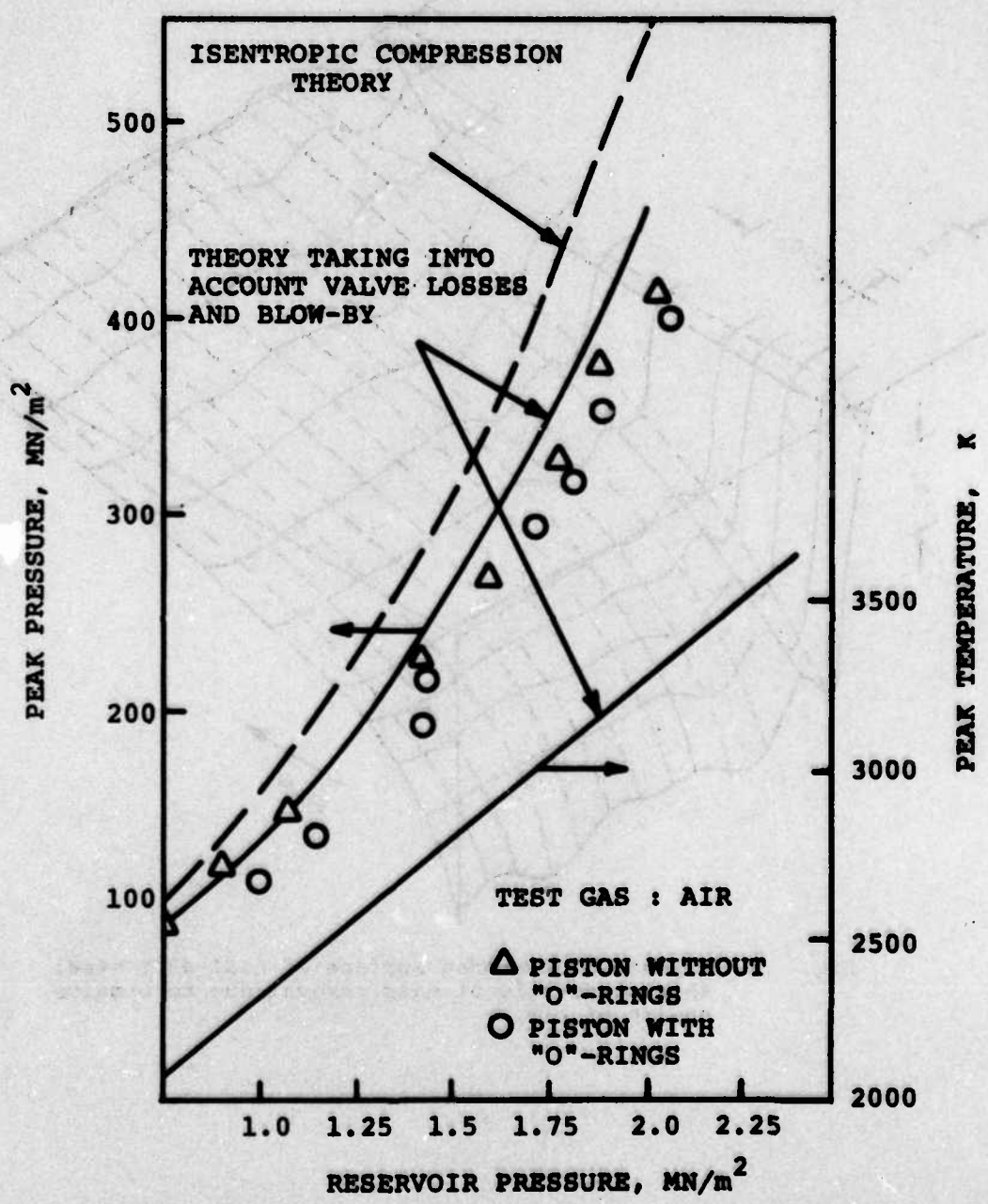

Fig. 29 Comparison of experimentally attained peak pressures with (a) isentropic compression theory and (b) theory taking into account valve losses and blow-by.

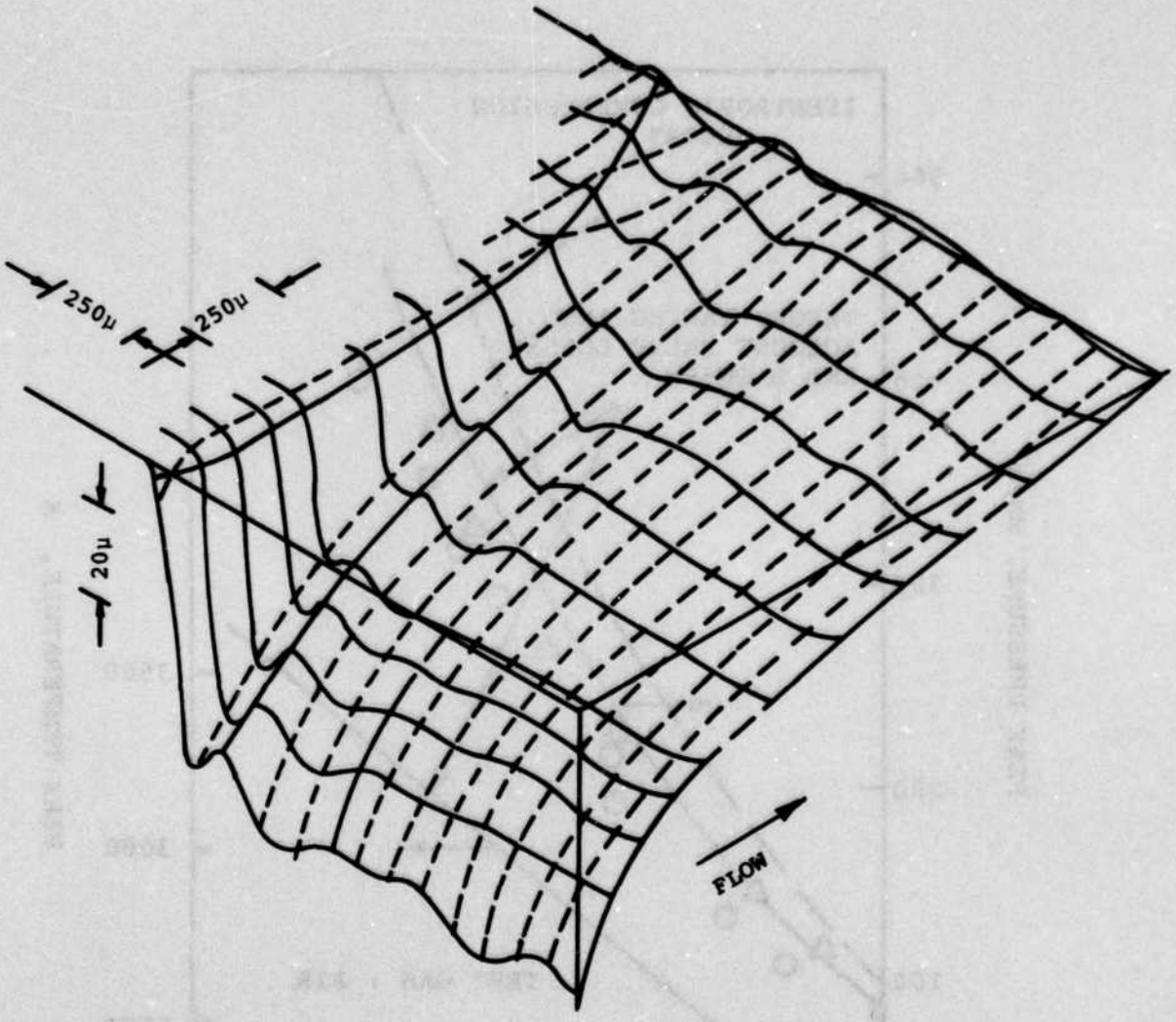

Fig. 30 Topograph of eroded surface of AISI 4340 steel showing details of mass removal due to erosive action of air.

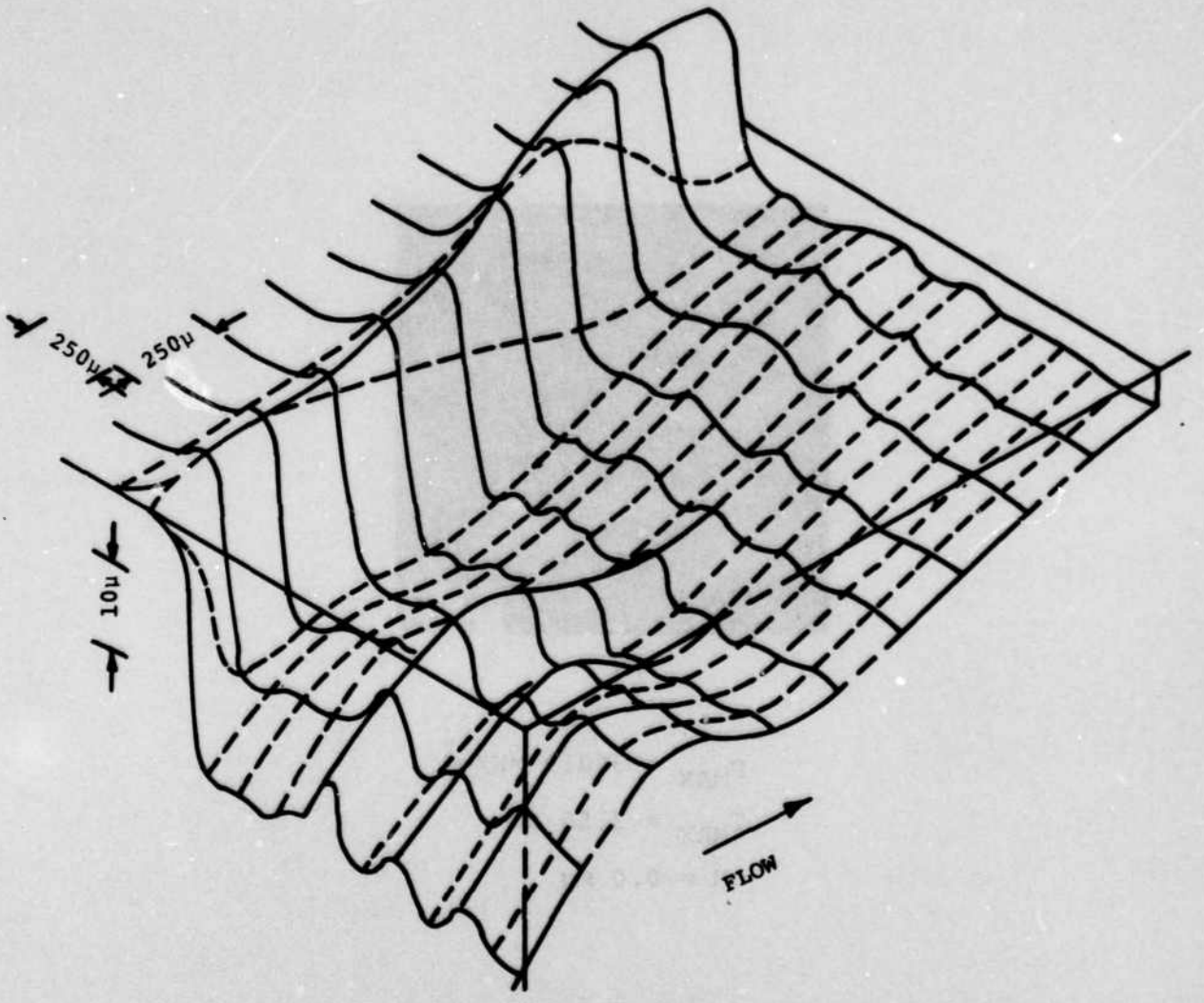

Fig. 31 Topograph of eroded surface of AISI 4340 steel showing details of mass removal due to erosive action of H_2.

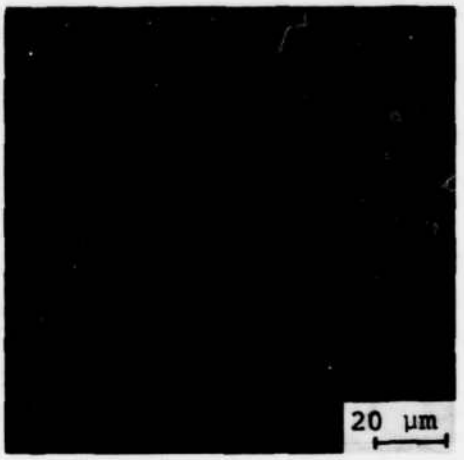

P_{MAX} = 368.9 MN/m^2

T_{MAX} = 3150 K

ΔM = 0.0 mg

Fig. 32 SEM photograph showing the inert erosive action of N_2 on AISI 4340 steel surface.

(A)

(B)

p_{max} = 362.0 MN/m^2

T_{max} = 3150 K

Δm = 0.0 mg

Fig. 33 SEM photographs of the surface of AISI 4340 steel subjected to the action of CO. Note at higher magnification, (B), the scale shows cracks.

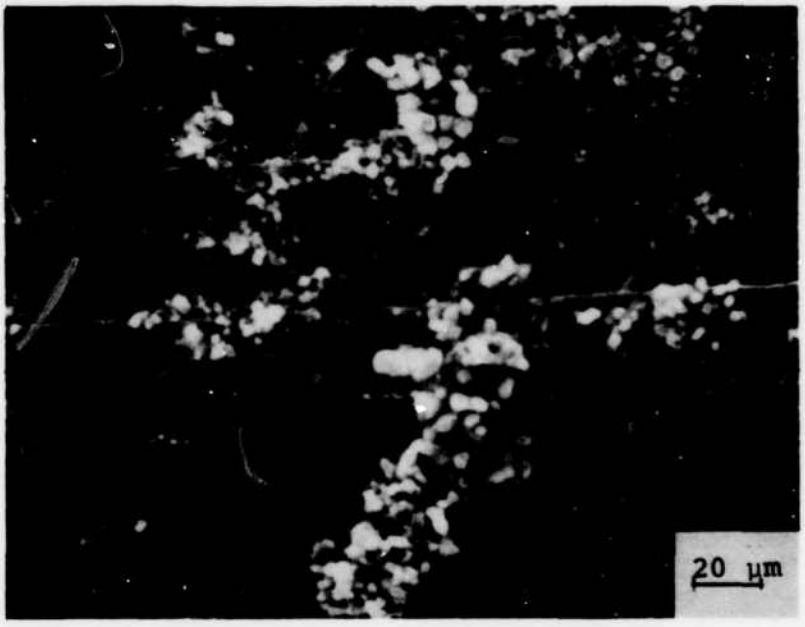

Fig. 34 SEM photograph showing that the surface is largely unaffected by the CO_2 interaction.

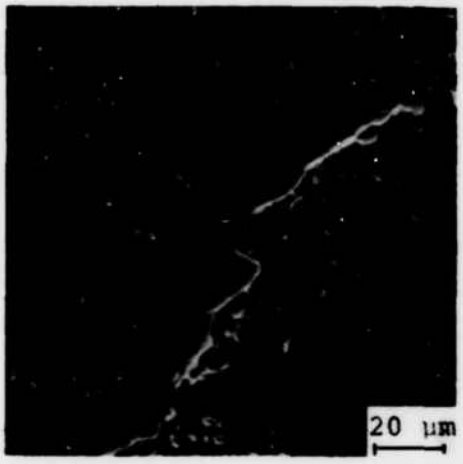

p_{max} = 368.9 MN/m^2
T_{max} = 3150 K
Δm = 1.44 mg

Fig. 35 SEM photograph of AISI 4340 steel test specimen showing the surface alterations resulting from H_2 interaction.

(A)

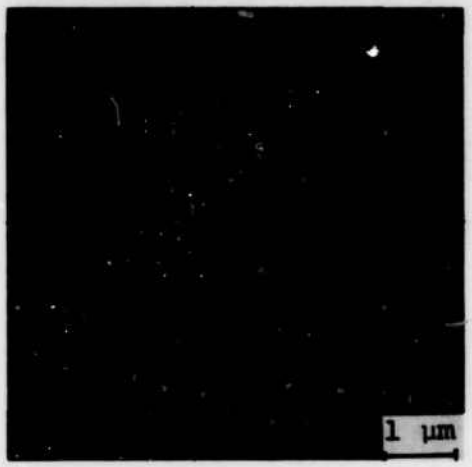

(B)

p_{max} = 334.4 MN/m^2

T_{max} = 3150 K

Δm = 1.61 mg

Fig. 36 SEM photographs of the surface of AISI 4340 steel subjected to the action of air. (A) Formation of oxide scale. (B) Region where the scale has been removed by the shearing forces of the flow.

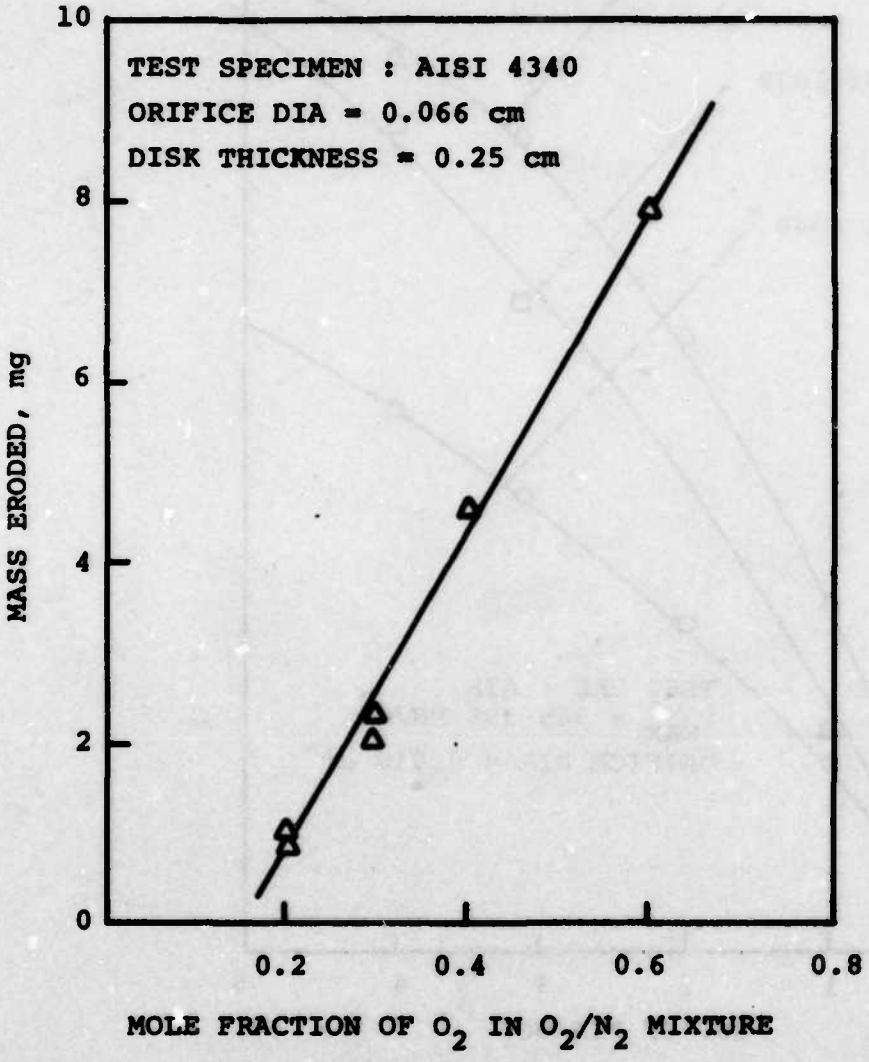

Fig. 37 Mass erosion of AISI 4340 vs mole fraction of O_2 in O_2/N_2 mixture, indicating the chemical nature of erosion.

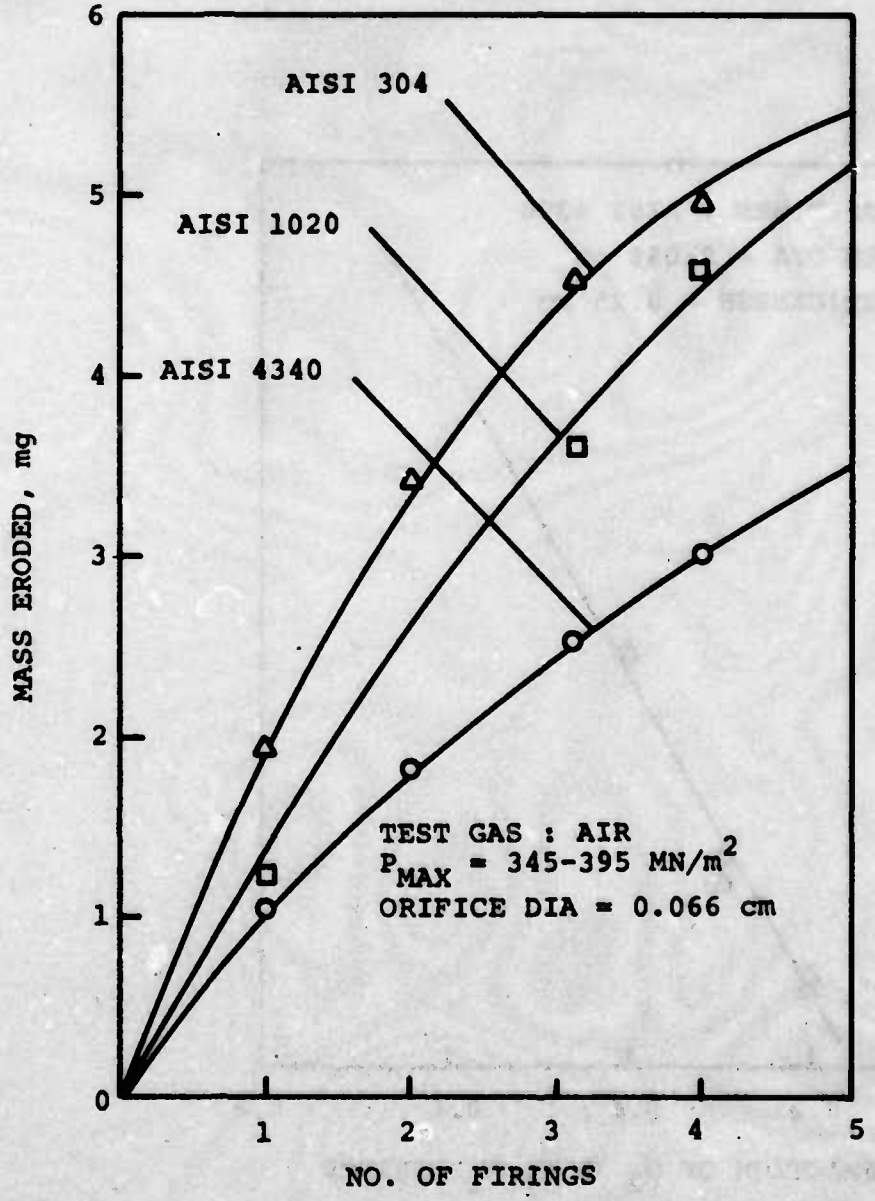

Fig. 38 Mass eroded versus number of firings for the three steel test specimens.

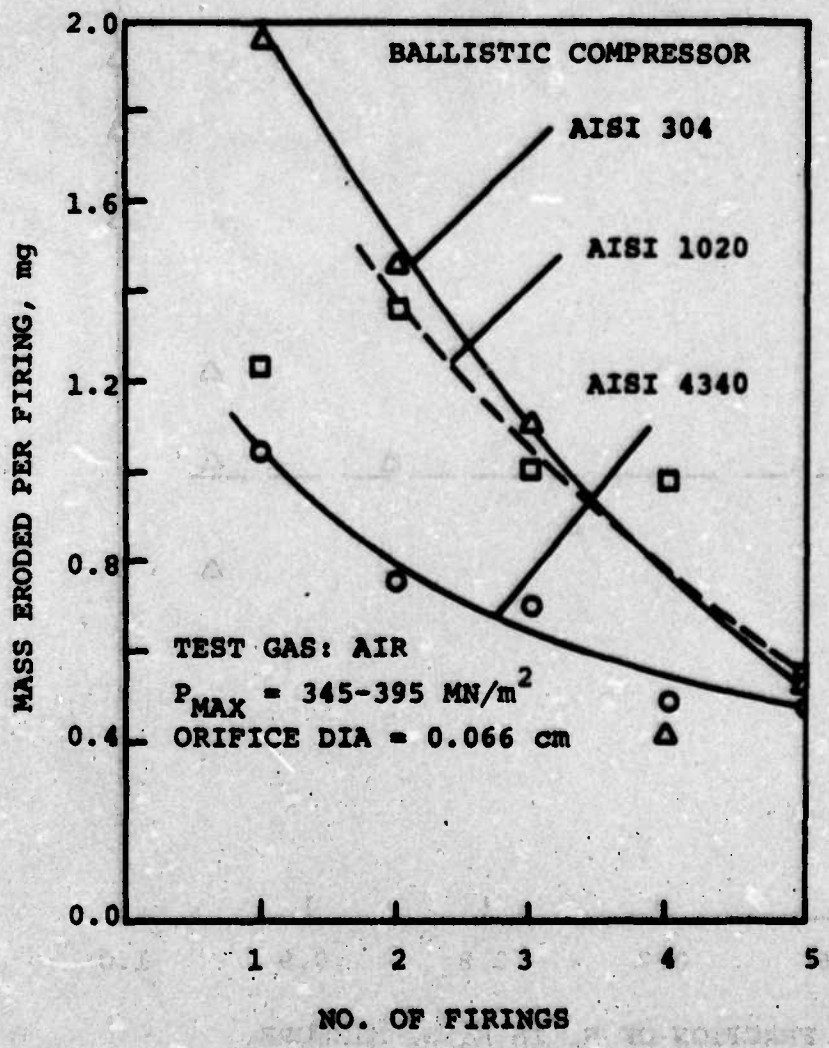

Fig. 39 Mass erosion per firing versus number of firings showing a particular exposure condition for which erosion decreases with increasing number of firings.

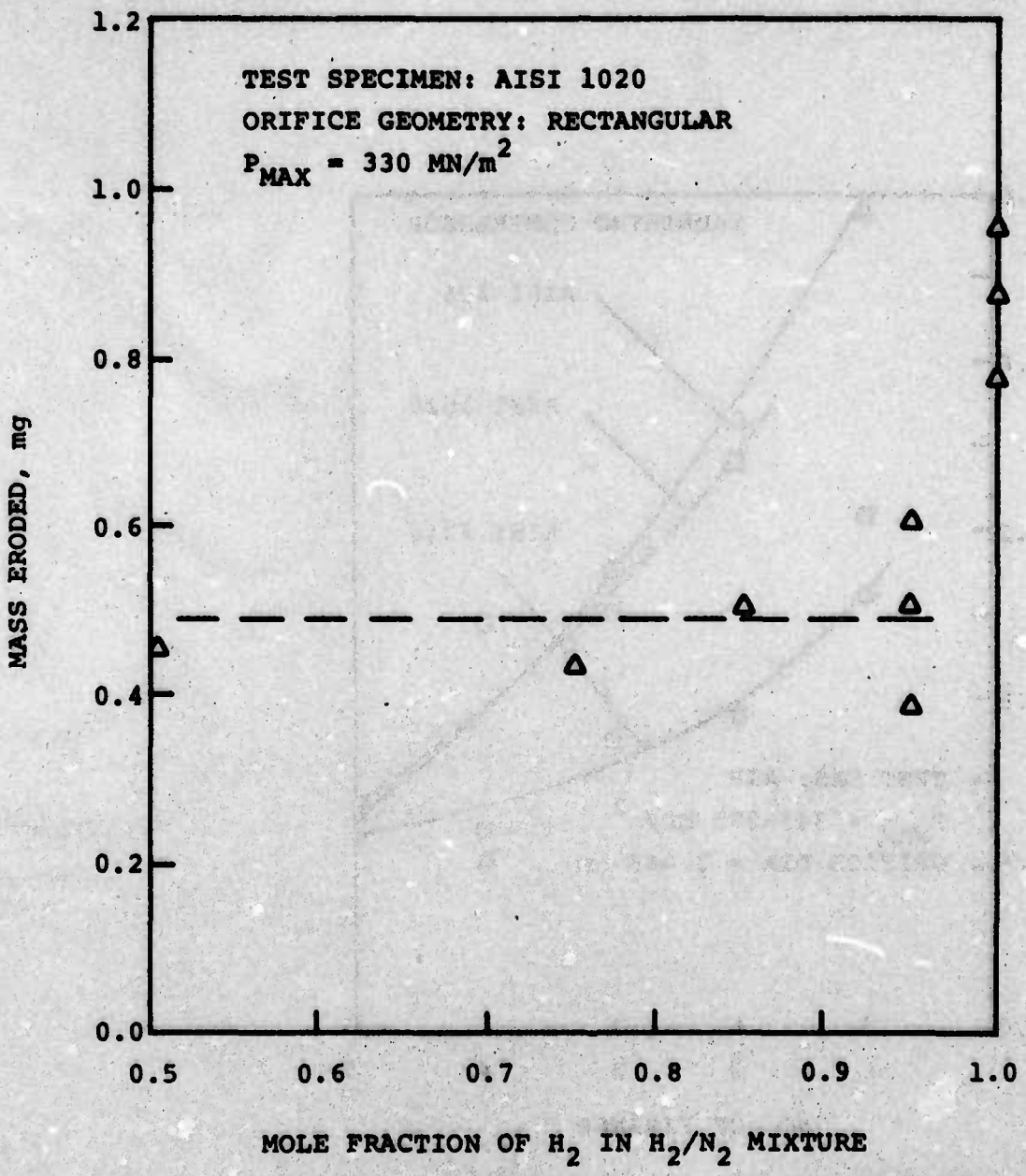

Fig. 40 Erosion of AISI 1020 steel vs mole fraction of H_2 in H_2/N_2 mixture, indicating that for H_2 concentrations less than 95% erosion is independent of H_2 concentration.

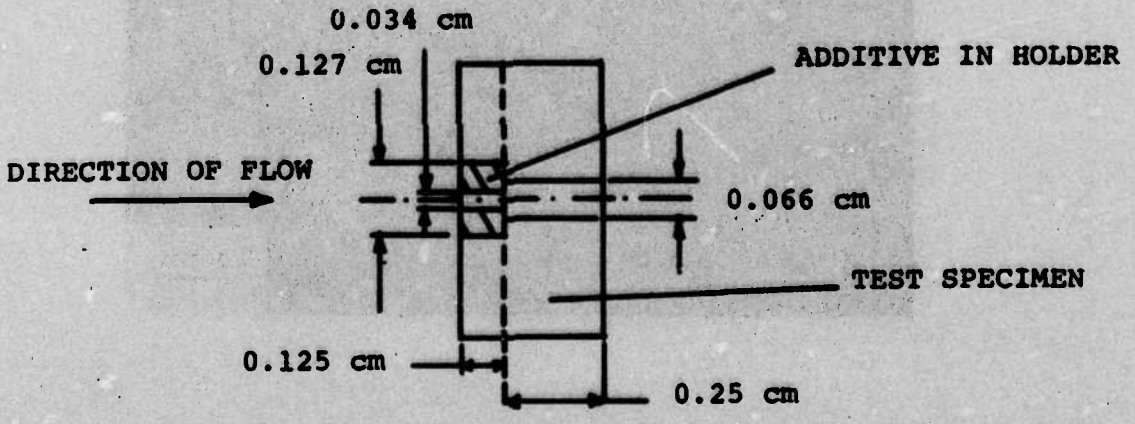

Fig. 41 Schematic representation of the test specimen configuration and positioning of the additive relative to the test specimen.

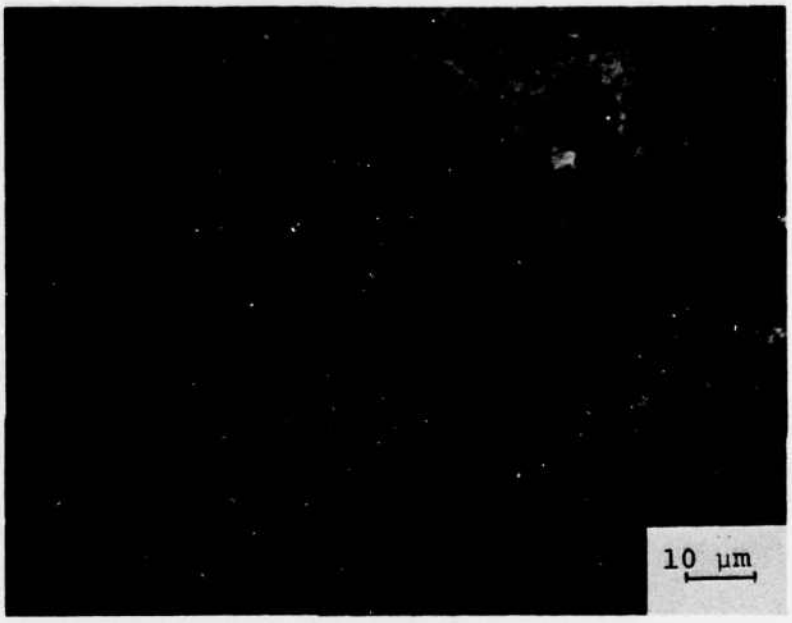

Fig. 42 SEM photograph of an eroded surface of AISI 4340 steel subjected to the action of IMR-4198 propellant gases.

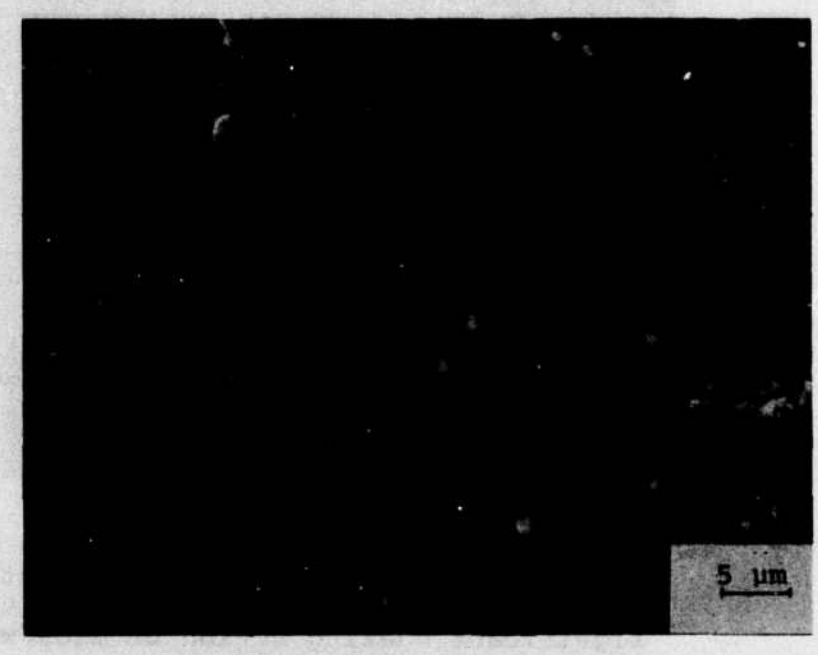

Fig. 43 SEM photograph of an eroded surface of AISI 4340 steel subjected to the action of IMR 4198 propellant gases showing the minor coating action of polyurethane foam additive.

Fig. 44 SEM photograph of an eroded surface of AISI 4340 steel subjected to the action of IMR 4198 propellant gases showing the significant coating action of TiO_2/wax erosion-reducing additive.

APPENDIX I

General Equilibrium Theory

Consider a closed system composed of several components. Let n_i the moles of species i present in the system. The Gibbs free energy can be expressed as

$$G = G(T, p, n_1, n_2 \ldots n_J) \tag{I-1}$$

Then

$$dG = \left(\frac{\partial G}{\partial T}\right)_{p,n_i} dT + \left(\frac{\partial G}{\partial p}\right)_{T,n_i} dp + \sum \left(\frac{\partial G}{\partial n_i}\right)_{T,p,n_J} dn_i \tag{I-2}$$

In the case of one-component system (i.e., $dn_i=0$), the change of the Gibbs free energy is given by

$$dG = -SdT + Vdp \tag{I-3}$$

Comparing equation (2) and (3) we obtain the following relations

$$S = -\left(\frac{\partial G}{\partial T}\right)_{p,n_i} \quad \text{and} \quad V = \left(\frac{\partial G}{\partial p}\right)_{T,n_i} \tag{I-4}$$

Thus equation (2) may be written as

$$dG = -SdT + Vdp + \sum \mu_i dn_i \tag{I-5}$$

where the chemical potential μ_i is defined as

$$\mu_i \equiv \left(\frac{\partial G}{\partial n_i}\right)_{T,p,n_J} = \bar{G}_i = \text{partial molal Gibbs free energy*}$$

---

*The partial molal property of L (where L is any property such as volume, entropy, etc., is defined as

$$\bar{L}_i \equiv \left(\frac{\partial L}{\partial n_i}\right)_{T,p,n_J}$$

Now, the criterion for equilibrium for a process proceeding at constant temperature and pressure is

$$\Delta G = 0 \tag{I-6}$$

Applying the equilibrium condition in equation (5) we have

$$\sum \mu_i dn_i = 0 \tag{I-7}$$

Let us now consider a general chemical reaction of the form

$$\sum \nu_i M_i \rightarrow \sum \nu_i' M_i \tag{I-8}$$

where ν_i denotes the stoichiometric coefficients and prime denotes the products. Applying the general equilibrium condition, Eq. (I-7) in reaction (I-8) we have

$$\sum \mu_i' dn_i' - \sum \mu_i dn_i = 0 \tag{I-9}$$

Dividing equation (I-9) by n_1 and noting that

$$\frac{dn_i}{n_1} = \frac{\nu_i}{\nu_1} \quad \text{and} \quad \frac{dn_i'}{n_1} = \frac{\nu_i'}{\nu_1} \quad \text{we have}$$

$$\sum \left(\mu_i' \nu_i' - \mu_i \nu_i \right) = 0 \tag{I-10}$$

Introducing now the activity a_i as

$$\mu_i \equiv \mu_i^* + RT \ln a_i \tag{I-11}$$

where $u_i^* = \bar{G}_i^*$ is the chemical potential evaluated at p = 1 atm.

Applying equation (I-11) in (I-10) and rearranging we have

$$\exp\left[- \frac{\Delta G^*}{RT} \right] = \frac{\Pi a_i^{\nu'}}{\Pi a_i^{\nu}} \tag{I-12}$$

where $\Delta G^* = \sum \bar{G}_i \nu_i' - \sum \bar{G}_i \nu_i$

The equilibrium constant K_a is defined as

$$K_a = \frac{\Pi a_i^{\nu_i'}}{\Pi a_i^{\nu_i}} \qquad \text{(I-13)}$$

In deriving equation (I-13) no assumption was made on the state of the species, i.e., whether they are solids, liquids or gases and therefore the equilibrium conditions derived are valid for a general system. In the next sections we will derive the equilibrium relations for ideal and non ideal gases and we will also discuss the equilibrium calculations in a heterogeneous system.

Chemical Equilibrium of Ideal Gases

The equation of state of an ideal gas is

$$p\Phi = RT \qquad \text{(I-14)}$$

where $\Phi = V/n$

For a multicomponent mixture

$$d\bar{G}_i = d\mu_i = \bar{V}_i dp - \bar{S}_i dT \qquad \text{(I-15)}$$

For an isothermal process and noting that for an ideal gas $\bar{V}_i = \Phi_i = \hat{u}$ then equation (I-15) becomes

$$d\mu_i = \frac{RT}{p} dp \qquad \text{(I-16)}$$

Integrating equation (I-16) between $p = 1$ atm ($\mu_i = \mu_i^*$) and $p = p$ we have

$$\mu_i = \mu_i^* + RT\ln p \qquad \text{(I-17)}$$

Comparing equation (I-17) with (I-11) we deduce that for an ideal gas

$$a_i = p_i \qquad \text{(I-18)}$$

Hence

$$K_p = \frac{\Pi p_i^{\nu_i'}}{\Pi p_i^{\nu_i}} = \exp\left[-\frac{\Delta G^\circ}{RT}\right] \qquad \text{(I-19)}$$

where ΔG° is the standard Gibbs free energy of the system.

The equilibrium constant can also be expressed in terms of the mole fractions of the species by using the relation

$$x_i = p_i/p \tag{I-20}$$

The corresponding expression of the equilibrium constant K_x

$$K_x = \frac{\Pi X_i^{\nu_i'}}{\Pi X_i^{\nu_i}} \; p^{(\Sigma\nu_i - \Sigma\nu_i')} \tag{I-21}$$

Chemical Equilibrium of Real Gases

We define a new property the fugacity of a gas i, f_i, such as

$$\mu_i \equiv \mu_i^* + RT\ln(f_i/f_i^*) \tag{I-22}$$

Comparison of equations (I-11) and (I-22) we have

$$f_i/f_i^* = a_i = \lambda_i/\lambda_i^* \tag{I-23}$$

where λ_i is the absolute activity of a substance.

The standard state of a real gas, i, we define as the state in which the gas has unit fugacity, i.e., $f_i^* = 1$, and in which the gas behaves as if it were ideal gas.

Thus from equations (I-23) and (I-18) we deduce that for an ideal gas

$$f_i = p_i \tag{I-24}$$

The fugacity coefficient γ_i is defined as

$$\gamma_i = f_i/p_i \tag{I-25}$$

This coefficient represents a measure of the departure of a real gas from ideal.

For a gas that obeys Abel's equation of state, i.e.,

$$p(\hat{V} - b) = RT \tag{I-26}$$

The fugacity coefficient γ is given by

$$\gamma = \exp(bp/RT) \tag{I-27}$$

Thus the non-ideal behavior of the gas increases as the pressure increases and as the temperature decreases.

The equilibrium constant of a non-ideal gas is given by the expression

$$K_f = \frac{\Pi f_i^{\nu_i'}}{\Pi f_i^{\nu_i}} \tag{I-28}$$

Chemical Equilibrium of Condensed Phases

The change in the partial molal Gibbs free energy is given by

$$d\bar{G}_i = d\mu_i = \bar{V}_i dp - \bar{S}_i dT \tag{I-29}$$

For an isothermal process

$$d\mu_i = V_i dp = RTd\ln f_i \tag{I-30}$$

Thus the fugacity at p=p is related to the fugacity at p = 1 atm by the relation

$$\ln \frac{f_i(p)}{f_i(1atm)} = \frac{1}{RT} \int_1^p \bar{V}_i dp \tag{I-31}$$

Hence

$$\frac{f_i(p)}{f_i^*} = \frac{f_i(p)}{f_i(1atm)} \frac{f_i(1atm)}{f_i^*}$$

or

$$a_i(p) = \frac{f_i(p)}{f_i(1atm)} a(1atm) \tag{I-32}$$

For a pure liquid or solid the activity at 1 atm is equal to unity (standard state).

For gas - solid reactions the general expression for the equilibrium constant is

$$K_a = \frac{\Pi a_i^{\nu'}(\text{gas})\,\Pi a_i^{\nu'}(\text{solid})}{\Pi a_i^{\nu}(\text{gas})\,\Pi a_i^{\nu}(\text{solid})} \qquad \text{(I-33)}$$

For pure solids at moderate pressures, a_i, for the solid is unity, then

$$K_a = \frac{\Pi a_i^{\nu'}(\text{gas})}{\Pi a_i^{\nu}(\text{gas})} . \qquad \text{(I-34)}$$

DISTRIBUTION LIST

No. of Copies	To
1	Office of the Director, Defense Research and Engineering, The Pentagon, Washington, D. C. 20301
12	Commander, Defense Documentation Center, Cameron Station, Building 5, 5010 Duke Street, Alexandria, Virginia 22314
1	Metals and Ceramics Information Center, Battelle Columbus Laboratories, 505 King Avenue, Columbus, Ohio 43201
1	Chemical Propulsion Information Agency, Applied Physics Laboratory, The Johns Hopkins University, 8621 Georgia Avenue, Silver Spring, Maryland 20910
	Deputy Chief of Staff, Research, Development, and Acquisition, Headquarters, Department of the Army, Washington, D. C. 20310
2	ATTN: DAMA-ARZ
	Commander, Army Research Office, P. O. Box 12211, Research Triangle Park, North Carolina 27709
1	ATTN: Information Processing Office
	Commander, U. S. Army Materiel Development and Readiness Command, 5001 Eisenhower Avenue, Alexandria, Virginia 22333
1	ATTN: DRCLDC, Mr. R. Zentner
	Commander, U. S. Army Communications Research and Development Command, Fort Monmouth, New Jersey 07703
1	ATTN: DRDCO-GG-DD
1	DRDCO-GG-DM
	Commander, U. S. Army Missile Research and Development Command, Redstone Arsenal, Alabama 35809
1	ATTN: Technical Library
1	DRSMI-RSM, Mr. E. J. Wheelahan
	Commander, U. S. Army Armament Research and Development Command, Dover, New Jersey 07801
2	ATTN: Technical Library
1	DRDAR-SCM, Mr. J. D. Corrie
1	DRDAR-SC, Dr. C. M. Hudson
1	DRDAR-PPW-PB, Mr. Francis X. Walter
	Commander, U. S. Army Natick Research and Development Command, Natick, Massachusetts 01760
1	ATTN: Technical Library

No. of Copies	To
	Commander, U. S. Army Satellite Communications Agency, Fort Monmouth, New Jersey 07703
1	ATTN: Technical Document Center
	Commander, U. S. Army Tank-Automotive Research and Development Command, Warren, Michigan 48090
2	ATTN: DRDTA, Research Library Branch
	Commander, White Sands Missile Range, New Mexico 88002
1	ATTN: STEWS-WS-VT
	Commander, Aberdeen Proving Ground, Maryland 21005
1	ATTN: STEAP-TL, Bldg. 305
	President, Airborne, Electronics and Special Warfare Board, Fort Bragg, North Carolina 28307
1	ATTN: Library
	Commander, Dugway Proving Ground, Dugway, Utah 84022
1	ATTN: Technical Library, Technical Information Division
	Commander, Edgewood Arsenal, Aberdeen Proving Ground, Maryland 21010
1	ATTN: Mr. F. E. Thompson, Dir. of Eng. & Ind. Serv., Chem-Mun Br
	Commander, Frankford Arsenal, Philadelphia, Pennsylvania 19137
1	ATTN: Library, H1300, Bl. 51-2
	Commander, Harry Diamond Laboratories, 2800 Powder Mill Road, Adelphi, Maryland 20783
1	ATTN: Technical Information Office
	Commander, Picatinny Arsenal, Dover, New Jersey 07801
1	ATTN: SARPA-RT-S
1	SARPA-FR-M-D, PLASTEC, A. M. Anzalone
	Commander, Redstone Scientific Information Center, U. S. Army Missile Research and Development Command, Redstone Arsenal, Alabama 35809
4	ATTN: DRSMI-RBLD, Document Section
	Commander, Watervliet Arsenal, Watervliet, New York 12189
1	ATTN: SARWV-RDT, Technical Information Services Office
	Commander, U. S. Army Foreign Science and Technology Center, 220 7th Street, N. E., Charlottesville, Virginia 22901
1	ATTN: DRXST, Military Tech., Mr. Marley
	Director, Eustis Directorate, U. S. Army Air Mobility Research and Development Laboratory, Fort Eustis, Virginia 23604
1	ATTN: Mr. J. Robinson, DAVDL-E-MOS (AVRADCOM)

No. of Copies	To
	U. S. Army Aviation Training Library, Fort Rucker, Alabama 36360
1	ATTN: Buildings 906 and 907
	Commander, U. S. Army Engineer School, Fort Belvoir, Virginia 22060
1	ATTN: Library
	Commandant, U. S. Army Quartermaster School, Fort Lee, Virginia 23801
1	ATTN: Quartermaster School Library
	Naval Research Laboratory, Washington, D. C. 20375
1	ATTN: Dr. J. M. Krafft - Code 8430
	Chief of Naval Research, Arlington, Virginia 22217
1	ATTN: Code 471
	Air Force Materials Laboratory, Wright-Patterson Air Force Base, Ohio 45433
2	ATTN: AFML/MXE/E. Morrissey
1	AFML/LC
1	AFML/LLP/D. M. Forney, Jr.
1	AFML/MBC/Stanley Schulman
	National Aeronautics and Space Administration, Washington, D. C. 20546
1	ATTN: Mr. B. G. Achhammer
1	Mr. G. C. Deutsch - Code RW
	National Aeronautics and Space Administration, Marshall Space Flight Center, Huntsville, Alabama 35812
1	ATTN: R. J. Schwinghamer, EH01, Director M&P Laboratory
1	Mr. W. A. Wilson, EH41, Building 4612
1	Ship Research Committee, Maritime Transportation Research Board, National Research Council, 2101 Constitution Ave., N. W., Washington, D. C. 20418
	P. R. Mallory Company, Inc., 3029 East Washington Street, Indianapolis, Indiana 46206
1	ATTN: Technical Library
1	Materials Sciences Corporation, Blue Bell Office Campus, Merion Towle House, Blue Bell, Pennsylvania 19422
1	The Charles Stark Draper Laboratory, 68 Albany Street, Cambridge, Massachusetts 02139
	Wyman-Gordon Company, Worcester, Massachusetts 01601
1	ATTN: Technical Library
	Lockheed-Georgia Company, 86 South Cobb Drive, Marietta, Georgia 30063
1	ATTN: Materials & Processes Engrg. Dept. 71-11, Zone 54

No. of Copies	To
	Director, Army Materials and Mechanics Research Center, Watertown, Massachusetts 02172
2	ATTN: DRXMR-PL
1	DRXMR-PR
1	DRXMR-AP
1	DRXMR-X
1	DRXMR-CT
1	DRXMR-D
1	Dr. J. Johnson
43	Author

Army Materials and Mechanics Research Center Watertown, Massachusetts 02172 EROSIVE EFFECTS OF VARIOUS PURE AND COMBUSTION-GENERATED GASES ON METALS, PART II, A. C. Alkidas, S. O. Morris, C. W. Christoe, L. H. Caveny and M. Summerfield, Princeton University, Princeton, NJ Technical Report AMMRC CTR 77-25, October 1977, 123 pp. illus - tables, Contract No. DAAG46-75-C-0088, D/A Proj. 1T161102AH42, AMCMS Code: 611102.11.H42 Final Report, 1 June 1975 - 31 January 1976	AD __________ UNCLASSIFIED UNLIMITED DISTRIBUTION Key Words Metal erosion Propellant gas Gun tubes Alloys

The chemical erosion characteristics of steel alloys by high pressure and high temperature reactive gases (pure and combustion-generated) were investigated. The data indicate that the primary mechanism of steel erosion under gun barrel conditions is the reaction of the combustion gases with the steel surface to form scale and the subsequent carrying-away of the scale by the high speed flow.

Army Materials and Mechanics Research Center
Watertown, Massachusetts 02172
EROSIVE EFFECTS OF VARIOUS PURE AND
COMBUSTION-GENERATED GASES ON
METALS, PART II, A. C. Alkidas,
S. O. Morris, C. W. Christoe,
L. H. Caveny and M. Summerfield,
Princeton University, Princeton, NJ
Technical Report AMMRC CTR 77-25, October 1977,
123 pp. illus - tables, Contract No.
DAAG46-75-C-0088, D/A Proj. 1T161102AH42,
AMCMS Code: 611102.11.H42
Final Report, 1 June 1975 - 31 January 1976
AD __________
UNCLASSIFIED
UNLIMITED DISTRIBUTION
Key Words
Metal erosion
Propellant gas
Gun tubes
Alloys

The chemical erosion characteristics of steel alloys by high pressure and high temperature reactive gases (pure and combustion-generated) were investigated. The data indicate that the primary mechanism of steel erosion under gun barrel conditions is the reaction of the combustion gases with the steel surface to form scale and the subsequent carrying-away of the scale by the high speed flow.

Army Materials and Mechanics Research Center
Watertown, Massachusetts 02172
EROSIVE EFFECTS OF VARIOUS PURE AND
COMBUSTION-GENERATED GASES ON
METALS, PART II, A. C. Alkidas,
S. O. Morris, C. W. Christoe,
L. H. Caveny and M. Summerfield,
Princeton University, Princeton, NJ
Technical Report AMMRC CTR 77-25, October 1977,
123 pp. illus - tables, Contract No.
DAAG46-75-C-0088, D/A Proj. 1T161102AH42,
AMCMS Code: 611102.11.H42
Final Report, 1 June 1975 - 31 January 1976
AD __________
UNCLASSIFIED
UNLIMITED DISTRIBUTION
Key Words
Metal erosion
Propellant gas
Gun tubes
Alloys

The chemical erosion characteristics of steel alloys by high pressure and high temperature reactive gases (pure and combustion-generated) were investigated. The data indicate that the primary mechanism of steel erosion under gun barrel conditions is the reaction of the combustion gases with the steel surface to form scale and the subsequent carrying-away of the scale by the high speed flow.

Army Materials and Mechanics Research Center
Watertown, Massachusetts 02172
EROSIVE EFFECTS OF VARIOUS PURE AND
COMBUSTION-GENERATED GASES ON
METALS, PART II, A. C. Alkidas,
S. O. Morris, C. W. Christoe,
L. H. Caveny and M. Summerfield,
Princeton University, Princeton, NJ
Technical Report AMMRC CTR 77-25, October 1977,
123 pp. illus - tables, Contract No.
DAAG46-75-C-0088, D/A Proj. 1T161102AH42,
AMCMS Code: 611102.11.H42
Final Report, 1 June 1975 - 31 January 1976
AD __________
UNCLASSIFIED
UNLIMITED DISTRIBUTION
Key Words
Metal erosion
Propellant gas
Gun tubes
Alloys

The chemical erosion characteristics of steel alloys by high pressure and high temperature reactive gases (pure and combustion-generated) were investigated. The data indicate that the primary mechanism of steel erosion under gun barrel conditions is the reaction of the combustion gases with the steel surface to form scale and the subsequent carrying-away of the scale by the high speed flow.